ornl

ORNL/SUB/93-SM037/2

# OAK RIDGE NATIONAL LABORATORY

LOCKHEED MARTIN

# Innovative Grinding Wheel Design for Cost-Effective Machining of Advanced Ceramics

## FINAL REPORT

R. H. Licht
P. Kuo
S. Liu
D. Murphy
J.W. Picone
S. Ramanath

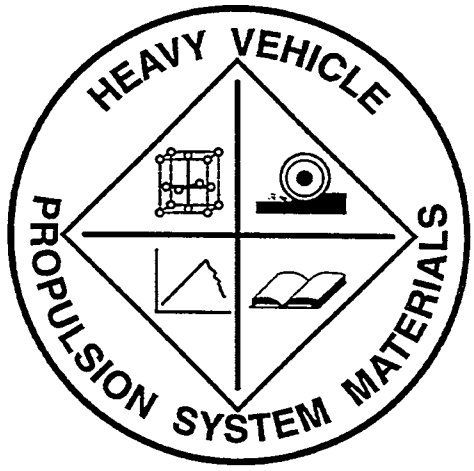


MANAGED AND OPERATED BY
LOCKHEED MARTIN ENERGY RESEARCH CORPORATION
FOR THE UNITED STATES
DEPARTMENT OF ENERGY

ORNL-27 (3-96)

## DISCLAIMER

**Portions of this document may be illegible in electronic image products. Images are produced from the best available original document.**

ORNL/Sub/93-SM037/2

# INNOVATIVE GRINDING WHEEL DESIGN FOR COST-EFFECTIVE MACHINING OF ADVANCED CERAMICS

R. H. Licht
P. Kuo
S. Liu
D. Murphy
J. W. Picone
S. Ramanath

Date Published: Feb. 2000

FINAL REPORT

Prepared by
Norton Company
Superabrasives R&D
Worcester, Massachusetts 01615-0008

Funded by
U.S. Department of Energy
Assistant Secretary for Energy Efficiency and Renewable Energy
Office of Transportation Technologies
Heavy Vehicle Propulsion System Materials Program
EE 07 01 00 0

for
OAK RIDGE NATIONAL LABORATORY
Oak Ridge, Tennessee 37831-6285
Managed by
LOCKHEED MARTIN ENERGY RESEARCH CORPORATION
for the
U.S. DEPARTMENT OF ENERGY
under Contract DE-AC05-96OR22464

# TABLE OF CONTENTS

Research sponsored by the U.S. Department of Energy, Assistant Secretary for Energy Efficiency and Renewable Energy, Office of Transportation Technologies, as part of the Heavy Vehicle Propulsion System Materials Program, under contract DE-AC05-96OR22464 with Lockheed Martin Energy Research Corporation.

# 1. EXECUTIVE SUMMARY

This Final Report covers the Phase II Innovative Grinding Wheel program. Norton Company successfully completed this second phase of a program to develop a novel grinding wheel for cost-effective cylindrical grinding of advanced ceramics.

Advanced ceramic materials are vital for energy conservation and pollution reduction in new transportation systems. Major impediments to the commercialization of advanced ceramics are reliability and cost. Toward the objective of improving reliability and reducing manufacturing cost, the U.S. Department of Energy, Office of Transportation Technologies, under contract with Lockheed Marietta Energy Research, Corp. (LMER) at Oak Ridge National Laboratory (ORNL), has sponsored research as part of the Heavy Vehicle Propulsion System Materials Program. The goal of this program, managed at ORNL, was to develop highly reliable and cost-effective structural ceramics for engine applications. The Cost-Effective Ceramic Machining (CECM) Program was part of Heavy Vehicle Propulsion System Materials in recognition of the importance of machining to commercializing advanced ceramics. The CECM recognized that ceramic machining, predominantly diamond grinding, is a major cost factor in advanced ceramics manufacturing. The abrasive wheel performance significantly influences the grinding costs. Additionally, the quality of the grinding operation greatly affects ceramic surface integrity, tolerance, and manufacturing yield.

In 1995, Norton Company successfully completed the 16-month Phase I technical effort to define requirements, design, develop, and evaluate a next-generation grinding wheel for cost-effective cylindrical grinding of advanced ceramics [1]. An improved superabrasive metal-bond specification for low-cost machining of ceramics in external cylindrical grinding mode was identified. Grinding test results of 76-mm- (3-inch-) and 203-mm- (8-inch-) diameter wheels indicated that a superior, innovative grinding wheel (IGW) for cylindrical grinding of ceramics had been developed using a modified metal-bond technology. The following are examples of superior performance observed in the small diameter in-house grinding wheel tests. The spindle power consumed by this wheel was as much as 30% lower compared to a standard resin bonded wheel with 100 diamond concentration. The wheel wear with this improved metal bond was an order of magnitude lower than the resin-bonded wheel, which would significantly reduce ceramic grinding costs through fewer wheel changes as a result of retruing and abrasive wear. The projected manufacturing cost of this experimental wheel was not appreciably different from standard resin- and metal-bond superabrasive wheels, and therefore this experimental wheel would have a significant cost advantage in grinding ceramics. Preliminary evaluation of ceramic specimens did not show evidence of unusual grinding damage.

Most production grinding of cylindrical ceramic parts is done on machines that use 305-mm- (12-inch-) to 406-mm- (16-inch-) diameter wheels. A Phase II program was initiated in March 1996 to scale-up the new superabrasive wheel specification to these larger diameters, to make further wheel enhancements, and to perform in-house and independent validation grinding tests.

This Phase II program final report reviews the efforts at Norton in process scale-up of the Phase I experimental metal-bond wheel to full size 400-mm (16-inch) diameter. In Task 1, Process Scale-up a new segmented-wheel approach was evaluated and selected over the continuous-rim design used for smaller wheels in Phase I. The segmented-wheel approach was expected to facilitate prototype fabrication of larger diameter wheels. Norton requested a modification of the original statement of work to change the test wheel diameter requirement from 356 mm, to a range of between 356 mm and 406 mm. This larger diameter capability is preferable for some of the newer OD grinding machines and current grinding trends in the ceramic industry. The successful manufacture of the larger diameter wheels would be expected to expedite new wheel commercialization at the conclusion of this Phase II contract.

A core material was chosen that would more than exceed the required spin-test speeds for test wheels by a factor of 3. Abrasive segment manufacturing trials that demonstrated improved segment property consistency were successfully completed. Wheel assembly trials that demonstrated net shape segment manufacture and successful segment-core adhesion were completed. Two cements were evaluated. Partial wheel assemblies were made for segment adhesion burst tests. In three wheel tests, failure occurred at over 200 m/s with the failure at the cemented interface. Fractography confirmed successful interface preparation and gave expected failure patterns. Several full size, 393-mm-diameter wheels were manufactured for burst testing and grinding tests. The manufacturing trials successfully demonstrated segment curvature and side angle control for the rim and segment-to-segment interfaces. Speed tests of the wheels to be used in grinding tests rated them at up to 120 m/s. Burst tests of 4 wheels would conservatively rate this design maximum operating speed (MOS) to at least 90 m/s. Further enhancements of the cement and core would be expected to increase the MOS.

Confirmatory grinding tests were performed in Task 2, In-House grinding Tests, and Task 3, Independent Validation Tests at customer sites. The principal workpiece material used in the all grinding tests was Norton Advanced Ceramics NT551 silicon nitride. This material is currently NAC's principal material used for ceramic engine components and is the material used for diesel engine valves under the DOE program, Advanced Ceramic Manufacturing Technology Development. The standard test pieces manufactured for the Innovative Grinding Wheel Tasks 2 and 3 tests were cylindrical NT551, approximately 3 inch long by 1 inch diameter. In addition to the standard specimens, Task 3 also included NT551 diesel engine valves, NT551 rolling contact fatigue (RCF) specimens, and alumina disks in the NAC test; and magnesia partially stabilized zirconia used for fuel injector components in the Caterpillar test.

Norton's Higgins Grinding Technology Center (HGTC), formerly the World Grinding Technology Center, completed preliminary in-house tests of the large diameter wheels under Task 2. These tests were in both plunge and traverse grinding modes at three grinding speeds and several grinding conditions. The experimental metal-bonded wheel significantly outperformed both the standard vitrified- and resin-bonded wheels. The experimental metal-bonded wheel demonstrated superior wheel life with less need for truing and dressing during the extended grinding tests. The improvements with the experimental metal-bonded wheel were more pronounced at higher material removal rate conditions. The IGW achieved cut rates of over 5 times of that practical by a standard resin-bond diamond grinding wheel, and demonstrated G-ratios over an order of magnitude greater. This advantage was more pronounced when considering that the standard resin-bond wheel had a higher diamond concentration.

Independent customer validation tests of the experimental metal-bond innovative grinding wheel were performed by Caterpillar Corporation; Chand Kare Technical Ceramics, Eaton Manufacturing Technologies Center, and Norton Advanced Ceramics (NAC). All these independent tests reported excellent results and operator preference for the IGW as opposed to standard diamond wheel products when grinding NT551 silicon nitride and other ceramics. The general trends from these tests showed that the IGW gave lower and more stable wheel wear, grinding force, and power over a wide range of material removal rates.

- NAC with the HGTC completed a grinding experiment comparing the IGW to a standard vitrified wheel for traverse finish grinding of ceramic diesel engine valves. The IGW was tested at cut rates over 6 times higher and traverse rates 2.5 times greater than achieved with the vitrified wheel; the IGW met the surface finish specification at all grinding test conditions. A supplemental NAC test at NRDC evaluated the IGW machining NT551 silicon nitride rolling contact fatigue specimens and cylindrical plunge grinding of aluminum oxide disks. In these preliminary trials at NRDC, no significant differences were noted compared to a standard resin-bonded wheel.
- Eaton tested the wheel at three speeds up to 18,000 surface feet per minute (SFPM). The Eaton test showed higher G-ratio, lower wheel wear, lower grinding force, and better surface finish compared to an even coarser grit resin-bonded wheel. The IGW performance was less sensitive to grinding speed than the resin-bonded wheel and the differences were more pronounced at lower grinding speeds.
- Caterpillar demonstrated G-ratio superiority of the IGW in centerless grinding on both NT551 silicon nitride and Mg-PSZ. Weibull analysis of post-ground zirconia bend bars suggested less machining damage for the IGW.
- Chand, testing at lower grinding speeds than the other tests, reported significantly lower specific energy with the IGW with surface roughness, form holding, and truing time similar to that of the standard resin-bonded wheel. Surprisingly, the IGW had slightly higher wheel wear (the opposite result from all other tests).

During the development of cost-effective machining processes or development of new grinding wheels, it is critically important to maintain and characterize the surface integrity of the ground ceramic. Surface integrity refers to: (1) finish and tolerance, (2) degree of machining damage, and (3) grinding-induced residual stress. Norton researchers characterized the surface integrity of the ground surfaces to ensure that the improved metal-bonded grinding wheel does not cause unusual grinding damage. We performed comprehensive ceramic surface characterization including surface finish, component flexural strength, failure origin analysis, and surface residual stress. There was no indication of unusual surface integrity problems with the new IGW. Most notably, the IGW showed excellent surface finish stability at very high material removal rates in several tests. Flexural testing of traverse-ground specimens did not result in significantly different strength differences or any observed severe machining damage with the IGW. Actually, severe damage was observed in isolated examples with the standard resin-bonded wheel, not the IGW, during the in-house HGTC test and the Caterpillar test. Also, the observed lower normal force and specific grinding energy observed for the IGW in several tests would tend to suggest the tendency for lower grinding damage with this new wheel. Residual stress studies were performed at Brookhaven National Laboratory under an ORNL HTML User Center project. Traverse- and plunge-ground cylindrical surfaces ground using the IGW or standard resin-bond wheel were compared. No significant differences in residual stress profiles were noted, except that a more severe stress gradient was noted for the plunge-ground surface created by the resin-bond wheel.

In conclusion, the Innovative Grinding Wheel Phase II program successfully demonstrated manufacturing scale-up of 16-inch-diameter wheels for cylindrical grinding. The new, experimental metal-bonded grinding wheel demonstrated significant improvements over conventional resin- and vitrified-bonded wheels when grinding silicon nitride and other advanced ceramics. The new wheel product offering should result in significant cost-effective improvements in the cylindrical grinding of advanced ceramics, while maintaining the required component quality achieved by conventional grinding wheels. Additionally, the new product should be applicable for other machining operations such as centerless, surface, and ID grinding.

# 2. LIST OF TABLES

# 3. LIST OF FIGURES

# INNOVATIVE GRINDING WHEEL DESIGN FOR COST-EFFECTIVE MACHINING OF ADVANCED CERAMICS -- PHASE II

R.H. Licht, P. Kuo, S. Liu, D. Murphy, J.W. Picone, S. Ramanath
Norton Company, Worcester and Northboro, Massachusetts

## 4. ABSTRACT

This Final Report covers the Phase II Innovative Grinding Wheel (IGW) program in which Norton Company successfully developed a novel grinding wheel for cost-effective cylindrical grinding of advanced ceramics. In 1995, Norton Company successfully completed the 16-month Phase I technical effort to define requirements, design, develop, and evaluate a next-generation grinding wheel for cost-effective cylindrical grinding of advanced ceramics [1] using small prototype wheels. The Phase II program was initiated to scale-up the new superabrasive wheel specification to larger diameters, 305-mm to 406-mm, required for most production grinding of cylindrical ceramic parts, and to perform in-house and independent validation grinding tests.

Wheel manufacturability studies were completed in Task 1. A segmented wheel approach was selected, which was expected to facilitate prototype fabrication of larger-diameter wheels. Partial wheel assemblies and full size wheels were speed tested (non-destructive) and burst tested (destructive) demonstrating the new design had sufficient wheel strength for the high speed required for grinding tests in this program. Further enhancements of the cement and core would be expected to increase the MOS. The manufacturing trials successfully demonstrated suitable control of the segment curvatures.

Confirmatory grinding tests were performed in Task 2, (in-house grinding tests) and Task 3, (independent validation tests at customer sites). The principal workpiece material used in the all grinding tests was Norton Advanced Ceramics (NAC) NT551 silicon nitride, currently used for ceramic engine components including diesel engine valves.

Norton's Higgins Grinding Technology Center (HGTC) completed preliminary in-house tests under Task 2 at three grinding speeds and several grinding conditions, in both plunge and traverse grinding modes. The experimental metal-bonded wheel significantly outperformed both the standard vitrified and resin-bonded wheels. The IGW achieved cut rates of over 5 times of that practical by a standard resin-bond diamond grinding wheel, and demonstrated G-ratios over an order of magnitude greater.

In Task 3, independent customer validation tests of the experimental metal-bonded IGW were performed by Caterpillar Corporation, Chand Kare Technical Ceramics, Eaton Manufacturing Technologies Center, and Norton Advanced Ceramics. All these independent tests reported excellent results and operator preference for the IGW vs standard diamond wheel products when grinding NT551 silicon nitride and other

ceramics. The general results of these tests showed that the IGW gave lower and more stable wheel wear, grinding force, and power over a wide range of material removal rates.

Researchers characterized the surface integrity of the ground surfaces of the new wheels vs standard wheels including surface finish, component flexural strength, failure origin analysis, and surface residual stress. There was no indication of unusual surface integrity problems with the new IGW. Most notably, the IGW showed excellent surface finish stability at very high material removal rates in several tests and no significant differences in the strength of ground surfaces compared to standard wheels.

The new wheel product offering should result in significant cost-effective improvements in the cylindrical grinding of advanced ceramics, while maintaining the required component quality achieved by conventional grinding wheels.

# 5. INTRODUCTION

Ceramic machining, predominantly diamond grinding, is a major cost factor in advanced ceramics manufacturing. The abrasive wheel performance significantly influences the grinding costs. Additionally, the quality of the grinding operation greatly affects ceramic surface integrity, tolerance, and manufacturing yield.

## 5.1. CERAMIC MACHINING MARKET

Beginning with ceramic pottery that required no machining, today we have ceramics that are ground to surface finishes typically a few hundred nanometers down to several angstroms. Finishes in the range of 0.1-0.3 μm (4-12 μin.) are required for most wear and engine components while finer finishes are required for parts such as thin film substrates, ceramic mirrors, and ceramic bearing components. Advanced ceramic materials are inorganic, usually covalent-bonded polycrystalline structures, which are strong, refractory, and have high hardness. Therefore they are inherently difficult to machine or polish. Typically, the finishing of ceramics into useful components requires an abrasive (~70% of the time) or a non-abrasive machining process.

The worldwide market for resin and metal-bonded diamond wheels for industrial (not construction) applications is approximately $570 M. Approximately 20% of this is for the ceramic grinding market [2]. The ceramic market may be classified into four major segments: industrial ceramics, electronic ceramics, technical ceramics, and advanced ceramics. The advanced ceramics market (ceramic bearings, engine components, etc.) are characterized by the key requirements of close tolerances, good retained strength after grinding and good surface finish. Even though the advanced ceramics market is small, the growth rate is high. The most common method for finishing of ceramic components has been using diamond abrasive wheels. The primary reason for the widespread use of diamond is its high hardness as required by the hardness of the workpiece.

## 5.2. INDUSTRY REQUIREMENTS - COST AND QUALITY CONSIDERATIONS

### 5.2.1. DOE Cost-Effective Ceramic Machining Initiative

Advanced ceramics possess unique properties of high-temperature durability, corrosion resistance, strength, hardness, stiffness, and wear resistance. These properties make advanced ceramics attractive to many applications in the transportation, energy, military, and industrial markets. Major impediments to the commercialization of advanced ceramics are reliability and cost. Toward the objective of improving reliability and reducing manufacturing cost, the U.S. Department of Energy, Office of Transportation Technologies, under contract with Lockheed Martin Energy Systems (LMES), Inc., sponsored research as part of the Ceramic Technology Project (CTP). The goal of the CTP, managed at ORNL, is to develop highly reliable and cost-effective structural ceramics for advanced heat engine applications such as automotive gas turbine, piston, and diesel engines. The Cost-Effective Ceramic Machining (CECM) Program was established in 1991 as part of the CTP in recognition of the importance of machining to commercializing advanced ceramics. The CECM led a series of workshops to identify industry and government needs. Two ORNL workshops identified abrasives and grinding wheels as a major issue and opportunity [3,4]. While ceramic machining can involve several abrasive and non-abrasive techniques, the majority of advanced ceramic machining operations involve diamond grinding operations. The Phase I program was performed in response to LMES Request for Proposal (RFP) No. SM037-87 and was managed under the CECM Program. The RFP emphasized cylindrical grinding of silicon nitride and other advanced ceramics. Norton believes this emphasis on silicon nitride and cylindrical grinding is consistent with the majority of transportation component needs. We are also confident that innovative wheel compositions optimized for cylindrical grinding of advanced ceramics can be relatively easily optimized for other machining operations such as centerless, surface, and ID grinding.

### 5.2.2. Ceramic Machining Cost Considerations

It is widely recognized in the advanced ceramics community that the machining operation is the largest single manufacturing cost category. A survey of all Norton industrial ceramic businesses showed that typical machining costs range from 20% - 70% of the total cost of manufacturing depending on product requirements [3,5]. Advanced ceramic manufacturers such as Norton Advanced Ceramics identified machining cost as a major impediment to widespread use of ceramic engine components. The reasons for the high machining costs are: (1) machining is capital and labor intensive, (2) expensive diamond abrasive is consumed, and (3) production rates are relatively low. The requirement for wheel dressing has also been identified as a significant factor in abrasive cost.

5.2.3. Reliability - Ceramic Surface Integrity

In addition to cost considerations, the second major challenge to introducing a new grinding-wheel system is maintaining ceramic quality and surface integrity. For example, relatively economical cut rates can be accomplished by grinding in the brittle mode of material removal. However, for some applications it may be necessary to change to finer-grit-size wheels and much lower removal rates in order to work in the ductile mode and minimize subsurface damage. Unfortunately, the subsurface median cracks are extremely difficult to see so that parts damaged by machining can not be picked out by inspection.

It is critical to have close cooperation and support between the grinding wheel manufacturer and the ceramic material supplier. Norton Company, with both abrasive and industrial ceramics branches, could take advantage of a customer-supplier relationship within the same parent organization, which maximized the synergy of this program.

An essential element to our approach was to quantify surface integrity and assess surface damage caused by the new products. Grinding wheel performance should be evaluated by not only grinding system factors such as force, power, wheel wear, cut rate, G-ratio, and dressing characteristics; but also on ceramic surface integrity considerations such as retained strength, surface finish, surface damage, and residual stress. It was essential that a next-generation grinding wheel that could significantly reduce machining costs would not compromise surface integrity on the machined ceramic parts.

Surface integrity assessment was an essential part of confirming that an acceptable new grinding wheel was developed. Budget considerations in the Phase I program limited the scope of the surface integrity characterization to selected samples ground by standard and the best performing experimental wheels. The characterization included surface finish, microscopic surface examination, C-ring compression tests on disks, and ceramic rod flexure strength. In Phase II, independent wheel validation program, it was recommended that more extensive retained strength studies be done to quantify grinding damage, and that residual stress in the ground surface be characterized and compared to standard grinding conditions. Residual stresses left behind from machining at and below the surface can influence the final mechanical properties of the workpiece [6-9]. Surface compressive residual stress tends to improve both flexural strength and wear resistance [6, 7, 9]. A meaningful residual stress distribution measurement on curved surfaces is a procedure that requires some development.

5.2.4. Grinding Wheel Dressing Considerations

The requirements of any typical advanced ceramic component manufacturer are to produce quality components of acceptable tolerances, part geometry, surface finish, and part strength at cost viable material removal rates. This implies that there are several requirements that have to be satisfied simultaneously. It is possible, for example, to hold the tolerance by using strong diamond types. However the resulting part strength may decrease because of the damage caused by grinding with "flattened" and worn abrasive particles.

One of the most critical parameters in controlling the cost and quality in a ceramic machining operation is determining the precise point at which truing or dressing is required. Truing refers to regenerating the original profile on the wheel and also making it run concentric to the axis of rotation. Dressing is the process used to expose the abrasive grit above the bond level for efficient grinding action.

Acceptable upper and lower control values for tolerance, finish, part strength, spindle power, etc., should be set in any grinding operation. Typically, a freshly trued and dressed wheel should meet all requirements simultaneously. As more components are ground, there would be a point in time when one of the requirements is not met, and the wheel must be trued and dressed. A schematic of the dressing operation control limits is shown in Figure 1 [10]. At time $t = t_0$ the acceptable tolerance, finish, strength, power values are set based on component performance requirements. During grinding time $t = t_n$ represents the point when one of the grinding limits (in this example spindle power) is exceeded. This indicates that it is time to either dress or true the wheel (depending on set grinding factors).

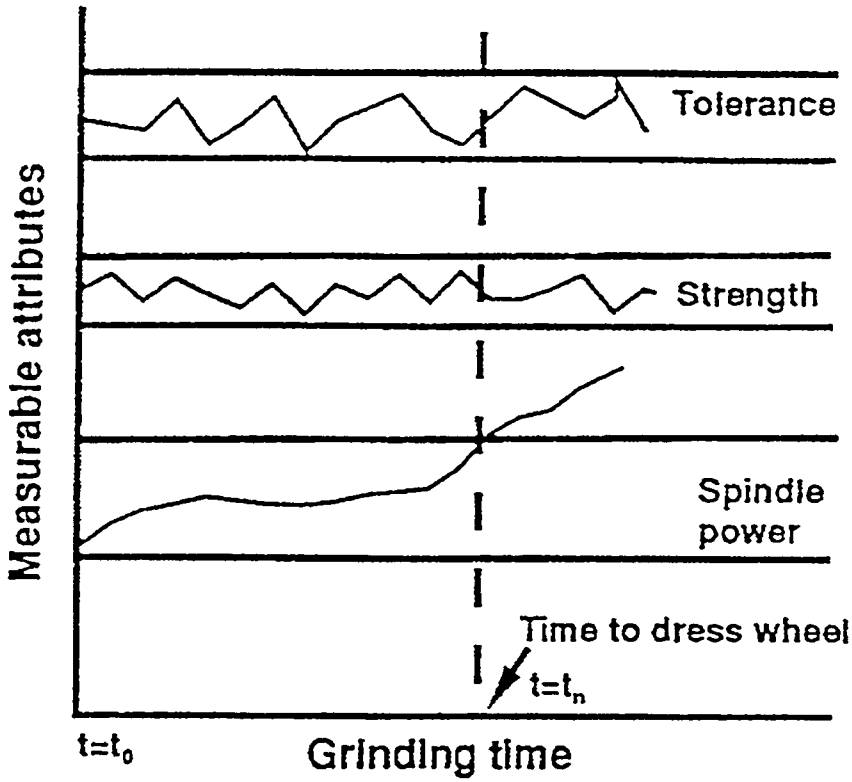


**Figure 1. Schematic figure of measurable attributes of a grinding process versus time showing the need for dressing.**

Truing and dressing are essentially non-productive causes of wheel wear that account for a significant portion of the abrasive costs in ceramic machining. Understanding the truing and dressing characteristics of a grinding wheel is essential to any wheel development program.

5.2.5 Wheel Bond Selection

There are primarily three major bond types that hold the abrasives: resin, glass or vitrified, and metal bond [11, 12]. Each existing bond system has advantages and disadvantages for grinding ceramics. Table 1 summarizes the characteristics of these bond systems.

**Table 1. Bond types and their characteristics.**

| RESIN (Polymer Matrix) | VITRIFIED (Glass Matrix) | METAL (Metal Matrix) | |
|---|---|---|---|
| **Multilayer** | **Multilayer** | **Multilayer** | Single Layer |
| • Easy to use<br>• Least cost<br>• Easy to true/dress<br>• Freeness of cut<br>• Range of ceramic work materials<br>• Good finish<br>• Readily available | • Controlled porosity<br>• Free cutting<br>• Easy to true<br>• May not need dressing<br>• Intricate forms<br>• High contact areas (creepfeed)<br>• Holds form longer | • Durable<br>• High stiffness (for thin wheels)<br>• Good form holding<br>• Good heat removal<br>• High speed potential<br>• Can withstand occasional shock loads<br>• Electro-discharge dressing | • Free cutting<br>• High stock removal<br>• High accuracy forms<br>• Controlled abrasive density and spacing |
| • Lower life<br>• Poor form holding<br>• Lower removal rates<br>• Frequent dressing required | • Speeds limited<br>• Not readily usable for thin cut-off wheels<br>• Prone to cracking due to misuse | • Existing bonds are difficult to dress<br>• High grinding power | • Lower life due to single layer<br>• Not easily trueable |

Resin-bond products are good starting points for grinding a wide range of advanced ceramics, producing quality surfaces with good part strength. Although, the resin-bonded wheels do not possess adequate life, and require frequent truing and dressing, these wheels are the most widely used, all-purpose wheels for grinding ceramics. Vitrified-bonded wheels can provide better life but need to be handled with caution because of the brittle nature and lower strength of the bond. Vitrified-bond products also pose considerable limitations for use in higher-speed grinding. Conventional metal bonds have been found to be exceptionally durable and consume more power in grinding fine-grain-size ceramics, requiring frequent dressing to remove the worn abrasives, and

expose sharp ones. However, metal bonds have the advantage of higher strength and higher wheel-speed capability. High-speed grinding has shown significant potential for ceramic grinding [13]. Metal bonds also have the ability to be dressed by new, electrodischarge techniques such as Electrolytic In-Process Dressing (ELID) [14].

Our initial focus of bond design in this program was to work in metal-bond systems with the objective of developing a system that possesses the most favorable attributes of resin and metal bonds. Further discussion of bond material characteristics is described in the Results Section, 7.1, Analysis of Grinding Wheel Requirements.

In order to understand the grinding process, we need to look at the interactions at the grinding zone as shown in Figure 2 [11]. They include abrasive/work, bond/work, chip/work and chip/bond interactions. While abrasive/work interaction leads to material removal, the other three result in rubbing and energy loss, which lead to adverse surface quality. The bond/work energy loss may be reduced by lowering the contact area between bond and work through experimental modification of the bond. This was one of our approaches in this program. The chip/bond interaction leads to wear of the bond. The size of the chip is very important and could be controlled by changing the grinding parameters like wheel speed and depth of cut, and wheel parameters like abrasive size and combination. For efficient grinding, we need sharp cutting points, good chip clearance, strong abrasive retention, and self-sharpening abrasive in a bond matrix that is resistant to attritious wear yet possesses good lubricating properties. We believe all these requirements can be designed into a metal bond.

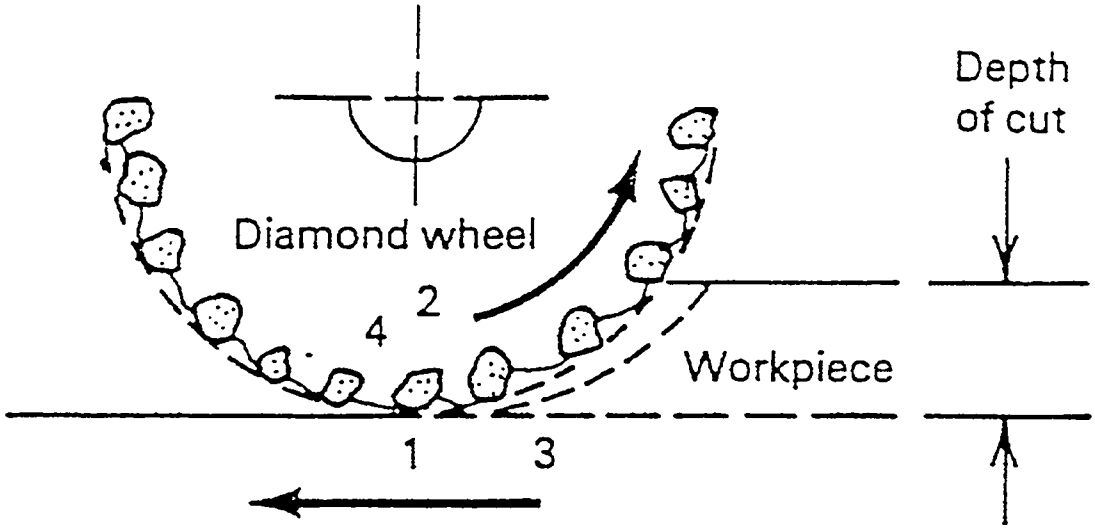


**Figure 2. Schematic illustrating interactions in the grinding zone of a grinding wheel/workpiece interface. 1. Abrasive/work interface; 2. Chip/bond interface; 3. Chip/work interface; 4. Bond/work interface.**

5.2.6. Ceramic Material Selection

In both Phase I and Phase II, there were two major considerations in selecting the ceramic materials for assessing the grinding performance of new wheels. The first was the material had to be commercially available and relevant to transportation technology components. The second criterion was that the materials must have reduced volume-flaw characteristics so as not to mask severe grinding damage that could be produced with new grinding products or incorrect dressing.

The intent of the Innovative Grinding Wheel Phase I and II Programs was to develop a wheel for cylindrical grinding of components such as engine valve stems. The ceramic materials selected were commercially viable for heat engine components. The Phase I program evaluated three advanced ceramic materials:

- NCX-5102 silicon nitride – Northobor R&D Center's (NRDC) HIP'ed $Si_3N_4$ - 4% $Y_2O_3$ was developed for high temperature (1371°C) gas turbine applications. NCX-5102 was developed by NRDC to demonstrate high ceramic reliability under a previous CTP contract [15].
- AZ67H zirconia toughened alumina (ZTA) -- This material is an 80% $Al_2O_3$ transformation toughened with a second phase tetragonal zirconia polycrystal (TZP). AZ67H showed promise in ceramic roller follower tests [16, 17] and is currently produced by Norton Advanced Ceramics for several wear-component applications such as metal-forming dies.
- NC-520 sialon from NRDC -- NAC's sialon (NT451) was the original base material under their Advanced Ceramic Manufacturing Technology (ACMT) program [18] under CTP.

The Phase II program material selection plan was to select a single test material for both internal and independent validation tests. The desired material was to be a silicon nitride based material used primarily for cylindrical engine components. Sialon was proposed as the original standard ceramic workpiece. However, before the start of the Phase II program, NAC developed a superior, more cost-effective silicon nitride for engine components, designated NT551. The ACMT ceramic valve manufacturing program also replaced sialon with NT551. Therefore, NT551 was chosen as the standard workpiece material for IGW Phase II.

- NT551 silicon nitride – NAC's NT551 is a sinterable silicon nitride.

All materials chosen for Phases I and II were classified as fully dense and contain reduced flaw populations so that any severe grinding damage produced by new wheels would not be hidden. As an example, for NCX-5102, the DOE-sponsored Program in Advanced Processing [15] has shown that as volume flaws in silicon nitride are reduced, failure will occur from grinding-related surface breaks, even in tensile testing of large-volume, longitudinally ground specimens [19, 20].

Details of the NT551 silicon nitride fabrication and properties are in Section 7.2.2. Ceramic Specimen Preparation and Characterization -- Task 2.A, on Page 23.

## 5.3 SUMMARY OF RESULTS FROM PHASE I

Phase I of the Innovative Grinding Wheel Program was initiated at the end of 1993. The program was completed in March 1995 and the final report was issued [1]. The objectives of the Phase I program were: to define requirements, design, develop and evaluate a next-generation grinding wheel for cost-effective, cylindrical grinding of advanced ceramics. The scope of the program was a cooperative effort that involved three Norton groups. The overall program was led by Norton Company Abrasives. Under this group the Abrasives R&D group led the technical effort while wheel manufacturing and eventual wheel commercialization would be the responsibility of the Superabrasives Division. Norton Company Abrasives R&D designed and developed a novel metal-bond system, and performed the wheel tests at the Norton Higgins Grinding Technology Center. The second group, Norton Diamond Film Division, conducted a parallel and complementary research and development effort that incorporated a novel design chemical vapor deposition (CVD) diamond film wheel system. The third group, the Northboro R&D Center, supplied ceramic specimens for the grinding tests and evaluated surface integrity in the ground ceramics. NDF and NRDC are divisions of Saint-Gobain Industrial Ceramics, Inc. (SGIC), a subsidiary of Norton Company. The program was divided into two technical tasks: (1) Analysis of Required Grinding Wheel Characteristics, and (2) Design and Prototype Development.

The major work in Task 1 of Phase I was a thorough analysis of wheel bond characteristics. Norton researchers reviewed the characteristics of the three major bond types that hold the diamond abrasives: resin, glass or vitrified, and metal bonds. Each bond system has advantages and disadvantages for grinding ceramics (Table 1. Bond types and their characteristics on Page 6) . Our focus of bond design in this program was to work in metal-bonded systems with the objective of developing a system that possesses the most favorable attributes of all current bond systems. Specifically, experimental metal bonds were designed to give intermediate grinding action between standard resin and metal bonds.

Task 1 was also designed to determine the structural and composition requirements for next generation grinding wheels. This analysis included the mechanical, thermal and coolant absorption characteristics of the system; type and characteristics of the abrasive grit; analysis of the wheel stiffness characteristics; identification of economic targets for wheel and process costs; and development of wheel-behavior models.

Task 1 culminated in a large experimental matrix of 76-mm screening wheels, used to grind sialon disks in a cylindrical plunge test. Some experimental bonds demonstrated significant improvements over standard resin-bonded wheels. Additionally, the experimental metal bond demonstrated the ability to grind significantly more than standard metal bonds without loading. By using this screening test approach, we were able to test approximately 45 superabrasive wheel variables before down selecting to the most promising bonds for the Task 2, 203-mm-diameter tests.

The novel CVD diamond wheel approach was incorporated into this program as a part of Task 1. The work was designed to include a small-wheel screening test that complemented the main Superabrasive metal-bond approach. The higher risk CVD diamond wheel approach was to be a feasibility study and was not planned for continuation into Task 2, Design and Prototype Development. The initial CVD wheel design was unsuccessful. A thin CVD diamond wheel was redesigned and tested. While significant grinding improvements were noted from the initial screening test, the results were not promising for cylindrical grinding compared to conventional grinding wheels.

Task 2 of Phase I was to design and construct prototype wheels and evaluate grinding performance on different grades of advanced ceramic rods. Grinding characteristics included surface roughness, spindle power, grinding forces, wheel dressing characteristics, wheel loading characteristics, wheel wear, and coolant compatibility. Three materials manufactured by SGIC were used that met the market applicability and performance criteria, NC-520 sialon, NCX-5102-HIP'ed $Si_3N_4$, and AZ67H-20% ZTA.

In Task 2, a series of the most promising metal bonds from Task 1 were scaled up to 203-mm- (8-in.-) diameter test wheels. The 203-mm-diameter test wheel made in this bond contained 75 concentration of 320 grit diamond abrasives. The wheels were tested on a CNC instrumented cylindrical grinder in both plunge and traverse test conditions. The experimental wheel successfully ground all three types of advanced ceramics for extended time without the need for wheel dressing. The spindle power consumed by this wheel during test grinding of NC-520 sialon is as much as 30% lower than with a standard resin-bonded wheel with 100 grit diamond concentration, which is typically used in this application. The wheel wear with this improved metal bond was an order of magnitude lower than the resin-bonded wheel, which would significantly reduce ceramic grinding costs through fewer wheel changes for retruing and replacements. The projected manufacturing cost of this experimental wheel was not appreciably different from standard resin- and metal-bonded superabrasive wheels, and therefore this experimental wheel would have a significant cost advantage in grinding ceramics.

An essential element to our approach was to quantify surface integrity and assess surface damage caused by the new products. It was essential that a next-generation grinding wheel that could significantly reduce machining costs would not compromise surface integrity on the machined ceramic parts. The C-ring compression test [21] from Task 1 ring specimens was determined to have limited usefulness as a qualitative assessment of grinding damage, but the experimental results did not show evidence of unusual grinding damage to the ceramic disks. For the Task 2 large-wheel test, optical examination and flexure test of three types of ceramic rods ground by experimental metal-bond wheels and standard resin wheels did not show any unusual grinding damage. The traverse ground sialon rods had strengths similar to the resin-bonded wheel flat-ground MOR specimens and there was no noticeable difference between the resin- and metal-wheel ground specimens. Therefore, in Phase I, results indicated that the innovative experimental wheel did not create unusual or excessive machining damage compared to the standard resin-bond product while retaining its enhanced performance and cost effectiveness.

# 6. OBJECTIVE/SCOPE

The overall objectives of this Phase II program were: (1) to improve or develop manufacturing technologies that enable the scale-up of Phase I, 203-mm- (8 in.-) diameter wheel to 356-mm- to 406-mm- (14-in.- to 16-in.-) diameter grinding wheels; and (2) to validate the performance of the new wheels in cylindrical grinding of advanced ceramics both in-house and at independent test sites. Innovative wheel designs optimized for cylindrical grinding could be relatively easily optimized for other machining operations such as centerless, surface and ID grinding.

In the completed Phase I, grinding test results of 76-mm- (3-in.-) and 203-mm- (8-in.-) diameter wheels indicated that a superior, next-generation grinding wheel for cylindrical grinding of ceramics had been developed. Most production grinding of cylindrical ceramic parts is done on machines that use 305-mm- (12-in.-) to 406-mm- (16-in.-) diameter wheels. A Phase II program was initiated to scale-up the new Superabrasive wheel specification to these larger diameters, to make further wheel enhancements, and to perform independent validation tests.

Task 1 of Phase II addressed wheel processing and wheel variable issues to achieve grinding action for the larger wheels similar to that successfully attained for the smaller Phase I wheels. In Phase II, Norton utilized a segmented wheel design for greater size capability and product consistency, unlike the continuous rim approach employed in Phase I. Also in Task 1, Norton selected and enhanced the wheel core, cement, and segment design for higher speed operation, and determined the maximum operating speed for the new wheel system.

In Task 2, we fabricated large test wheels, and performed a cylindrical in-house grinding test at Norton's Higgins Grinding Technology Center prior to independent validation testing. In Task 3, large experimental test wheels were manufactured for independent validation at ceramic manufacturers. The following organizations performed validation tests: Norton Advanced Ceramics, Caterpillar Corporation, Chand Kare Technical Ceramics, and Eaton Manufacturing Technologies Center. Eaton tested the new wheel product under high-speed grinding conditions, building upon their R&D efforts for the DOE/ORNL Cost-Effective Ceramic Machining Program. The NAC and HGTC wheel validation activity would complement their valve grinding development efforts in process under the DOE/ORNL Advanced Ceramic Manufacturing Technology Program. Task 4 performed a more comprehensive evaluation of ceramic surface integrity of ground ceramic specimens from the Task 2 and 3 grinding tests.

# 7. RESULTS

## 7.1. PROCESS SCALE-UP -- TASK 1

### 7.1.1. Task Overview

In the completed Phase I program, superior grinding performance was demonstrated on both 76-mm- (3-in.-) and 203-mm- (8-in.-) diameter wheels. However, the most useful wheel size range for OD cylindrical production grinding of advanced ceramics is 305-mm- (12-in.-) to 406-mm- (16-in.-) diameter wheels. The first task of the Phase II program was to scale-up the new Superabrasive wheel specification to these larger diameters.

Task 1 of Phase II addressed wheel processing and wheel variable issues to demonstrate similar or improved grinding action for the larger wheels as that successfully attained for the smaller, Phase I wheels. Also in Task 1, Norton needed to develop or modify the wheel core for higher speed operation, and determine the maximum operating speed for the new wheel system.

### 7.1.2. Experimental Design and Definition -- Task 1.A

The basic experimental bond selected in Phase I was used as the starting wheel system for the Phase II program. This baseline wheel specification is AD320-75MXL1993. Work in this subtask included: (1) understanding the proposed grinding conditions scheduled to be performed, and selecting the wheel specifications and bond variables consistent with this Phase II test plan; (2) reviewing data generated from previous tests for scale-up consideration; and (3) addressing material and manufacturing issues in scaling-up from 203-mm- (8 in.-) diameter wheels to 356-mm- (14 in.-) wheels running up to 126 m/s (25,000 surface feet per minute, SFPM). The variables such as diamond type, grit size (particularly the coarser grit), diamond concentration, coating, level of bond porosity, core material, hub design, and wheel manufacturing parameters were considered in the scale-up experimental design for the new wheel specifications. These variables were designed to be consistent with the planned grinding test system conditions, such as wheel-work contact geometry, wheel speed, infeed, and grinding force/grain.

The Norton team held a preliminary design review meeting and selected a segmented wheel approach instead of a continuous rim approach. Norton also requested, and LMES approved, a modification to expand the SOW that changed the test wheel diameter requirement from 356-mm, to include a range in diameter between 356-mm and 406-mm. This larger-diameter capability is preferable for some of the newer OD grinding machines and current grinding trends in the ceramic industry. The successful manufacture of the larger-diameter wheels will expedite new wheel commercialization at the conclusion of this Phase II contract.

7.1.3. Strength Characterization and High Speed Core Development -- Task 1.B

7.1.3.1. Introduction. One advantage of using a metal-bond system is the inherent bond-strength/high-speed capability. Bond-strength tests in Phase I demonstrated that a typical metal bond has more than twice the flexural strength of a resin bond used for ceramic grinding. For smaller-diameter Phase I wheels, a standard wheel-hub composition that was adequate for the required testing parameters was selected. The wheels were speed tested to approximately 91 m/s (18,000 SFPM), and were rated for at least 61 m/s (12,000 SFPM) grinding speed. The ultimate wheel-speed capability of this abrasive rim-hub combination, not determined in Phase I, was done in Phase II. If higher speeds are required for future applications, a different hub material could be selected to maximize wheel speed capability.

To make wheels strong enough to meet the requirements of the Phase II high-speed grinding test plan, the wheel core had to be redesigned. Calculations were performed to establish the minimum strength requirement including proper built-in safety factor. We analyzed the strength and microstructure of the standard wheel core material used for the Phase I 203-mm-diameter wheels. Such information served as our baseline for designing the new wheel core and its manufacturing process.

7.1.3.2. Wheel Strength Design. Finite element analysis was performed to estimate the minimum strength requirements for wheel core and abrasive section under various wheel designs and at a peripheral wheel speed of 200 m/s (39,370 SFPM). Since stress on the wheel ($\sigma$) is proportional to the square of the wheel speed, the strength requirements for a wheel to be run at another speed ($V_2$) can be calculated directly from the following relationship:

$$\frac{\sigma_1}{\sigma_2} = \left(\frac{V_1}{V_2}\right)^2$$

Considering the anticipated desired testing speed at Eaton for up to 127 m/s, and with proper built-in safety factor, a core material must have a minimum yield strength of approximately 150 MPa. The actual core material chosen has a yield strength of approximately 450 MPa.

A comparison analysis of stress produced between continuous abrasive rim and segmented abrasive rim was also performed. The corresponding tangential and radial stresses at any position between arbor hole and the wheel OD are shown in Figure 3 for a continuous rim wheel and Figure 4 for a segmented-rim wheel. The wheel model was constructed with the following dimensions: 127-mm-diameter arbor hole, 392-mm outside diameter, and 6.4-mm diamond depth. The tangential stresses created at the interface between core and diamond section in a wheel with a continuous rim is about five times of that for a segmented-rim wheel.

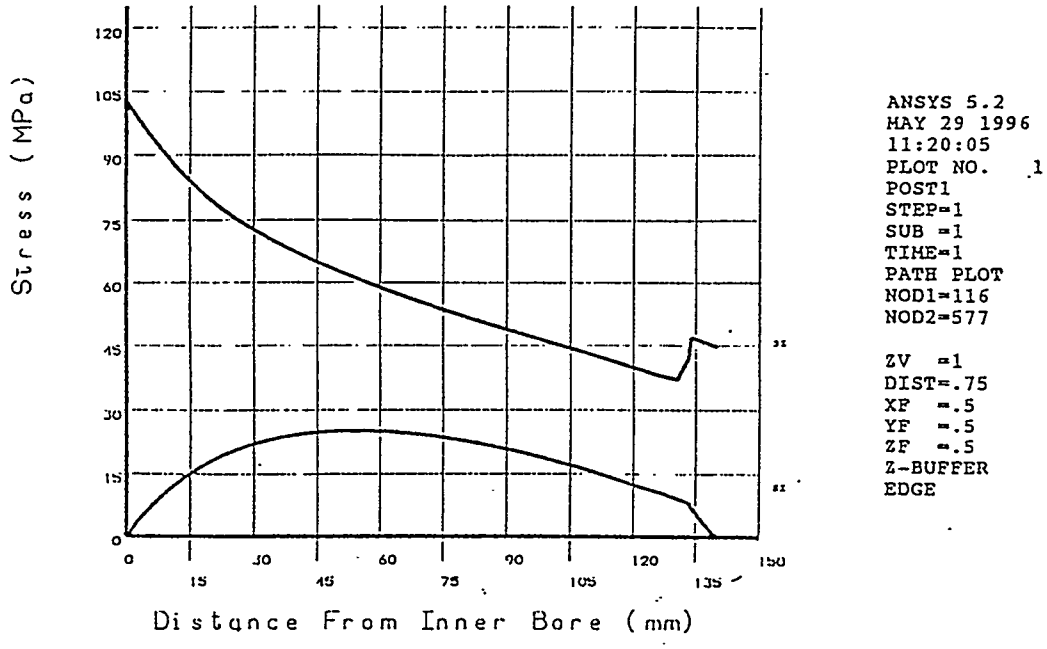


**Figure 3. Tangential (SZ) and radial (SX) stress distribution on a continuous rim wheel. Metal bond wheel at 200 m/s.**

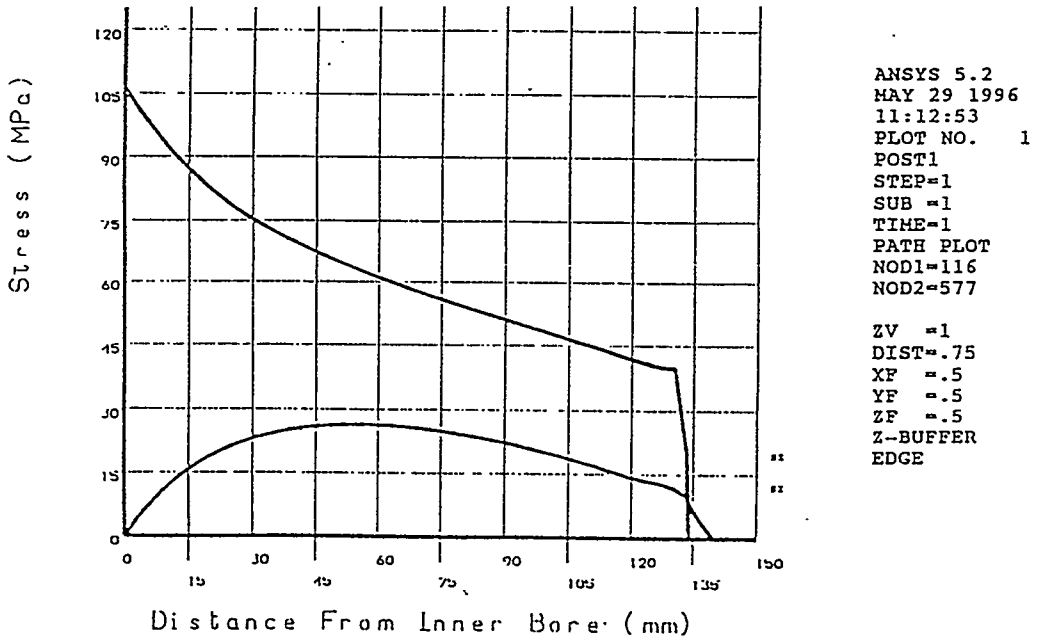


**Figure 4. Tangential (SZ) and radial (SX) stress distribution on a segmented wheel. Segmented metal bond wheel at 200 m/s.**

For operational safety consideration, we decided to re-direct our wheel-fabrication approach from continuous-rim to segmented. This change of wheel-fabrication approach also removed a physical constraint in wheel size for this program. During Phase II planning stage, we had an internal wheel size limitation of 356-mm- (14 in.-) diameter due to hot press furnace capacity. With the new segmented wheel design, we could make larger-diameter wheels, approximately 393-mm (15.5-in.). This larger-size wheel is more consistent with the current needs of ceramic manufacturers.

For bond-strength characterization, we attempted to initially do bond tensile testing. However, due to the relatively brittle nature of the specimens, we had difficulty preparing specimens that would yield required specimen gage breaks. Ultimately, we adopted a spin test method, which more closely simulates real-life conditions, to verify that the experimental bond and wheel design will be sufficiently strong for anticipated high speed grinding applications. In several preliminary spin tests, described below in Task 1.C., we passed the target threshold speed for planed independent tests in Task 3 with a sufficient safety factor. We confirmed that the core material selected for the larger wheel can pass the required speed limit with a sufficiently large safety factor.

7.1.4. Manufacturing and Characterization of Large Wheels -- Task 1.C

The segmented wheel design was selected for manufacturing trials after review and consultation with the LMES Program Manager. The general wheel design and related drawings for the large Phase II wheels were completed. All drawings for the graphite mold parts, thermocouple, and wheel core for the initial continuous rim design and the revised segmented-wheel manufacturing approach were completed.

7.1.4.1. Abrasive Segment Manufacturing Trials. An objective of the manufacturing trials was to ensure consistency with the larger diameter wheels of the new segmented design compared to smaller test wheels from Phase I. We characterized the relationship between fabrication control parameters and bond properties. Three different compositions and three temperatures were used to form this study matrix.

Different furnace equipment is required to make wheel segments and continuous-rim wheels. Therefore, considerable emphasis was spent in correlating furnace operating parameters and final properties of the segments. The furnace run profile and all the control parameters were identified and specified.

With the final furnace run profile, we have demonstrated that we could make very consistent segments. For example, we evaluated the hardness of laboratory made segments of the same specification. For approximately 40 Rockwell B-scale data points, both within a segment and within a batch of segments, the standard deviation was $\pm$ 0.9% and the high-to-low hardness range was 2.7% of the mean. This was considered very consistent. In addition, we duplicated these results in a production manufacturing environment.

The existing manual furnace control procedures were sufficient to produce prototype wheels for this program. We did a preliminary assessment of automated furnace control methodologies that may be implemented later during production.

7.1.4.2. Wheel Assembly Trials. There were two design and manufacturing objectives in the scale-up of large-size experimental wheels by the segmented rim approach:

(1) Segment Geometry -- The objective was to make the segments to near-net-shape to avoid laborious machining by grinding. The design required that the segments be prepared with exact inside curvature and side angles to match the outside diameter of the core, so that the segments can be butted together tightly;

(2) Segment-Core Adhesion -- To select the proper type of cement that will bond the segments to the prefabricated core, and retain sufficient strength to hold segments against centrifugal force and shear force during grinding.

These objectives were achieved as discussed below:

(1) For near-net-shape control, we achieved an exact curvature match between the outside diameter of the wheel core and the inside curvature of the as-fired segments. This eliminated the need for any ID grinding.

Due to the expansion and contraction of the metal bond with process temperatures, and surface condition requirements, minor finishing grinding was necessary. This was particularly true for the side angle and chord length control. The angle-grinding fixture was prepared and we identified a suitable grinding-wheel specification for this operation. Segmented-wheel expertise developed for Norton Company vitrified-bonded wheel products was applied in support of this project.

(2) Several factors that can affect the ultimate wheel assembly operation were addressed. We reviewed properties of various cementing materials for joining the diamond section to the prefabricated core. Three candidate cements were considered. Building upon the experience of the Norton Vitrified Wheel R&D group, two of the three candidates, designated Cement A and B, were evaluated. Shear strength, burst strength, and thermal stability were the primary considerations for the final cement selection. In addition, the surface roughness and cleanness of segment and core surfaces were considered to be critical to the retained bonding strength between the two parts at the joint line.

For obtaining proper interface adhesion, the surface roughness of wheel core and segments were monitored. Significant attention was given to cleaning the surfaces of segments and core to obtain sufficient bonding strength between the two parts at the joint line.

7.1.4.3. Partial Wheel Assembly Burst Tests. Three partial-wheel specimens with only four segments were made for burst speed study, as shown in Figure 5. Either Cement A or B was used in fastening four segments on the wheel core. Table 2 gives the burst test results, and the estimated Norton rated maximum operation speed (MOS) for similar wheels of this design based on this burst-speed data.

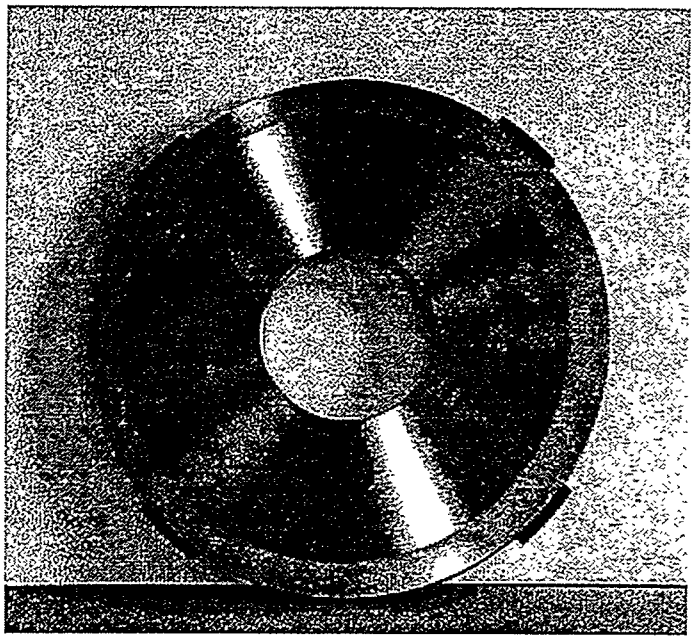

**Figure 5. A preliminary burst testing wheel with four segments.**

**Table 2. Burst test results, four abrasive segments per wheel.**

| Wheel No. | Cement | Burst Speed (m/s) | Estimated Norton Rated MOS (m/s) | No. of Broken Segments |
|---|---|---|---|---|
| 1 | A | 262 | 148 | 3 |
| 2 | B | 219 | 124 | 1 |
| 3 | B | 202 | 115 | 1 |

The traces of broken segments remaining on the wheel cores indicated that all the broken segments had separations initiated from the edge of the segment. The separation likely created a large bending moment on the loose end of the segment at the high burst test speeds. The bending moment eventually led to the fracture through the segment. Therefore, it was predicted that fully assembled wheels will yield even higher burst speeds since the segments will have support from adjacent segments, unlike these partial burst test wheels. We also concluded that both types of adhesives can provide sufficient strength to achieve high grinding speeds desired for this project.

In most of the cases, the separations occurred partly at the core-cement interface and partly at the segment-cement interface. Figure 6 shows a typical fracture surface appearance when one or more segments and core became separated. The fractography

suggested that we had successful surface preparation. The separation occurred partly at the core-cement interface and partly at segment-cement interface indicating successful interface preparation. These results also indicated that the joint line is the weakest region of the wheel. The only exception to the pattern in Figure 6 occurred for Wheel No. 1 (Table 2) where one of the three segments that broke off had separation primarily at the segment-cement interface. In this particular case, there was a clear sign of surface contamination on the ID surface of this segment prior to cementing.

During the course of adhesive strength study, we identified some manufacturability limitations in the properties of Cement A and decided to discontinue work on this cement and specify Cement B.

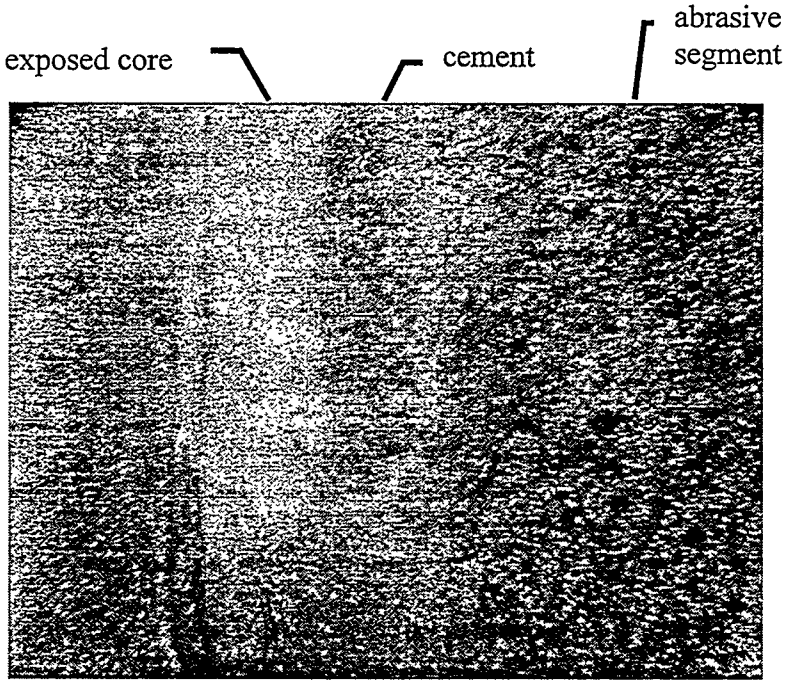


**Figure 6. Typical fracture surface in the segmented test wheel after the burst test.**

7.1.4.4. Full Size Test Wheel Manufacturing. Seven, 393-mm- (15.5-in.-) nominal-diameter segmental wheels were made. Figure 7 shows one of the first full-size, metal-bonded segmental diamond wheels, and Figure 8 shows a magnified view of the segmental rim section. The manufacturing trials successfully demonstrated segment curvature control for the rim interface, and suitable side angle grinding of segments resulted in close butting of segment-to-segment interfaces.

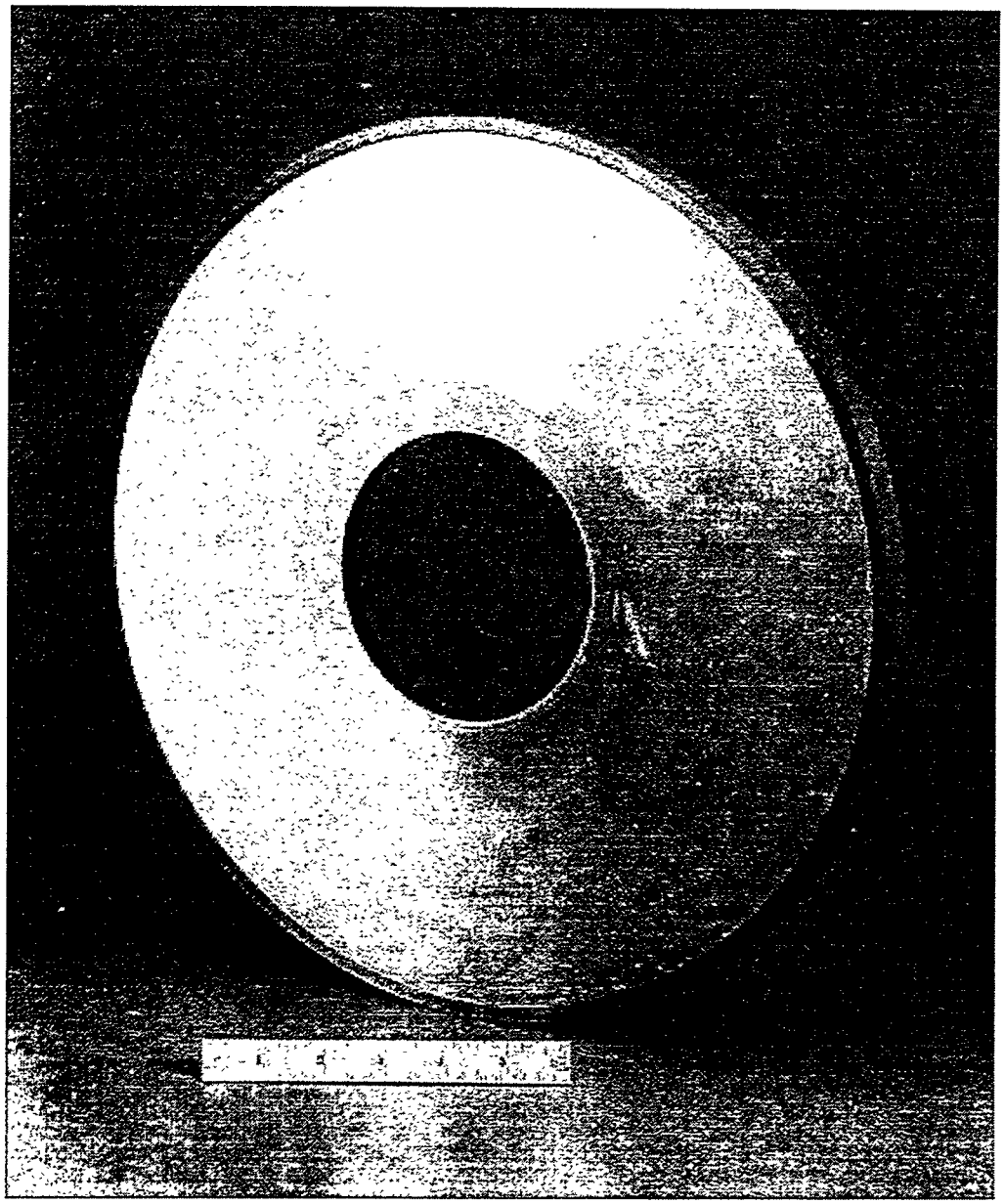

**Figure 7. Full-size (393 mm in diameter by 15-mm-thick with 127 mm hole) segmental experimental metal-bonded wheel for the HGTC in-house grinding test.**

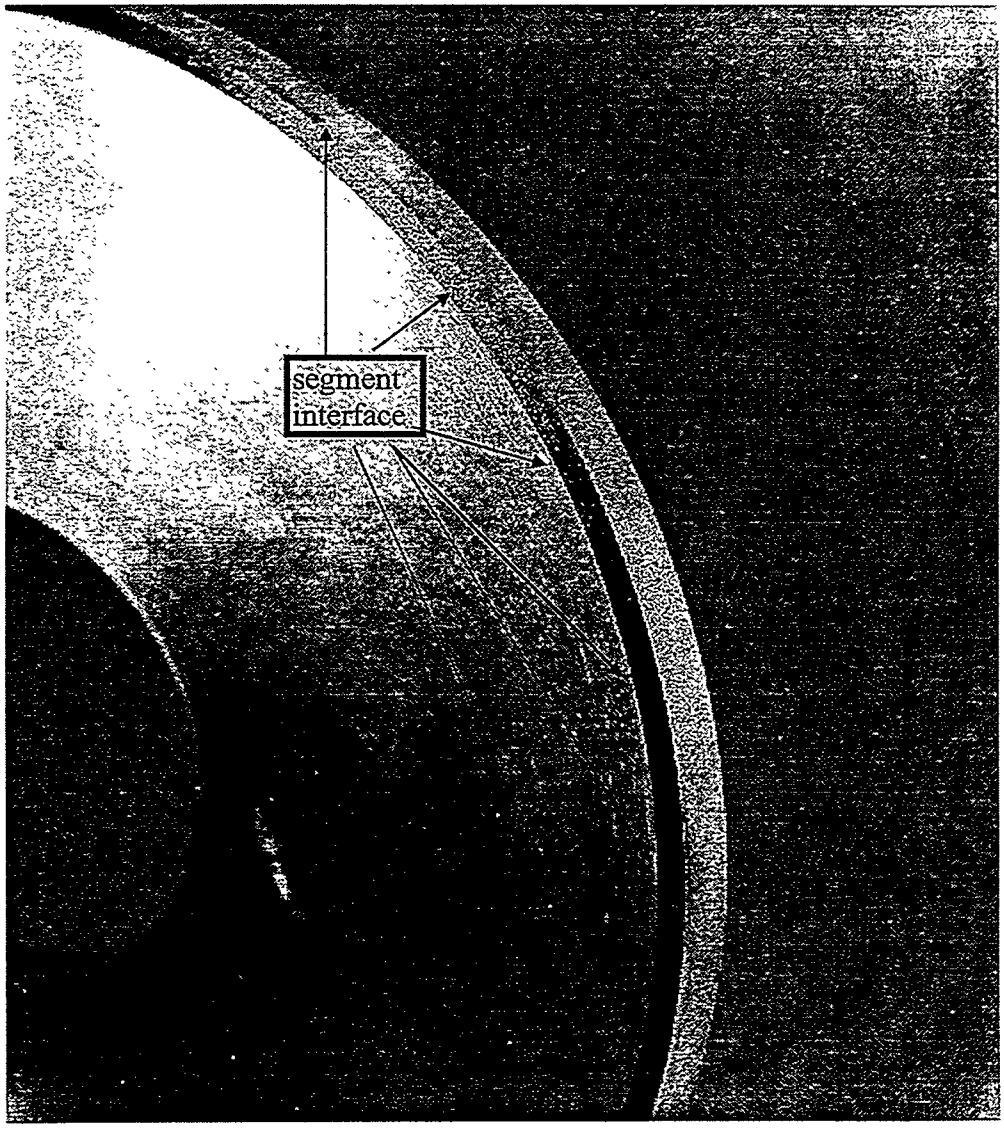


**Figure 8. An enlarged view of the Figure 7 wheel highlights the segmental rim of this experimental grinding wheel.**

Three of these wheels were used in preliminary grinding tests at Norton Company's Higgins Grinding Technology Center (HGTC) under Task 2. These three wheels were successfully speed tested to pass 120 m/s (23,622 ft/min.) peripheral speed. The other wheels were burst tested to evaluate the burst speed of completed prototype segmented wheels (see Section 7.1.4.5.).

We successfully implemented automation of furnace-cycle-control methodologies. The results showed that the product quality and consistency were significantly improved as shown in the figures below. Figure 9 represents the early pilot-stage results and Figure 10 represents the current results from batch to batch. The entire segment-manufacturing process can now be done in a production environment.

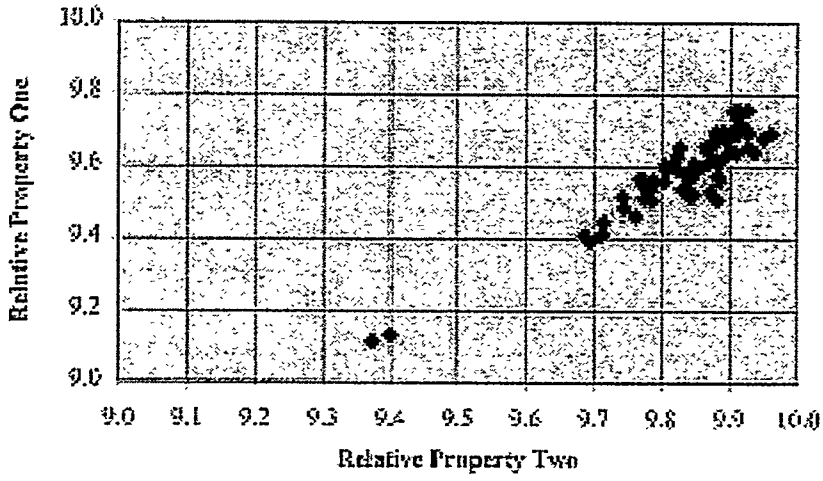


**Figure 9. QC measurements on early pilot runs.**

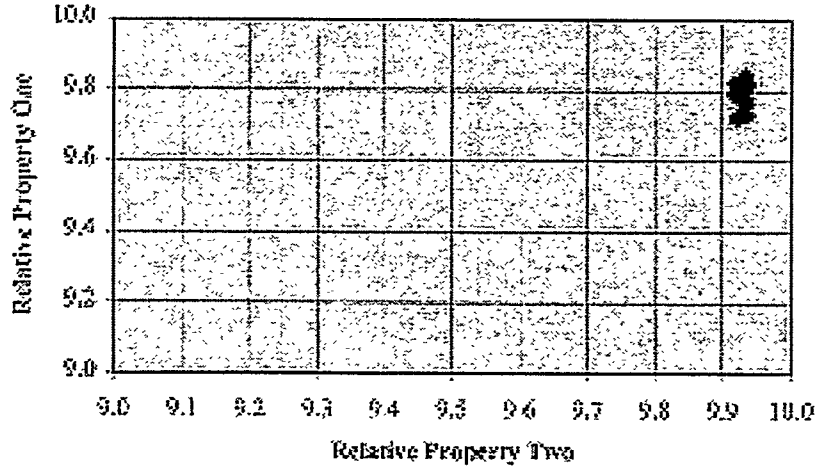


**Figure 10. QC measurements on latest production runs.**

7.1.4.5. Burst Strength of Full-Size Prototype Wheels. To characterize the maximum operating speed of this new type of segmented wheel, full-size wheels were purposely spun to destruction to determine the burst strength and rated maximum operating speed. Table 3 summarizes the burst-test data for the 393-mm-diameter experimental metal-bonded wheels.

**Table 3. Experimental metal-bonded wheel burst strength data.**

| Wheel # | Wheel Diameter (in.) | Burst RPM | Burst speed (m/s) | Burst speed (SFPM) | Norton Rated MOS (m/s) |
|---|---|---|---|---|---|
| 4 | 15.449 | 9950 | 204.4 | 40242 | 115.8 |
| 5 | 15.472 | 8990 | 185.0 | 36415 | 104.8 |
| 7 | 15.463 | 7820 | 160.8 | 31657 | 91.1 |
| 9 | 15.459 | 10790 | 221.8 | 43669 | 125.7 |

According to these data, the experimental ceramic grinding wheels of this design would qualify for an operational speed up to 90 m/s (17,717 SFPM). Higher operational speeds can be easily achieved by some further modifications in fabrication processes and wheel designs.

For wheels 5 and 7, both had one segment that flew off the wheel cores. Examination of segment and core separation traces on both wheels showed that the failures occurred at the interface between segment and cement. Both wheels 4 and 9 had several segments that flew off the wheel cores. The separation traces as shown in Figure 11 indicated that the ultimate metal bond strength had been reached.

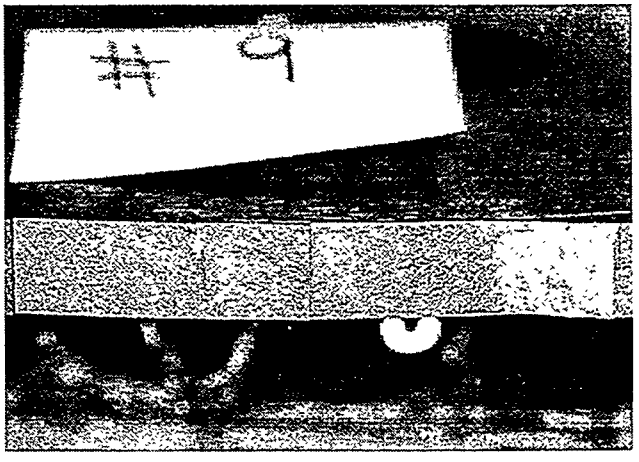


**Figure 11. Fractured surface of metal-bonded segments.**

7.1.4.6. Summary of Task 1 Process Scale-up. The following is a summary of the manufacturing process validation trials performed during the successful manufacture of the three, experimental full-size segmented wheels:

1) Temperature Control -- The furnace temperature characterization was completed.
2) Hot Press Run Profile -- The furnace run profile was retuned to improve the product quality and yield. When the process was transferred from R&D to production for pilot runs, some scatter in product properties was encountered. After some process modifications, a later pilot production batch was very successful in achieving wheel properties within the tight control boundaries.
3) Segment Curvature Control -- Perfect curvature match was achieved, which eliminated the need for ID grinding on segments.
4) Angle Grinding for Butting Segment Faces -- Current process procedures and practices for grinding of segments to match one another were defined. (See segment interfaces, Figure 8 on page 20.) Operation efficiency can be further improved by making some adjustments in prior operational steps.
5) Wheel Assembly – Effective procedures for segments and core surface preparation, and wheel assembly were developed. In this subtask, six wheels were assembled (three full wheels and three partial wheels) uniformly and without any manufacturing difficulties.

The objectives of Task 1 were achieved. Scale-up of the Phase I wheel from 204 mm to 393 mm in diameter has been successfully accomplished. The original project objectives were to scale-up the wheel to only 356 mm. Based on conservative speed tests, these test wheels have been qualified for grinding at speeds up to 80 m/s for the Task 2 in-house test.

## 7.2. IN-HOUSE WHEEL TESTING -- TASK 2

### 7.2.1. Task Overview

Task 2.A involved the fabrication and characterization of the cylindrical ceramic specimens to be used in the Task 2.B in-house grinding test and the Task 3 independent-validation grinding tests. The in-house grinding test was performed on the initial full-size wheel prototypes (393-mm-diameter). This in-house test objective was to evaluate and select optimum wheel variables, and to confirm overall performance advantages of the new wheel system before committing to the series of four independent validation tests.

### 7.2.2. Ceramic Specimen Preparation and Characterization -- Task 2.A

7.2.2.1. Silicon Nitride Selection and Fabrication. We selected Norton Advanced Ceramics' NT551 silicon nitride as the program's base material. NT551 is currently under development for diesel engine valves [18].

More than 200 ceramic rods were fabricated for use in the Tasks 2 and 3 grinding tests. Three separate 15-kilogram powder batches were made of the NT551 silicon nitride powder composition. Each slurry batch was spray dried and the powder surface area was determined. Specimen rods were cold isostatically pressed using a wet bag technique. A total of 211 green rods, and accompanying characterization tiles (2 x 2 in.) were made.

All rods and tiles went through a binder burnout furnace followed by a high-temperature, gas pressure sintering cycle. The initial densification run was done at the Northboro R&D Center and the remaining two furnace runs were done at Norton Advanced Ceramics manufacturing plant in East Granby. We achieved theoretical density (3.29 g/cm$^3$) for all specimens in all three of the furnace runs. The densified rod specimen dimensions were nominally 25 mm x 90 mm (1 in. x 3.5 in.). Table 4 summarizes the furnace batches and specimen quantities fabricated.

**Table 4. NT551 silicon nitride specimen batch ID.**

| Batch ID | Description | Quantity of Rod Specimens |
|---|---|---|
| N22 | NRDC Furnace run | 23 |
| NAC1 | 1$^{st}$ NAC Furnace run | 92 |
| NAC2 | 2$^{nd}$ NAC Furnace run | 96 |
| Total | | 211 |

7.2.2.2. Silicon Nitride Characterization. Rod samples from each of the three furnace batches were sliced, polished, and tested to evaluate batch consistency. Table 5 contains the Vickers Hardness and fracture toughness data for a rod from each batch. The fracture-toughness technique used for these specimens was the Indentation Fracture Method (Anstis, et al. [22]).

Room-temperature flexural strength and indentation strength fracture toughness were determined from standard ASTM C1161-B specimens machined from tiles [23]. The tiles were from the two large NAC batches. Table 6 contains the strength and toughness data from these two tiles. The differences between fracture toughness data in Table 5 and Table 6 are expected differences due to the test method.

**Table 5. NT551 batch properties.**

| Batch | Specimens | Mean Vickers Hardness (GPa), Load = 10 kg | Std Dev | Mean $K_{IC}$ MPa $m^{1/2}$ | Std Dev |
|---|---|---|---|---|---|
| N22 | 5 | 13.29 | 0.05 | 4.47 | 0.18 |
| NAC1 | 5 | 13.08 | 0.10 | 4.63 | 0.11 |
| NAC2 | 5 | 13.17 | 0.18 | 4.52 | 0.12 |

**Table 6. NT551 room temperature flexural strength and fracture toughness.**

| Room Temperature Flexural Strength ASTM C1161-B | | | Fracture Toughness Indentation Strength, Load = 10 kg | | |
|---|---|---|---|---|---|
| Sample | Batch NAC1 $\sigma_f$ (MPa) | Batch NAC2 $\sigma_f$ (MPa) | Sample | Batch NAC1 $K_{IC}$ (MPa $m^{1/2}$) | Batch NAC2 $K_{IC}$ (MPa $m^{1/2}$) |
| 1 | 1092.0 | 786.4 | 1 | 6.45 | 6.58 |
| 2 | 840.4 | 934.7 | 2 | 6.37 | 6.70 |
| 3 | 1104.4 | 970.9 | | | |
| 4 | 982.0 | 1035.9 | | | |
| 5 | 930.5 | 919.8 | | | |
| Mean | 989.8 | 929.5 | | 6.41 | 6.64 |
| Std.Dev | 99.478 | 82.017 | | 0.04 | 0.06 |

The rod specimens for this program, as illustrated in Table 5 and Table 6, show good batch-to-batch consistency and are typical for NT551 silicon nitride. Typical properties of NT551 silicon nitride from NAC's Advanced Ceramic Manufacturing Technology program are given in Table 7.

**Table 7. Typical properties of Norton Advanced Ceramics NT551 silicon nitride.**

| Properties | NT551 Sinter/HIP |
|---|---|
| **Young's modulus** GPa) | 310 |
| **Hardness,** Vickers (GPa) | 13.4 |
| **Flexural strength** | |
| RT (MPa) | 890-970 |
| 850°C (MPa) | 850 |
| **Fracture toughness** (Indentation Strength Method) (MPa·$m^{1/2}$) | 6.5-6.9 |
| **Density** (g/$cm^3$) | 3.29 |

7.2.3. Preliminary Grinding Tests in HGTC -- Task 2.B

7.2.3.1. Introduction and Test Design. Norton Company Higgins Grinding Technology Center completed a comprehensive, in-house grinding test of the experimental metal-bond vs standard wheels. Grinding was done on NT551 $Si_3N_4$ rods using a Studer CNC OD/ID grinder at the HGTC. Figure 12 shows the grinding test arrangement and the new metal-bond wheel's capability to plunge grind a $Si_3N_4$ rod of 25.4-mm diameter into a fine needle form (approx. 1.1 mm in diameter).

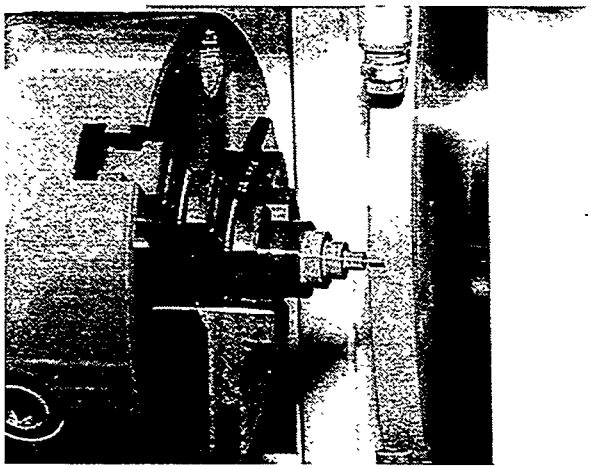

**Figure 12. In-house grinding test setup.**

Three, 393-mm-diameter experimental metal-bonded segmental wheels (#4, #5 and #6) were tested. The #6 wheel was the target grade while the other wheels were with slight grade variations. Most of the wheel tests were done on #6 as presented below. Testing was done at three speeds: 32 m/s (6252 SFPM), 56 m/s (11,000 SFPM), and 80 m/s (15,750 SFPM). One vitrified-bonded diamond wheel and one resin-bonded diamond wheel were included in the test matrix for comparison. The resin wheel was tested at all three speeds. The vitrified wheel was tested at 32 m/s (6252 SFPM) only. The testing of the vitrified diamond wheel was not in the original statement of work, and added during the program to assure superiority over the current best bond systems.

Over one thousand plunge grinds of 6.35-mm- (0.25 in.-) wide and 6.35-mm- (0.25 in.-) deep were performed. The following Table describes the general testing conditions.

**Table 8. General grinding test conditions.**

| | | |
|---|---|---|
| Machine: | Studer S40 CNC | |
| Wheel Specifications: | AD320-75MXL1994 | (experimental metal bond) |
| | SD320-R4BX619C | (resin bond) |
| | SD320-N6V10 | (vitrified bond) |
| Wheel Speed: | 32, 56, and 80 m/s (6252, 11,000, and 15,750 SFPM) | |
| Coolant: | Inversol 22 @60% oil and 40% water | |
| Coolant Pressure: | 270 psi | |
| Material Removal Rate (MRR')*: | Varying, starting at 3.2 $mm^3/s/mm$ (0.3 $in.^3/min/in.$) | |
| Work Material: | NT551 $Si_3N_4$, 25.4 mm diameter X 88.9 mm long | |
| Work Speed: | 0.21 m/s (42 SFPM), constant | |
| Work Starting diameter: | 25.4 mm (1 inch) | |
| Work finish diameter: | 6.35 mm (0.25 inch) | |

*The normalized material removal rate (MRR') used in all the in-house data analysis is the volume material removed per time per unit wheel width.

The final truing and dressing conditions established for the metal-bonded wheels were as follows:

**Truing Operation:**

| | |
|---|---|
| Wheel: | 5SG46IVS |
| Wheel Size | 152-mm diameter (6-inches) |
| Wheel Speed: | 3000 rpm; at +0.8 ratio relative to grinding wheel |
| Lead: | 0.015 in. |
| Compensation: | 0.0002 in. |

**Dressing Operation:**

| | |
|---|---|
| Stick: | 37C220H-KV (SiC) |
| Mode: | Hand Stick Dressing |

Tests were performed in a cylindrical OD plunge mode in grinding NT551 silicon nitride rods. To preserve the best stiffness of work material during grinding, the 88.9 mm (3.5 in.) samples were held in a chuck with approximately 31 mm (1.22 in.) exposed for grinding. Each set of plunge grind tests started from the far end of each rod. First, the wheel made a 6.35-mm- (0.25 in.-) wide and 3.18-mm- (0.125 in.-) radial depth of plunge to complete one test. The work rpm was then re-adjusted to compensate for the loss of work speed due to reduced work diameter. Two more similar plunges were performed at

the same location to reduce the work diameter from 25.4 mm (1 in.) to 6.35 mm (1/4 in.). The wheel was then laterally moved 6.35 mm (1/4 in.) closer to the chuck to perform the next three plunges. Four lateral movements were performed on the same side of a sample to complete the twelve plunges on one end of a sample. The sample was then reversed to expose the other end for another twelve grounds. A total of 24 plunge grinds was done on each sample. Figure 13 shows the various specimens produced by the metal-bonded wheel during Task 2 performance evaluation.

**Figure 13. Various test specimens produced in in-house tests.**

7.2.3.2. Grinding Performance at 32 m/s (6252 SFPM) Wheel Speed. The initial comparison tests for the metal, resin, and vitrified wheels were conducted at 32 m/s peripheral speed at three material removal rates (MRR') from approximately 3.2 $mm^3/s/mm$ (0.3 $in.^3/min/in.$) to approximately 10.8 $mm^3/s/mm$ (1.0 $in.^3/min/in.$), where MRR' is material removal rate per unit wheel width as described in Table 8. Figure 14 shows the performance differences, as depicted by G-ratios, among the three different types of wheels after twelve plunge grinds. G-ratio is the unitless ratio of volume material removed over volume of wheel wear. The data showed that the N grade vitrified wheel had better G-ratios than the R grade resin wheel at the higher material removal rates. The experimental metal-bonded wheel (M #6) was far superior to both of the resin wheel and vitrified wheel at all material removal rates. Since the metal-bonded wheel was extremely durable, there was no measurable wheel wear after twelve grinds. In Figure 14, the G-ratio is an estimate for the metal bond at all material removal rates and

an estimate for the low MRR resin wheel test, because wheel wear was not measurable. Another important observation is that the metal-bond wheel is a 75 diamond concentration wheel, while the resin and vitrified wheels are 100 concentration and 150 concentration, respectively, resulting in additional cost-effectiveness of the experimental wheel.

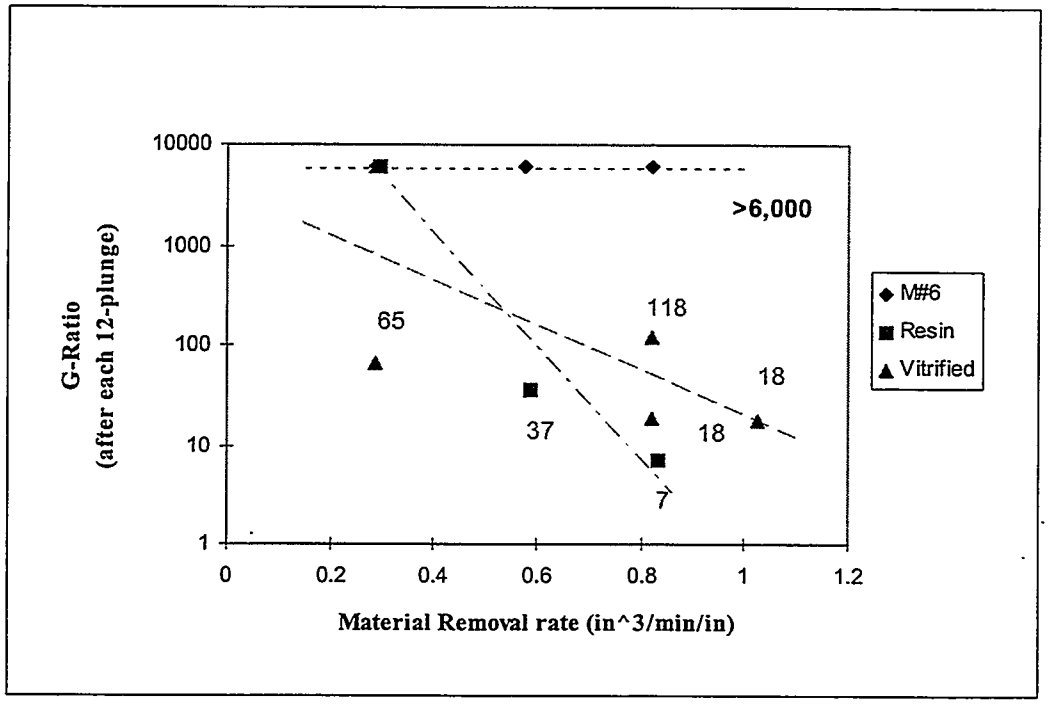


**Figure 14. G-ratio vs material removal rate at 32 m/s grinding speed. M#6 is the experimental IGW metal-bonded wheel.**

Figure 15 shows the difference in grinding power consumption at various material removal rates for the three different wheel types. The resin wheel had a slightly lower power consumption than the other two wheels; however, the experimental metal-bonded wheel and vitrified-bonded wheel had comparable power consumption at the low speed.

Figure 16 and Figure 17 show the preliminary surface finish (Ra) and waviness (Wt) data measured on samples ground by the three wheels at the low test speed. The waviness value, Wt, is the maximum peak-to-valley height of the waviness profile. All surface-finish data reported below were on surfaces created by cylindrical plunge grinding without sparkout. These surfaces are normally rougher than traverse grinding.

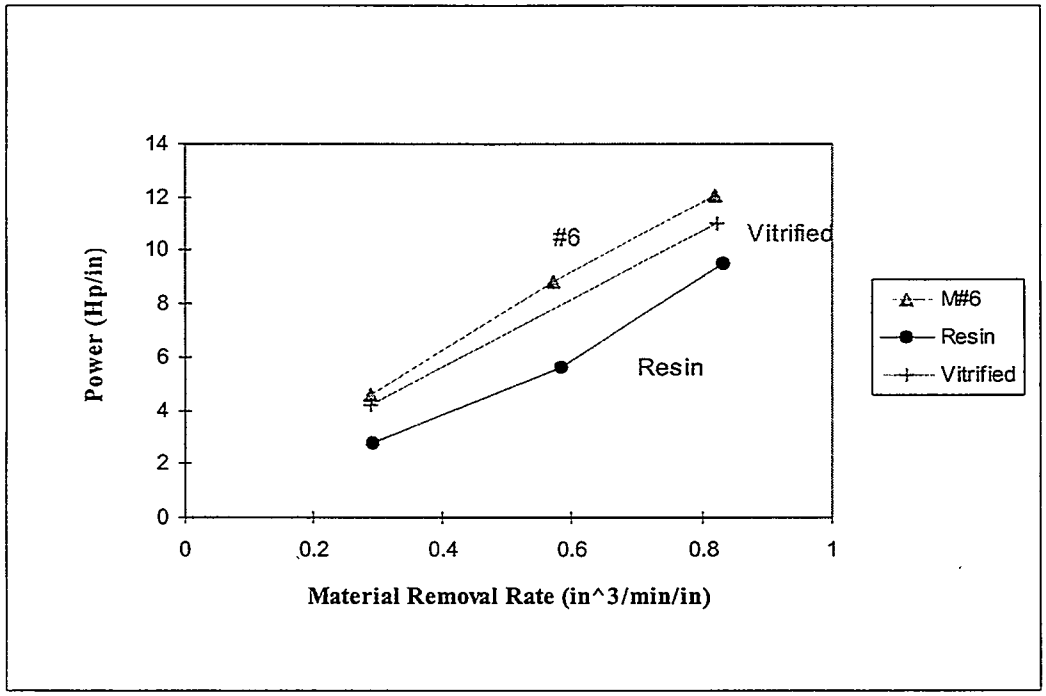


**Figure 15. Power vs MRR' of different wheels at 32 m/s grinding speed.**

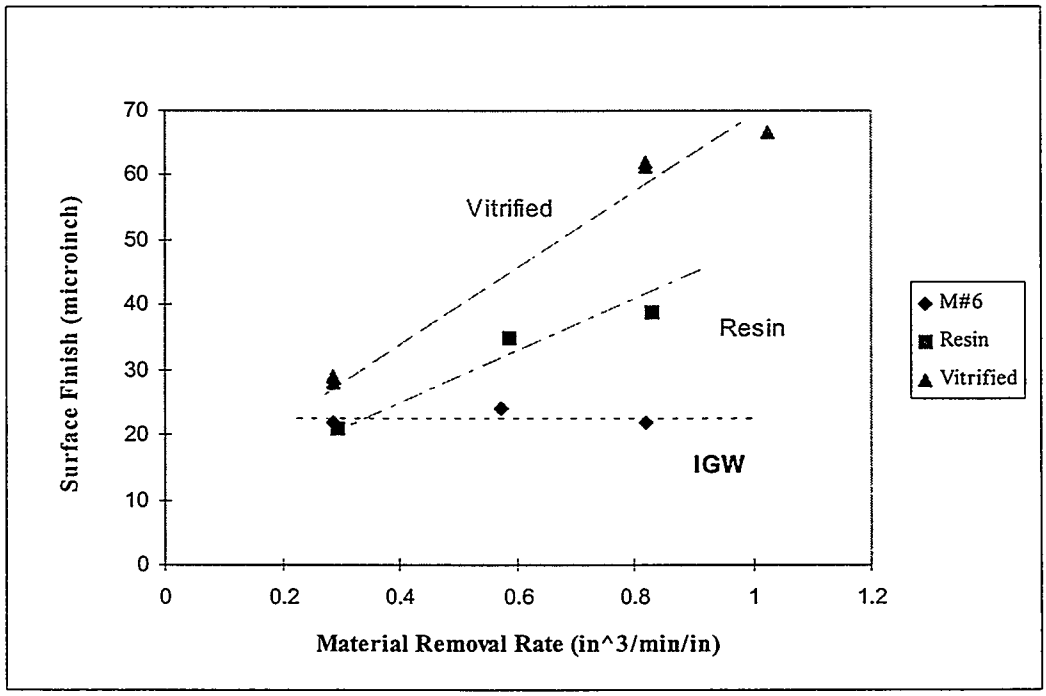


**Figure 16. Surface finish, Ra, vs MRR' at 32 m/s grinding speed.**

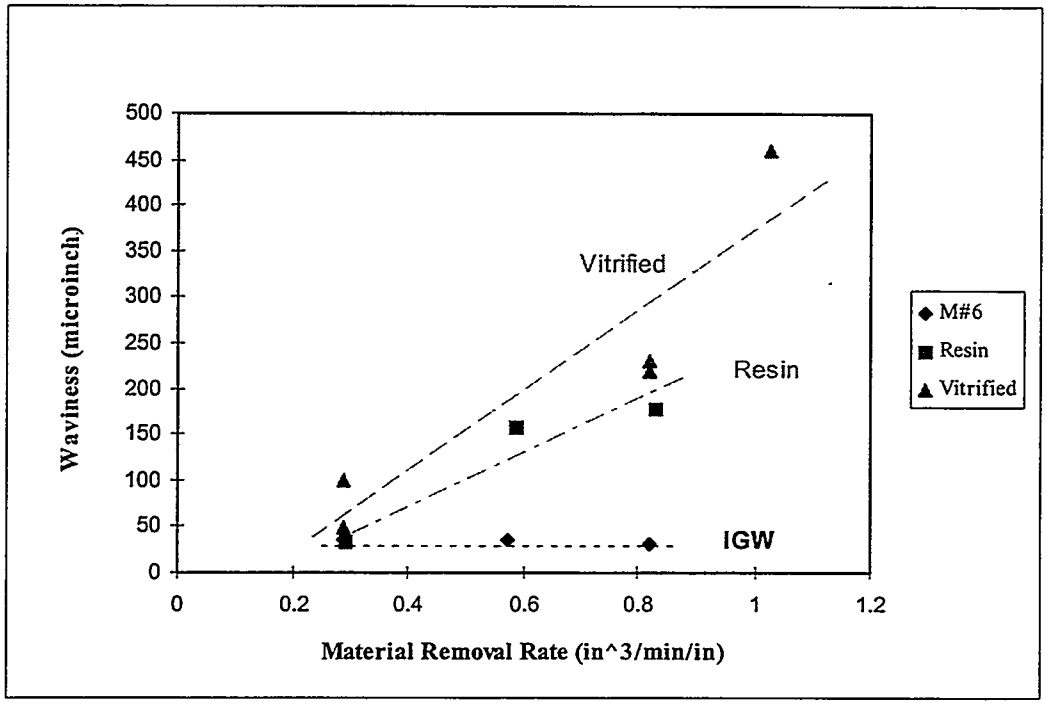


**Figure 17. Waviness, Wt, vs MRR' at 32 m/s grinding speed.**

In general, the average surface finish and waviness of samples plunge ground by the new metal-bonded wheel were in the order of 0.50 μm Ra and less than 1.0 μm Wt. The surface finish and waviness were worse for specimens ground by the resin and vitrified wheels. In addition, the roughness and waviness on the samples ground by the experimental metal-bonded wheel maintained at a constant level at all material removal rates up to 10.8 $mm^3/s/mm$ (1.0 $in.^3/min/in.$) during this series of tests. In contrast, the samples ground by the resin and vitrified wheels showed constant deterioration in surface finish and waviness at higher material removal rates. Specimens were sent to the Northboro R&D Center for further contact and non-contact profilomentry, as part of Task 4.

7.2.3.3. Grinding Performance at 80 m/s (15,750 SFPM) Wheel Speed. Due to original design limit, the vitrified-bonded wheel was not evaluated in this high speed round of performance testing. Figure 18 shows the average power consumption versus material removal rate for the new metal-bonded wheel and resin-bonded wheel. The resin wheel and metal wheel had comparable power consumption at material removal rate of 8.6 $mm^3/s/mm$ (0.8 $in.^3/min/in.$). For the metal-bonded wheel, power appears proportional to MRR'. The highest MRR' that was conducted in this test was 47.3 $mm^3/s/mm$ (4.4 $in.^3/min/in.$), but we believe the wheel did not reach its practicable limit. We believe the material removal rate successfully attained with the experimental wheel is not now achievable for any commercial wheel.

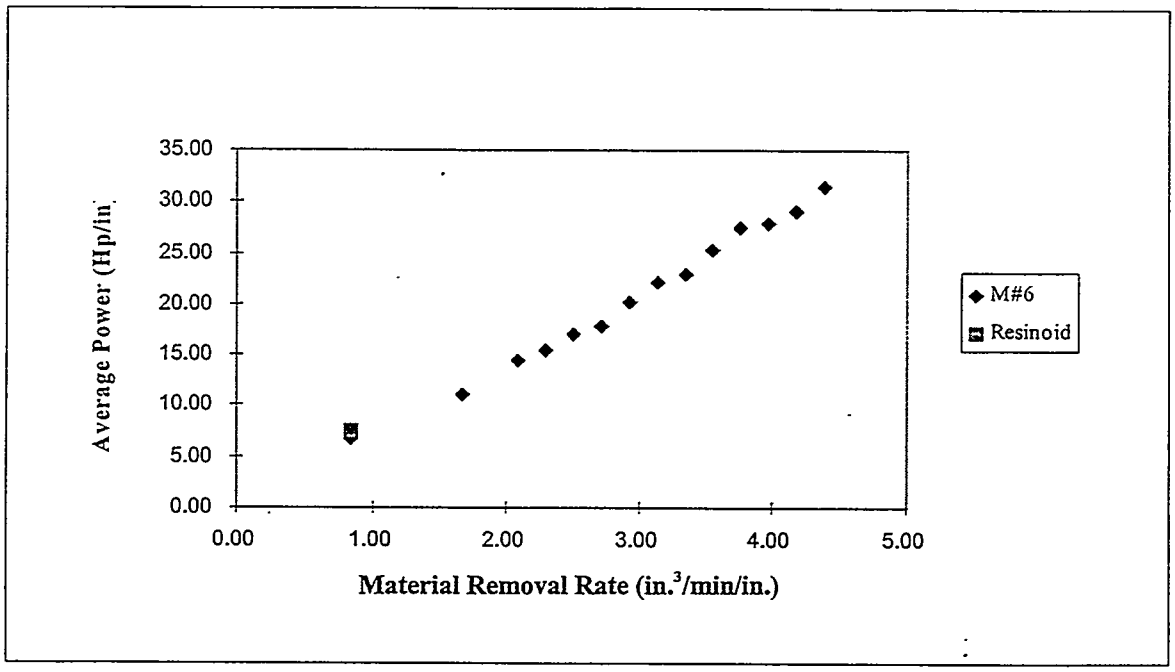


**Figure 18. Average power vs MRR' at 80 m/s grinding speed.**

Figure 19 shows that the power consumption for the experimental wheel at each material removal rate was fairly steady during the twelve grinds. This indicates that the wheel maintained its sharp cutting points during the entire length of the test at all material removal rates.

Figure 20 shows the estimated G-ratios for the resin wheel and the new metal-bonded wheel (#6) at all material removal rate conditions. Since there was no measurable wheel wear after twelve grinds at each material removal rate for the metal-bonded wheel, a symbolic value of 10 μin. (0.25 μm) radial wheel wear was given for each case. This yielded an estimated G-ratio of 6000, but actual G-ratio was probably higher.

During the entire test, with material removal rates ranging from 8.6 $mm^3/s/mm$ (0.8 $in.^3/min/in.$) to 47.3 $mm^3/s/mm$ (4.4 $in.^3/min/in.$), the wheel was not trued or dressed. This wheel showed no measurable wheel wear after 168 plunges at 14 different material removal rates. The total amount of silicon nitride material ground was equivalent to 27,096 $mm^3$ per mm (42 $in.^3$ per in.) of wheel width. By contrast, the G-ratio for the 100-concentration resin wheel at 8.6 $mm^3/s/mm$ (0.8 $in.^3/min/in.$) material removal rate was approximately 583 after twelve plunges. In summary, the experimental metal wheel was able to grind effectively at over 5 times the practicable MRR compared to the standard resin-bonded wheel. Also, the experimental wheel had over 10 times the G-ratio compared to the resin wheel at the lower MRR, and the G-ratio difference would be much greater at higher material removal rates.

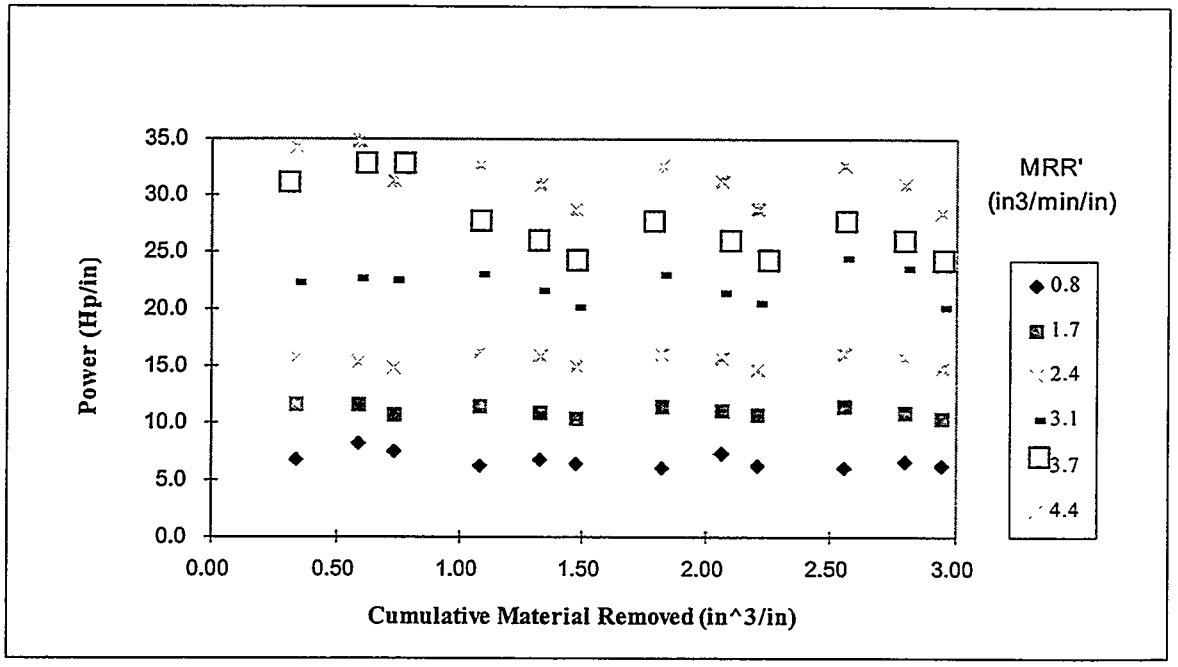


**Figure 19. Grinding power vs cumulative material removed (grinding time) of IGW wheel, M #6 at 80 m/s speed.**

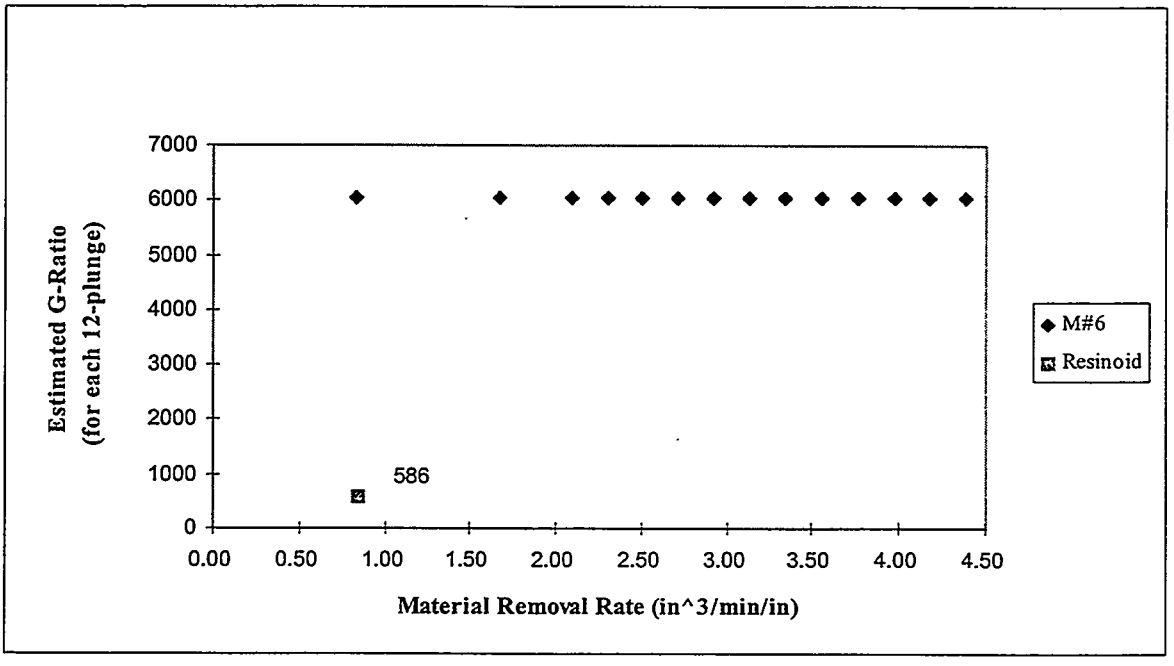


**Figure 20. Estimated G-ratio vs MRR' of the experimental metal-bonded and standard resin-bonded wheels at 80 m/s wheel speed.**

According to above results, one can illustrate the potential productivity gain when using the new metal-bonded diamond wheel capable of high material removal rates by the following example. For a hypothetical task of grinding a 25.4-mm-long by 25.4-mm-diameter silicon nitride rod to 6.35 mm in diameter with a 6.5-mm-wide wheel, four deep plunges are required. The straight grinding time required to complete this work will be around 3.5 minutes for grinding conditions producing a MRR' of 9.0 $mm^3/s/mm$ (0.84 $in.^3/min/in.$), and about 10 minutes for MRR' at 3.2 $mm^3/s/mm$ (0.3 $in.^3/min/in.$). However, with the experimental wheel, it only requires 40 seconds to complete the task at a MRR' of 47.3 $mm^3/s/mm$ (4.4 $in.^3/min/in.$).

Figure 21 shows that the samples ground by the experimental metal-bonded wheel (M #6) at all 14 material removal rates maintained constant surface finishes between 0.4 μm (16 μin.) and 0.5 μm (20 μin.). The resin wheel was not tested at these high material removal rates. At about 8.6 $mm^3/s/mm$ (0.8 $in^3/min/in$) material removal rate, the bars ground by the resin wheel had slightly better but comparable surface finishes (17 versus 20 μin.). Surprisingly, there was no apparent deterioration in surface finish when the rods were ground with the new metal-bonded wheel as the material removal rate increased. This is in contrast to the commonly observed surface finish deterioration with increase cut rates for standard wheels.

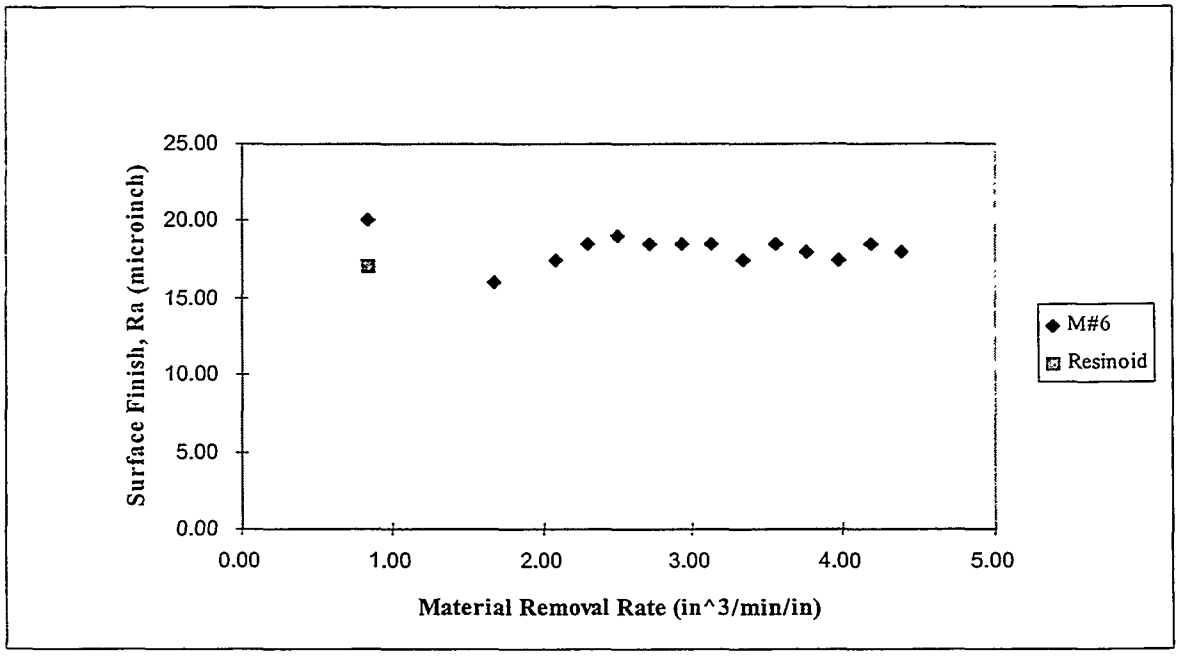


**Figure 21. Surface finish, Ra, vs MRR' at 80 m/s grinding speed.**

Prior to the above test series, a long-duration test of 96 plunges was performed on an experimental metal wheel at 80 m/s. The material removal rate was set at 5.4 $mm^3/s/mm$ (0.5 $in.^3/min/in.$). The total material removed was equivalent to 15,484 $mm^3$ per mm (24 $in.^3$ per in.) of wheel width. The power consumption was consistent throughout the 96 grinds. The G-ratio measured during this long-duration test was about 800. No truing or dressing on the wheel was required.

7.2.3.4. Summary, Grinding Performance as a Function of Wheel Speed. Figure 22 shows the linear relationship between power consumption and material removal rate under various wheel speeds and types of wheel. At 32 m/s (6252 SFPM) and 56 m/s (11,000 SFPM) speeds, the power consumption for the experimental metal-bonded wheel was higher than that of the standard resin wheel at all the material removal rates tested. However, the power consumption for the metal-bonded wheel became comparable or slightly less than that of resin wheel at the high wheel speed of 80 m/s (15,750 SFPM). Overall, the trend showed that the power consumption decreased with increasing wheel speed when grinding at the same material removal rate. This is true for both the resin wheel and the experimental metal-bonded wheel. This trend is probably due to the reduced chip thickness at the higher wheel speeds.

Figure 23 shows the relationship between G-ratio and material removal rate under various wheel speeds and wheel types. Here again, there was no measurable wheel wear on the metal-bonded wheel; it showed a straight horizontal line at constant G-ratio of approximately 6000 at all material removal rates and wheel speeds. For the resin wheel, the G-ratio decreases with increasing material removal rates at any constant wheel speed. G-ratio is shown to improve at higher wheel speed.

Figure 24 shows the improvement in surface finishes on the ground bars at higher wheel speed. Measurement of waviness showed similar trends. In addition, the samples ground by the new metal-bonded wheel had the lowest measured waviness under all wheel speeds and material removal rates tested under Task 2.

7.2.3.5. Task 2 In-house Grinding Test Summary. The following are some of the key performance advantages demonstrated by the innovative metal-bonded diamond wheels during the Task 2 evaluation.

1. The experimental metal-bonded wheel reached a material removal rate of 47.3 $mm^3/s/mm$ (4.4 $in.^3/min/in.$) at 80 m/s wheel speed without showing wheel wear or surface-finish deterioration on the ground parts. This is a significant improvement in grinding productivity and reduction of machining cost for the advanced ceramics industry.
2. At each of the material removal rates (from 8.6 $mm^3/s/mm$ to 47.3 $mm^3/s/mm$), the metal-bonded wheel demonstrated consistent grinding power consumption and surface finish in grinding NT551 silicon nitride samples even after extensive plunge grinds.

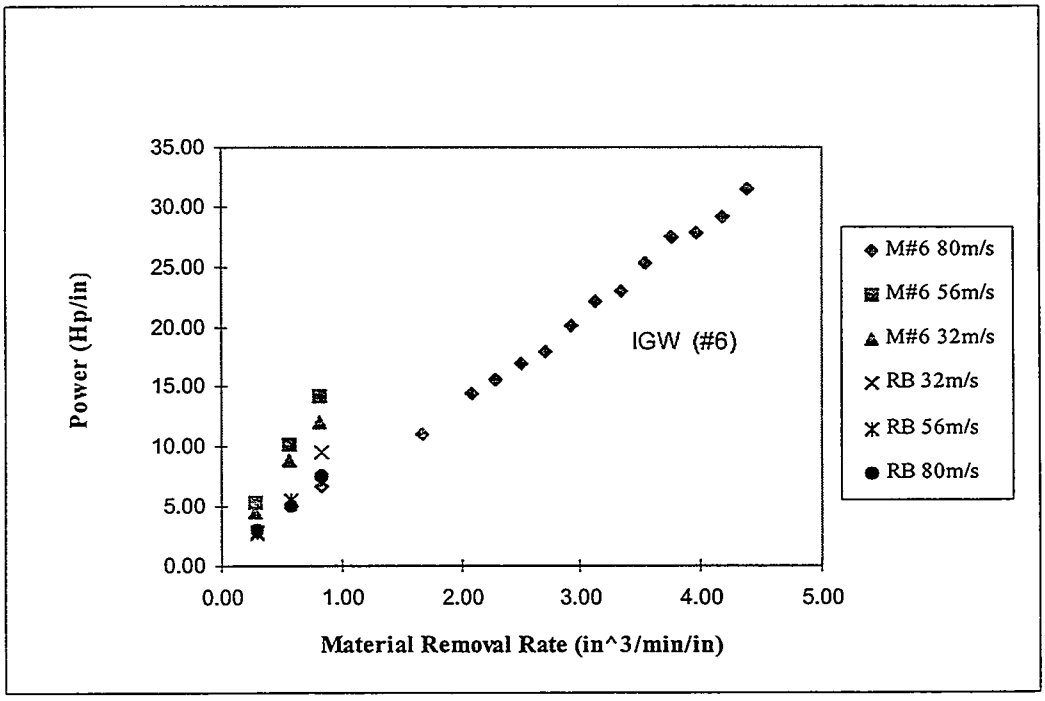


**Figure 22. Power vs MRR' of experimental bond (M #6) and the standard resin-bonded wheel at three wheel speeds.**

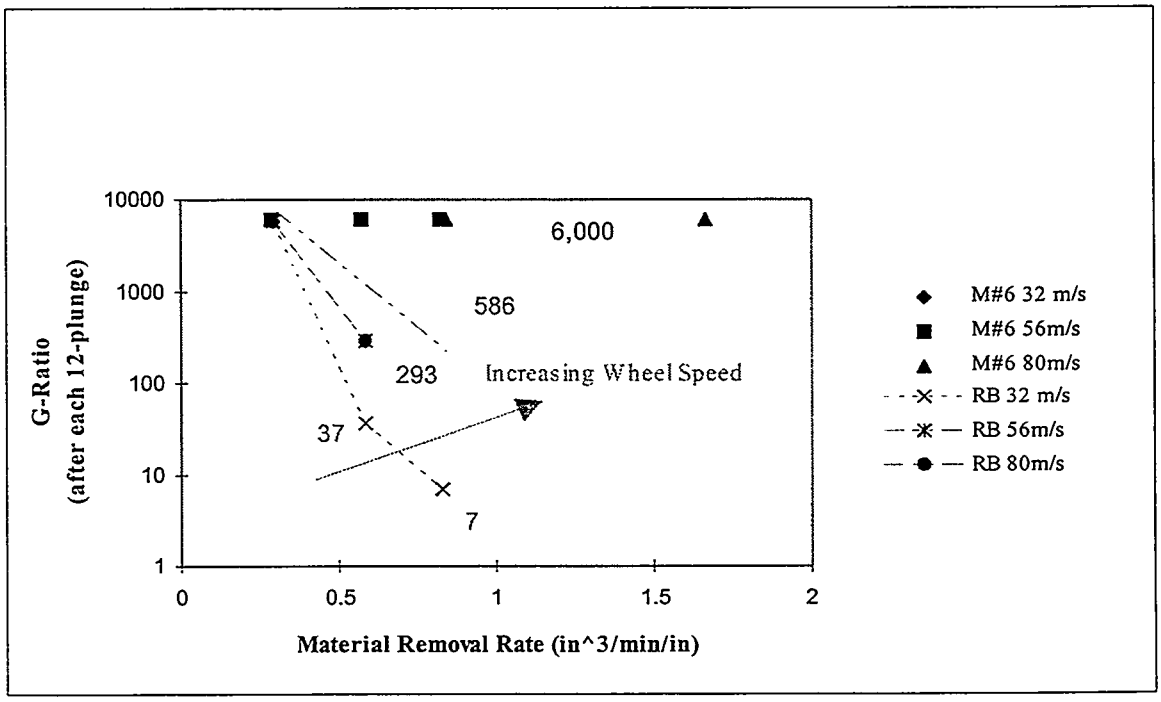


**Figure 23. G-ratio vs MRR' at 3 wheel speeds for the two types of wheels.**

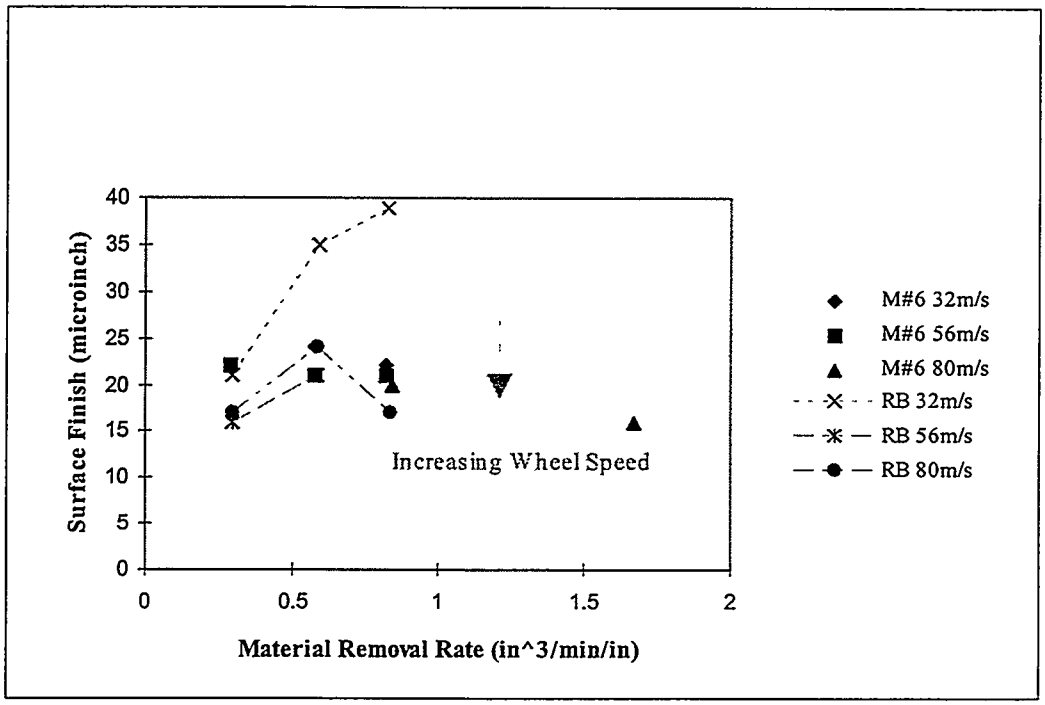


**Figure 24. Surface finish, Ra, vs MRR' at 3 wheel speeds for the experimental metal and standard resin-bonded wheels.**

3. At 32 m/s speed, the metal-bonded wheel had slightly higher power consumption than the resin wheel; but at 80 m/s the metal-bonded wheel had power consumption comparable to the resin wheel.
4. The metal-bonded wheel demonstrated superior wheel life compared to the resin and vitrified-bonded wheels. In addition, there was no need for truing and dressing during the extended grinding tests.
5. The current experimental wheel could be operated at wheel speeds up to 90 m/s.
6. A truing and dressing method for this new metal-bonded wheel was successfully developed; and further improvement in truing operation would be expected to yield additional wheel performance benefits.

Overall, the above results suggest that there are tremendous benefits to be realized by the ceramic industry when using this innovative metal-bonded diamond wheel for cylindrical grinding. In addition, this experimental wheel does not require frequent and difficult dressing, which is characteristic of a standard metal-bonded diamond wheel. This new bond demonstrated free cutting capability throughout the entire test matrix. Continuation of the program to Task 3 independent validation tests was definitely warranted and recommended to the ORNL Program Manager.

## 7.3. INDEPENDENT VALIDATION TESTS -- TASK 3

### 7.3.1. Introduction -- Selection of Sites and Wheel Specs -- Task 3.A

AlliedSignal Ceramic Components, Chand Kare Technical Ceramics, and Eaton Manufacturing Technologies Center were originally proposed to do independent validation tests, and submitted updated quotations after the start of this program.

Norton Company held preliminary meetings with AlliedSignal Ceramic Components, Eaton Corporation, and Chand Kare Technical Ceramics to establish testing conditions and to verify details of their statements of work. The fourth test site, Norton Advanced Ceramics Division of Saint-Gobain Industrial Ceramics, Inc., was planned to be performed at Norton Company's Higgins Grinding Technology Center under supervision of NAC. NAC elected to do additional testing at SGIC's Northboro R&D Center Machining Lab.

AlliedSignal Ceramic Components, one of the four independent validation test sites planned for in Task 3, withdrew their proposal due to scheduling difficulties. We reviewed a list of potential replacement test sites with the ORNL Program Monitor. Caterpillar Corporation submitted a proposal to become the fourth independent validation test site, to replace AlliedSignal Ceramic Components. After review with the ORNL Program Monitor, Caterpillar was selected.

We consulted with all the test sites on their Statements of Work and proposed test conditions and made mutually agreed upon modifications based on the internal grinding results of Task 2. For all test sites, the experimental wheel was standardized at 320 grit diamond, which we concluded was the best all-purpose grit size for testing the wheel in both rough and finish grinding conditions.

The initial NAC grinding evaluation plan was finalized with NAC and the HGTC. The experimental metal-bond wheel was to be evaluated as a finishing wheel by traverse grinding diesel valve profiles (stem and base) on the Studer grinder. We planned to evaluate the experimental wheel compared to the finishing operation done by HGTC on NAC's valves under the Advanced Ceramics Manufacturing Technology (ACMT) program [18]. Finish profile grinding represents one of the most time consuming valve grinding operations. Therefore, this proposed test was considered an effective method to demonstrate significant cost-effective improvements. Surface finish and power at various grinding conditions were the primary interests of this test. The test determined maximum cut rate that can be used while still achieving the 8 μin. Ra finish requirement. The required truing and dressing frequency/characteristics, and wear behavior of the experimental metal bond were also assessed.

The following were the wheel specifications selected for each independent grinding test subcontractor.

| | |
|---|---|
| Chand Kare: | (400-mm-diameter) 15.75 in. x 0.5 in. x 5.0002 in. 1A1SA Wheel of AD320-75MXL1994 |
| NAC: | (400-mm-diameter) 15.75 in. x 0.5 in. x 5.0002 in. 1A1SA Wheel of AD320-75MXL1994 |
| Eaton: | (400-mm-diameter) 15.75 in. x 0.5 in. x 5.0002 in. 1A1SA Wheel of AD320-75MXL1994 on customer hub |
| Caterpillar: | (400-mm-diameter) 15.75 in. x 0.5 in. x 9.0002 in. 1A1SA Wheel of AD320-75MXL1994 on customer hub |

7.3.2. Wheel Fabrication and Delivery-- Task 3.B

All experimental metal-bond test wheels (IGW) were fabricated and delivered to the four independent test sites. Several improvements were implemented for manufacturing-control and cost-reduction considerations during the fabrication of experimental wheels for the validation tests. Additionally, Norton supplied standard NT551 silicon nitride rod specimens and the recommended SG® Seeded-Gel truing wheels. Each test site supplied their own standard test wheels for comparison, consistent with their standard grinding operation practices.

7.3.3. Independent Validation Tests at Subcontractors -- Task 3.C

All four independent validation tests were initiated and completed during 1997.

7.3.3.1. Caterpillar Test -- Task 3.C.1. Caterpillar Technical Center in Peoria, Illinois, completed their grinding test on the experimental metal-bond innovative grinding wheel (IGW) and the final test report was submitted to Norton (Appendix 1). The following is a summary of the test. Centerless grinding test was done at two feed rates on both Norton Advanced Ceramics' NT551 silicon nitride and Caterpillar-supplied magnesia partially stabilized zirconia, Mg-PSZ.

**Grinding Test Procedure** -- Caterpillar's program consisted of two parts. The first part used Mg-PSZ rods, 6.5 mm in diameter, by 70-mm-long, to simulate a centerless grinding operation used to manufacture zirconia fuel injector components. The second part used NAC NT551 silicon nitride rods, approximately 25.4 mm in diameter by 90-mm-long, to simulate the centerless grinding of right circular cylinder structural components, such as valve guides or valve seats.

The centerless grinding was done on a Liokoping Centerless grinder, using Hocut 763-MY Undyed, a water-based coolant (5 percent by volume coolant). The innovative grinding wheel (specification: 15.5-in. x 0.5-in. x 9.0002-in. [1A1SA AD320-75MXL1994] was compared to a 320 grit, 100 concentration, vitrified-bonded diamond wheel (D1A1, 16-in. x 0.5-in. x 9-in.).

The maximum depth of cut for the Liokoping was controlled by the taper on the grinding wheel. For this trial, a 0.1 mm taper was placed on both the experimental metal-bond (IGW) and vitrified-bond grinding wheels. This taper allowed a maximum stock removal of 0.1 mm from the diameter, per pass. Since the depth of cut was fixed by the taper on the grinding wheel, the evaluation consisted of centerless grinding both the zirconia and silicon nitride specimens at two constant thrufeed rates (fast and slow).

**Summary of Caterpillar Results** -- Summaries of the grinding results are shown for zirconia and silicon nitride in Tables 9 and 10, respectively.

**Table 9. Summary of grinding results on Mg-zirconia rods.**

| Wheel | Thru-feed Rate (mm/s) | No. of Speci-mens | Wheel Wear ($mm^3$) | G-Ratio | Surf. Finish, Ra (μm) | % "Pull-Out" | Avg. Flex Strength ± Std Dev. (MPa) | Weibull Mod (no. of data points) |
|---|---|---|---|---|---|---|---|---|
| IGW | 3.3 | 15 | 46 | 292 | 0.42 | 9.01 E-05 | **642** ± 23 | **30** (14) |
| IGW | 10 | 15 | 159 | 83 | 0.77 | 1.4 E-04 | **638** ± 23 | **30** (15) |
| Vitr. Bond | 3.3 | 12 | 102 | 77 | 0.42 | 8.38 E-04 | **631** ± 59 | **12** (15) |
| Vitr. Bond | 10 | 15 | 206 | 64 | 0.71 | 1.17 E-04 | **608** ± 54 | **12** (15) |

**Table 10. Summary of grinding results on NT551 silicon nitride rods.**

| Wheel | Thru-feed Rate (mm/s) | No. of Speci-mens | Wheel Wear ($mm^3$) | G-Ratio | Surf. Finish Ra (μm) | % "Pull-Out" | Residual Stress, Radial (KSI) | Residual Stress, Axial (KSI) |
|---|---|---|---|---|---|---|---|---|
| IGW | 2.5 | 5 | none | N/A | 1.013 | 2.37E-04 | -36.3 +/- 6.5 | -46.2 +/- 5.6 |
| IGW | 7.3 | 5 | 161 | 238 | 0.70 | 1.27E-04 | -33.3 +/- 7.1 | -35.8 +/- 8.5 |
| Vitr. Bond | 2.5 | 4 | 263 | 117 | 0.99 | 1.81E-04 | -31.2 +/- 6.4 | -32.6 +/- 7.3 |
| Vitr. Bond | 7.3 | 5 | 12,095 | 3.2 | 1.566 | 5.66E-04 | -48.5 +/- 7.1 | -56.0 +/- 5.6 |

After each set of specimens was machined, the wheel wear was measured. The G-ratio was calculated for each grinding condition. In addition, the number of times the grinding wheel required dressing during the grinding of a group of specimens was noted.

After machining, the surfaces of both the zirconia and silicon nitride rods were quantified using 3-D surface analysis and scanning electron microscopy techniques. The residual stress of the silicon nitride surfaces after machining was determined using X-ray techniques. Finally, the effect of machining on the mechanical properties of the zirconia rods was determined by breaking the machined rods using 4-point bending techniques conforming to Military Standard 1942A.

**Conclusions** -- The following conclusions were drawn from the Caterpillar grinding data:

1. The Norton IGW demonstrated lower wheel wear than the vitrified-bonded wheel when centerless grinding either Mg-PSZ or NT 551 rods at either thrufeed rate. Increasing the thrufeed rate increased the difference in G-ratios between the two wheels because of the significantly higher wheel wear of the vitrified-bonded wheel.
2. When machining silicon nitride at the higher thrufeed rates (7.3 mm/s), the vitrified-bonded wheel started to break down producing rougher surface finishes with higher residual stresses than the IGW.
3. The flexural data on zirconia suggest that the IGW caused less grinding damage than the vitrified-bonded wheel. As determined by fractography, the critical flaws that caused failure in zirconia rods machined using the IGW were volume flaws (i.e., porosity), resulting in a higher Weibull modulus. However, the critical flaws that caused failure for zirconia machined with the vitrified-bonded wheel were both volume and surface flaws (i.e., pits in the machining grooves). These two failure modes caused a wider distribution of flexure strengths, and lower Weibull modulus, because the surface flaws caused failures at lower loads than the volume flaws. However, the average bend strength of the Mg-PSZ rods did not appear to be affected by the grinding wheel.
4. The truing and dressing of the IGW was no more difficult than the truing and dressing of the vitrified-bonded wheel. During machining, the IGW required less dressing than the vitrified-bonded wheel, especially at the higher thrufeeds.

7.3.3.2. Chand Kare Technical Ceramics Test – Task 3.C.2. Chand Kare completed their independent grinding test and submitted their final test report to Norton Company (Appendix 2). A summary of the test results is as follows:

**Grinding Test Procedure** -- Chand Kare evaluated Norton's new experimental metal-bond wheel (320 grit, 15.5 inch diameter, ½ inch wide) versus a standard resin-bonded wheel (Norton SD320R75B99E, 16 inch diameter, ½ inch wide) using two approaches: design of experiment and machine operator's evaluation.

The grinding tests were done on NT551 $Si_3N_4$ rods (supplied by Norton) under external cylindrical grinding mode. Chand Kare evaluated grinding power, specific energy, surface roughness, wheel wear, and wheel truing time. Grinding tests were

performed under external cylindrical grinding mode using an OD/ID grinder as illustrated in Figure 25. Center holes were drilled on both ends of the rods. During grinding, the rods were held using a chuck and a center hole as shown in Figure 25.

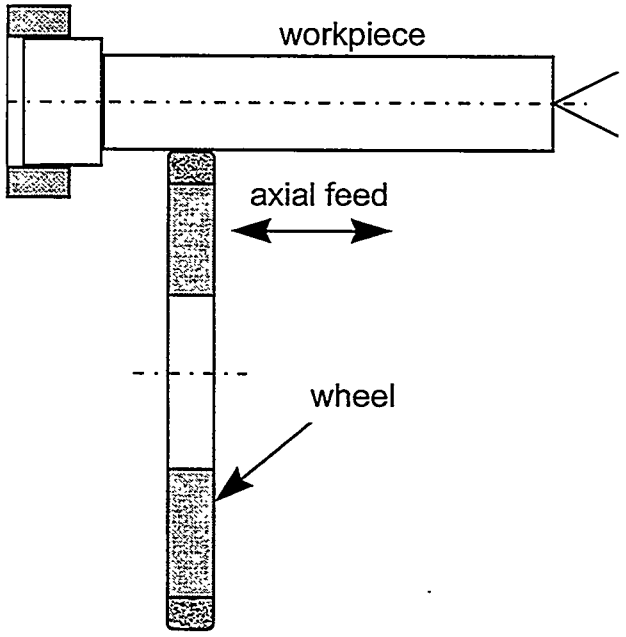


**Figure 25. Schematic of experimental setup.**

The wheels were trued using a brake controlled truing device with silicon carbide truing wheels. The truing parameters were: truing depth 0.001 in./pass, feed 0.55 in./s. The wheels were then dressed using aluminum oxide sticks.

For the design of experiment approach, the two wheels were tested under OD grinding mode with two levels of wheel speeds (24 m/s and 44 m/s; 4638 and 8567 SFPM), two levels of depths of cut (10 μm and 30 μm; 0.0004 and 0.0012 in.), and two levels of work speeds (0.19 m/s and 0.34 m/s; 36.9 and 66.7 SFPM). The workpiece axial feed velocity was fixed at 14 mm/s (0.55 in./s). A full factorial design was used which consisted of 16 tests as listed in Table 11. It should be noted that the high depth of cut of 0.0012 inch is not commonly used in production grinding with 320 grit resin wheels.

Wheels were re-trued and redressed before each test to maintain the same initial condition. Each test was performed on a separate rod. A total of 0.2 inch (in diameter) stock was removed for each test, which leads to about 30 minute grinding with the depth of cut of 0.0012 inches (83 passes) and 90 minute grinding with the depth of cut of 0.0004 inches (250 passes).

**Table 11. Chand Kare grinding test matrix.**

| Test number | Depth of cut, DOC (in) | Work speed, $v_w$ (SFPM) | Wheel speed, $v_s$ (SFPM) | Wheel type |
|---|---|---|---|---|
| 1 | 0.0012 | 36.9 | 4638 | XL metal bond |
| 2 | 0.0004 | 36.9 | 4638 | XL metal bond |
| 3 | 0.0012 | 66.7 | 4638 | XL metal bond |
| 4 | 0.0004 | 66.7 | 4638 | XL metal bond |
| 5 | 0.0012 | 36.9 | 8567 | XL metal bond |
| 6 | 0.0004 | 36.9 | 8567 | XL metal bond |
| 7 | 0.0012 | 66.7 | 8567 | XL metal bond |
| 8 | 0.0004 | 66.7 | 8567 | XL metal bond |
| 9 | 0.0012 | 36.9 | 4638 | resin bond |
| 10 | 0.0004 | 36.9 | 4638 | resin bond |
| 11 | 0.0012 | 66.7 | 4638 | resin bond |
| 12 | 0.0004 | 66.7 | 4638 | resin bond |
| 13 | 0.0012 | 36.9 | 8567 | resin bond |
| 14 | 0.0004 | 36.9 | 8567 | resin bond |
| 15 | 0.0012 | 66.7 | 8567 | resin bond |
| 16 | 0.0004 | 66.7 | 8567 | resin bond |

**Summary of Results from Chand Kare** -- The results from the statistical analyses indicated that grinding with the new experimental metal-bonded wheel required significantly lower specific energy than the resin-bond wheel tested.

Grinding power was monitored during tests using a power monitor and recorded at three times during the test, namely the 5$^{th}$ pass (newly trued and dressed wheel), 75$^{th}$ pass (after about 30 minutes grinding), and 245$^{th}$ pass (end of test).

Specific energy was calculated by dividing the power by the material removal rate, or

$$u = \frac{p}{\pi d_w a v_f}$$

where $p$ is the net grinding power, $a$ is the wheel depth of cut, $d_w$ is the workpiece diameter, and $v_f$ is the axial feed velocity.

Wheel type had the most significant influence for power data taken at all three times: (1) on a "new" wheel, (2) after 30 minutes, and (3) at the end of the grinding test. The experimental metal-bond wheel consumed much lower specific energy than the resin-bond wheel for all tests. For the "new" wheel test, work speed, wheel type, depth

of cut, and many interactions also had significant influence on specific energy. The analyses of variance of the specific energy after 30 minutes of grinding and at the end of the test both showed that the wheel type and the interaction of wheel type with wheel speed had a significant influence on specific energy. Again, the experimental metal-bonded wheel consumed much lower specific energy than the resin-bonded wheel. Furthermore, the experimental metal-bonded wheel resulted in more consistent specific energy than the resin-bonded wheel.

The surface roughness was not found to have any difference between the parts ground using the new experimental metal-bonded wheel and parts ground using the resin-bonded wheel. However, the new metal-bonded wheel resulted in slightly better and more consistent surface roughness. The most significant factor that influenced the surface roughness was depth of cut. Wheel speed is the next significant factor. From the main effect analysis it was shown that higher depth of cut leads to higher surface roughness, as expected. Higher wheel speed led to lower surface roughness as expected. In general, the parts ground with the experimental metal-bonded wheel had lower surface roughness than the resin wheel, but the difference was not statistically significant.

The results also indicate that the two wheels required basically the same truing time. The statistical analyses also indicate that both wheels have similar form holding capability under the test condition. In order to measure wheel wear, the form of the wheel was copied to an alumina rod by plunge grinding the rod before and after each test. The corner radius of each form on the alumina rod was then measured using a shadow graph comparator under a magnification of 50X. Measurements of the corner radii were taken on both the left and the right side of the wheel.

The main effects and interaction analysis showed that higher depth of cut, higher work speed, and lower wheel speed result in higher wheel wear as expected. The results also showed that the experimental metal-bonded wheel showed slightly higher wheel wear than the resin-bonded wheel. However, the difference was not statistically significant. The conclusion is that the two wheels have similar wear within the test conditions.

The Chand Kare machine operator evaluation concluded that the new experimental metal-bonded wheel was better than the tested resin-bonded wheel (SD320R75B99E) for grinding the NT551 silicon nitride ceramics.

The above Chand Kare results, in conjunction with in-house tests at HGTC, point to the improved versatility of the experimental "innovative grinding wheel" at several grinding operations and conditions. The several previous HGTC tests consistently showed significantly lower wheel wear with the experimental metal-bonded wheel versus the standard resin-bonded wheel. This wheel wear trend was not observed in the above Chand test, but this may be attributed to the different Chand machine and conditions, particularly the lower wheel speed.

7.3.3.3. Eaton Test – Task 3.C.3. The Eaton Manufacturing Technology Center grinding test was completed and the final test report was submitted to Norton (Appendix 3). The following is a summary of the test.

Eaton evaluated the innovative grinding wheel at speeds up to 18,000 SFPM (91 m/s). The test included an evaluation of the metal-bonded wheel by Electrocontact Discharge Dressing (EDD).

**Grinding Test Procedure** -- The two wheels selected for this study were the 15.75-inch-diameter, 320 grit Norton IGW, (specification: AD320-75MXL1994) and a 12-inch-diameter, 240 grit polyimide resin-bonded diamond wheel (D240-100-UI841). Both wheels were approximately 0.5 inches wide.

A modified Weldon 1632 OD grinder was used to plunge grind Norton NT551 silicon nitride cylindrical specimens. The Weldon was upgraded with hybrid ceramic bearings in the spindle and is capable of 14,000 RPM operation. Additionally, a Kistler piezoelectric washer system was installed in the ball nut of the wheel head axis to measure grinding forces in process. Spindle power was monitored using a Load Controls Inc. portable power monitor. Data were collected using a PC-based data acquisition system.

Grinding test conditions were:

Wheel speeds -- 6,000; 12,000; and 18,000 SFPM (30.5, 61, and 91 m/s)

Material removal rates, MRR' -- 0.1, 0.5, and 1.0 $in^3/min/in.$ (1.08, 5.4, and 10.8 $mm^3/s/mm$)

Coolant -- water soluble oil.

Truing was done after mounting each wheel and when necessary to remove any wheel wear. Dressing was done before each test but not in between passes for a given test condition. The resin wheel was trued and dressed using an Eaton-developed method for resin-bonded wheels.

Two different dressing methods were evaluated on the Norton metal-bonded innovative grinding wheel. First, was the Norton specified method using an SG wheel followed by sticking. Second, Eaton's Electrocontact Discharge Dressing system was evaluated. The Eaton EDD system differs from ELID in the following characteristics:

- In ELID, the grinding wheel is connected to the positive terminal of a voltage source. An electrode, located at some distance from the grinding wheel surface, is connected to the negative terminal. Electrolysis occurs by conducting electricity from the wheel to the electrode through a conductive coolant [24].
- EDD is analogous to spark dressing. A potential is placed across two electrodes. The metal-bonded wheel is then brought into contact with the electrodes. When the potential between the electrodes becomes sufficient, a spark jumps across, melting the bond away.

A constant 60V DC potential was placed across two sets of electrodes. The wheel was then either plunged into or traversed across the electrodes to dress the grinding wheel.

The NT551 workpieces were received for testing in the "as-fired" condition. Prior to testing, the workpieces were ground to a dimension of 1.000 inches (25.4 mm) using the 240 grit resin wheel. The workpiece was held in a six-jaw chuck and grinding was always done as close to the jaws as possible to maintain constant workpiece stiffness. A contact width of 0.400 inches was kept constant and the wheel was plunged to take the workpiece to a nominal diameter of 0.25 inches. The workpiece was indexed 0.500 inches after a plunge grind and the subsequent plunge made. Radial wheel wear was determined by measuring the step height differences between the ground and un-ground portion of the wheel face. The small wheel wear values were measured by optical comparator on a plunge ground reference sample.

**Summary of Results from Eaton** -- A summary of the grinding results is shown in Table 12. Figure 26 and Figure 27 are examples of specific grinding energy and radial wheel wear data vs wheel speed at the three MRR test conditions for the IGW and the resin-bonded comparison wheel. Figure 28 plots the radial wheel wear vs material removal rate at the low and medium speeds.

A courser, 240 grit wheel would be expected to have lower wheel wear and specific grinding energy. However, Figure 26 to Figure 28 show the finer grit Norton IGW still had lower specific energy and wheel wear vs the courser-grit resin bond. The superiority of the Norton IGW is more prominent at the lower speeds and higher material-removal-rate conditions.

**Conclusions from the Eaton Test** -- In general, the conventionally dressed finer grit Norton wheel cut with comparable or lower normal force and power, achieved a better surface finish, and had less wear than the coarser resin-bonded wheel. For both wheels, the amount of wear was reduced by increasing wheel speed. At the middle material removal rate using the resin wheel, wear was reduced by more than a factor of two by increasing wheel speed from 6,000 to 18,000 SFPM. The Norton wheel was much less sensitive to wheel speed effects in reducing wear than the resin.

The EDD dressed wheel resulted in lower specific grinding energy compared to the conventionally dressed Norton IGW. However, the EDD wheel also suffered from severe wheel wear, bond smearing, and grit pullout. It does not appear that this bond type is readily adaptable to an aggressive electrocontact based dressing system such as EDD.

Eaton examined the wheel face after grinding and noted a wheel segment that appeared not to contain diamond abrasive at the surface and was not improved with dressing. This is under investigation.

# Table 12. Summary of grinding data from the Eaton test.

240 Resin

| Test | Part Speed (ft/min) | In-feed Rate (in/rev) | Material Removal Rate ($in^3$/min/in) | Wheel Speed (ft/min) | Normal Force (lb) | Power (hp) | Specific Energy (in-lb/$in^3$) | Surface Finish Ra (µinch) | Surface Finish Rt (µinch) | Radial Wheel Wear (in) | G-Ratio |
|---|---|---|---|---|---|---|---|---|---|---|---|
| 1 | 42 | 0.0002 | 0.1 | 6,000 | 14 | 0.48 | 4,714,286 | 39 | 294 | 0.0015 | 65 |
| 2 | 42 | 0.0002 | 0.1 | 12,000 | 5 | 0.34 | 3,339,286 | 31 | 224 | 0.0006 | 163 |
| 3 | 42 | 0.0002 | 0.1 | 18,000 | 11 | 0.48 | 4,714,286 | 35 | 291 | 0.0005 | 195 |
| 4 | 42 | 0.001 | 0.5 | 6,000 | 63 | 2.75 | 5,401,786 | 59 | 445 | 0.0020 | 49 |
| 5 | 42 | 0.001 | 0.5 | 12,000 | 23 | 1.84 | 3,614,286 | 51 | 349 | 0.0010 | 98 |
| 6 | 42 | 0.001 | 0.5 | 18,000 | 20 | 1.75 | 3,437,500 | 43 | 321 | 0.0006 | 163 |
| 7 | 42 | 0.002 | 1.0 | 6,000 | | | | | | | |
| 8 | 42 | 0.002 | 1.0 | 12,000 | 45 | 3.77 | 3,702,679 | 62 | 455 | 0.0015 | 65 |
| 9 | 42 | 0.002 | 1.0 | 18,000 | 34 | 3.43 | 3,368,750 | 48 | 368 | 0.0007 | 140 |

Norton Innovative Grinding Wheel - Norton Dressing Method

| Test | Part Speed (ft/min) | In-feed Rate (in/rev) | Material Removal Rate ($in^3$/min/in) | Wheel Speed (ft/min) | Normal Force (lb) | Power (hp) | Specific Energy (in-lb/$in^3$) | Surface Finish Ra (µinch) | Surface Finish Rt (µinch) | Radial Wheel Wear (in) | G-Ratio |
|---|---|---|---|---|---|---|---|---|---|---|---|
| 1 | 42 | 0.0002 | 0.1 | 6,000 | 11 | 0.254 | 2,494,643 | 37 | 327 | 0.0006 | 124 |
| 2 | 42 | 0.0002 | 0.1 | 12,000 | 14 | 0.189 | 1,856,250 | 22 | 181 | 0.0006 | 124 |
| 3 | 42 | 0.0002 | 0.1 | 18,000 | 14 | 0.207 | 2,033,036 | 35 | 319 | 0.0005 | 149 |
| 4 | 42 | 0.001 | 0.5 | 6,000 | 35 | 1.193 | 2,343,393 | 58 | 386 | 0.0008 | 93 |
| 5 | 42 | 0.001 | 0.5 | 12,000 | 24 | 1.081 | 2,123,393 | 41 | 302 | | |
| 6 | 42 | 0.001 | 0.5 | 18,000 | 28 | 1.74 | 3,417,857 | 28 | 235 | 0.0006 | 124 |
| 7 | 42 | 0.002 | 1.0 | 6,000 | | | | | | | |
| 8 | 42 | 0.002 | 1.0 | 12,000 | 35 | 2.465 | 2,420,982 | 27 | 206 | 0.0006 | 124 |
| 9 | 42 | 0.002 | 1.0 | 18,000 | 32 | 3.244 | 3,186,071 | 33 | 215 | 0.0006 | 124 |

Norton Innovative Grinding Wheel - Electrolytic Discharge Dressing (EDD) Method

| Test | Part Speed (ft/min) | In-feed Rate (in/rev) | Material Removal Rate ($in^3$/min/in) | Wheel Speed (ft/min) | Normal Force (lb) | Power (hp) | Specific Energy (in-lb/$in^3$) | Surface Finish Ra (µinch) | Surface Finish Rt (µinch) | Radial Wheel Wear (in) | G-Ratio |
|---|---|---|---|---|---|---|---|---|---|---|---|
| 1 | 42 | 0.0002 | 0.1 | 6,000 | 10 | 0.159 | 1,561,607 | 44 | 417 | 0.0006 | 124 |
| 2 | 42 | 0.0002 | 0.1 | 12,000 | 12 | 0.159 | 1,561,607 | 55 | 467 | 0.0015 | 50 |
| 3 | 42 | 0.0002 | 0.1 | 18,000 | 6 | 0.191 | 1,875,893 | 36 | 279 | 0.0006 | 124 |
| 4 | 42 | 0.001 | 0.5 | 6,000 | | | | | | | |
| 5 | 42 | 0.001 | 0.5 | 12,000 | 22 | 0.762 | 1,496,786 | 60 | 414 | 0.0024 | 31 |
| 6 | 42 | 0.001 | 0.5 | 18,000 | 20 | 0.715 | 1,404,464 | 43 | 351 | 0.0008 | 93 |
| 7 | 42 | 0.002 | 1.0 | 6,000 | | | | | | | |
| 8 | 42 | 0.002 | 1.0 | 12,000 | 40 | 1.59 | 1,561,607 | 48 | 387 | 0.0018 | 41 |
| 9 | 42 | 0.002 | 1.0 | 18,000 | 38 | 1.462 | 1,435,893 | 41 | 297 | 0.0012 | 62 |

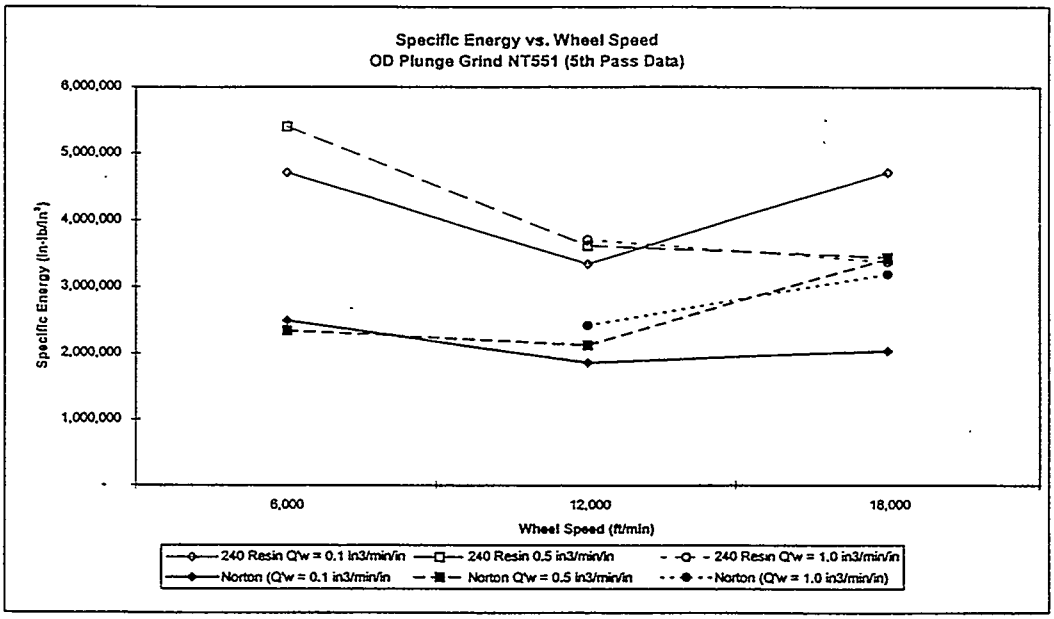


**Figure 26. Specific energy vs wheel speed for 240 grit Resin and 320 grit Norton IGW. Conventional dressing method.**

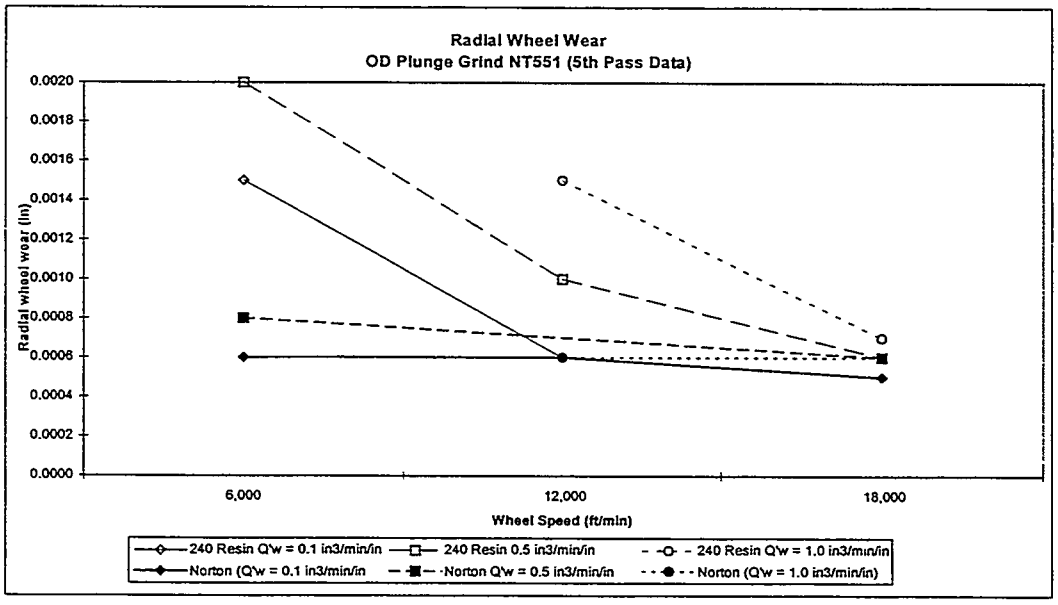


**Figure 27. Radial wheel wear vs wheel speed for 240 grit Resin and 320 grit IGW.**

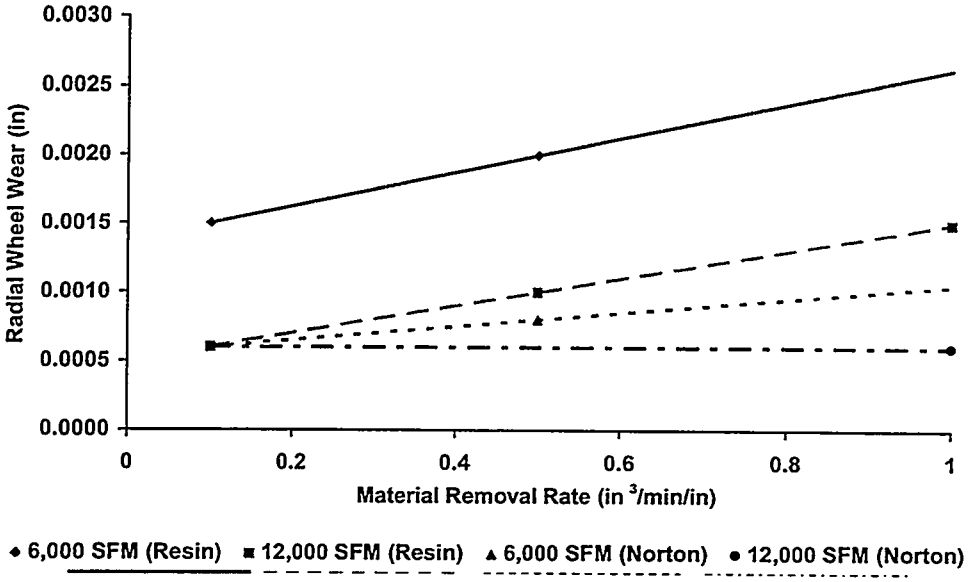


**Figure 28. Radial wheel wear vs material removal rate at 6000 and 12,000 SFPM for 240 grit Resin and 320 grit Norton IGW. Conventional dressing method.**

7.3.3.4. Norton Advanced Ceramics Test at HGTC – Task 3.C.4.1. The Norton Advanced Ceramics valve grinding test was performed at the Higgins Grinding Technology Center. Below is a summary of this valve finishing test. The internal test report is included in Appendix 4A.

A supplemental wheel evaluation test was performed for NAC by the Northboro R&D Center Machining Laboratory. This supplemental test is also described below in Section 7.3.3.5 on Page 54. The internal test report of the NAC validation test performed at NRDC is included in Appendix 4B.

**Valve Finishing Grinding Test at HGTC** -- The experimental metal-bonded wheel was evaluated in finish traverse grinding of diesel valve profiles (stem and base), giving excellent results as described below. This wheel was compared to the finishing operation done by HGTC on NAC's ceramic valves under the Advanced Ceramics Manufacturing Technology (ACMT) program [18]. The valve design was from Detroit Diesel Corporation's Series 49 engine. DDC is a subcontractor to NAC on the ACMT program. Finish profile grinding of a ceramic valve represents one of the most time consuming grinding unit operations.

This test was conducted on three NT551 silicon nitride valve blanks provided by NAC, using the Studer CNC OD grinder at the HGTC. Figure 29 shows the HGTC test area with the Studer machine in the background. Some of the Norton IGW team are shown with the test wheels and several ceramic test specimens in the foreground.

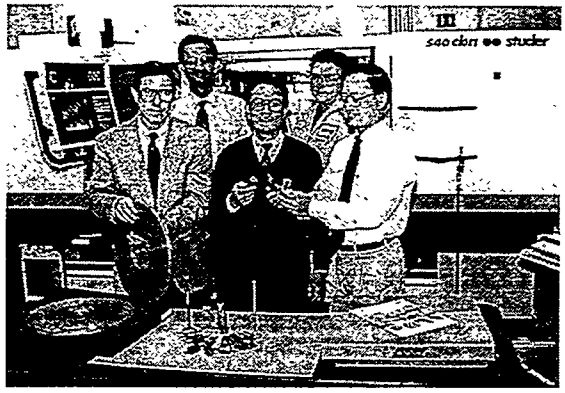

**Figure 29. HGTC valve grinding test. Norton researchers with wheels and ceramic parts. Studer CNC OD grinder is in the background.**

The wheel speed for the experimental innovative grinding wheel was 80 m/s (15,750 SFPM). One standard vitrified-bonded diamond wheel, previously used for NT551 silicon nitride valve grinding under ACMT, was also tested. However, power data were not able to be collected for the vitrified wheel on the second machine spindle. For comparison, we used power data generated from the ACMT valve grinding trials on the same machine at the same finishing conditions. The work speed was 1,000 rpm as in the ACMT trials.

Surface finish and power at various grinding conditions were the principal grinding parameters of interest in this test. Wheel wear was negligible. The test was to determine maximum cut rate that can be achieved while still maintaining no rougher than the 8 μin. Ra finish requirement for these Detroit Diesel Series 149 exhaust valves.

The experimental wheel was tested at the normalized grinding conditions shown below in Table 13 and Table 14. Note that the material removal rate per unit wheel width, MRR' (units are typically $in.^3/min/in.$), changes with depth of cut (or stock removed from diameter) but does not change with traverse rate. However, changing traverse rate does change volumetric material removal rate, MRR (units are typically $in.^3/min$). As shown in Table 14 of normalized conditions, the faster the traverse rate, the larger volume of the material removed per unit time.

The maximum material removed per unit time (MRR) in this test was greater than 6 times the practicable MRR for the vitrified standard wheel. The experimental IGW achieved the 8 μin. Ra (0.2 μm) finish requirement at all the grinding conditions tested. Figure 30 shows surface finish, Ra, vs the relative MRR' for all the experimental valve grinding test conditions in Table 13 and Table 14. It is likely, but was not experimentally confirmed because of time constraints, that the experimental metal-bonded wheel could grind at even a higher MRR and maintain the surface-finish specification. For comparison, the vitrified wheel typically achieved approximately 4 μin. Ra at the lowest traverse rate (normalized at 100).

**Table 13. Valve profile finishing test conditions.**

Normalized material removal rate per unit wheel width, MRR'

| Normalized Stock Removed from Diameter | 100 | 125 | 150 | 200 | 250 |
|---|---|---|---|---|---|
| 500 | | | | | 470 |
| 400 | 400 | | | 400 | |
| 300 | 300 | | 300 | | |
| 200 | 200 ** | 200 | | | |
| 100 | **100 *** | 100 | 100 | 100 | 100 |

Normalized Traverse Rate

**Table 14. Valve profile finishing test conditions.**

Normalized Volume Material Removed per Unit Time, MRR

| Normalized Stock Removed from Diameter | 100 | 125 | 150 | 200 | 250 |
|---|---|---|---|---|---|
| 500 | | | | | 1250 |
| 400 | 400 | | | 800 | |
| 300 | 300 | | 450 | | |
| 200 | 200** | 250 | | | |
| 100 | **100*** | 125 | 150 | 200 | 250 |

Normalized Traverse Rate

* Conditions used for initial 10-valve test under ACMT program (vitrified wheel).
** Conditions for most-recent 30-valve run-off test under ACMT(vitrified wheel).

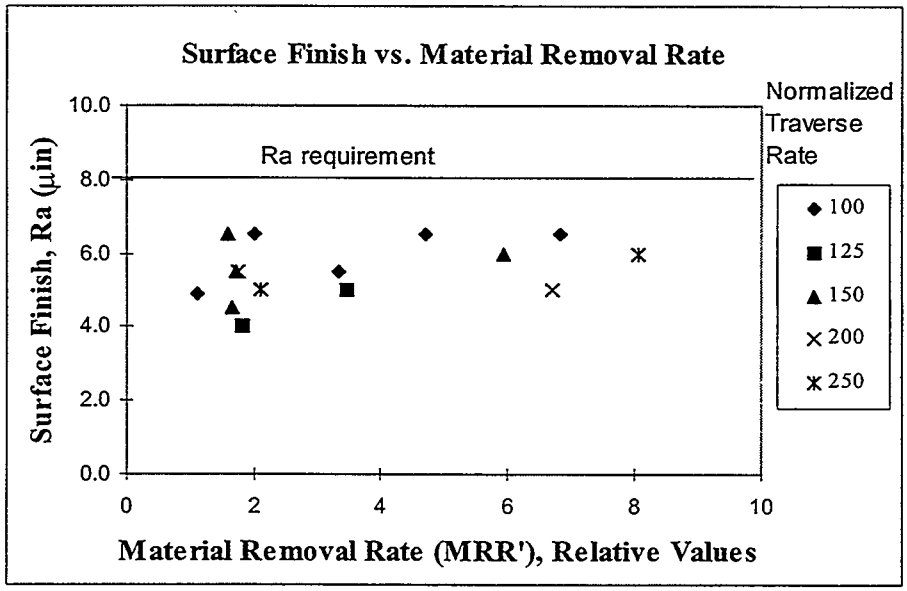


**Figure 30. Surface finish vs material removal rate for the experimental metal-bond wheel grinding NT551 valve stems at all traverse grinding conditions.**

There was evidence that the 320 grit experimental IGW would be an effective rough grinding wheel for valve profile grinding. During one test run, the experimental wheel removed (accidentally) 34 times the base depth of cut at the lowest traverse rate (i.e., MRR and MRR' = 34 times the base for the vitrified wheel valve grinding trial), and still generated a surface finish of only 12 µin. Ra.

The IGW wheel drew comparable grinding power to the vitrified wheel as shown in Figure 31. As shown in Figure 32, at a fixed material removal rate, the grinding power of the experimental grinding wheel decreased with increasing traverse rate. Since the grinding power data for the vitrified-bonded wheel in this test was not available, the data presented in these figures were from the ACMT program at the same 80 m/s wheel speed and the lowest depth of cut and traverse rate from Table 13 and Table 14.

It was observed that truing of the innovative grinding wheel was relatively difficult when the same conditions were used as for the vitrified wheel. This may be the cause of chatter marks on the valve stems. Truing and dressing of IGW needs to be optimized. Additional NAC evaluation of the IGW is being planned.

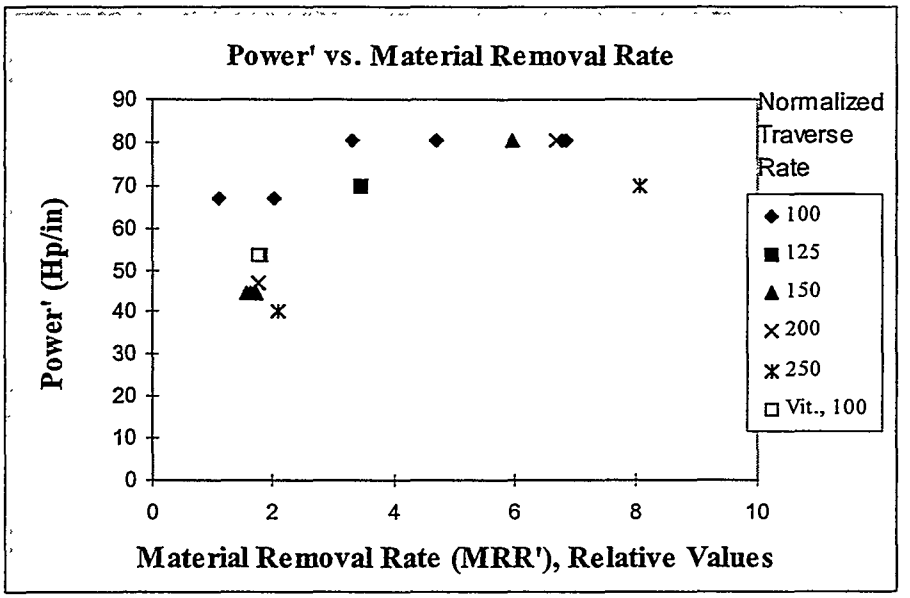


**Figure 31. Grinding power per unit wheel width vs material removal rate per unit wheel width for the experimental wheel at all valve finishing conditions vs the standard vitrified wheel.**

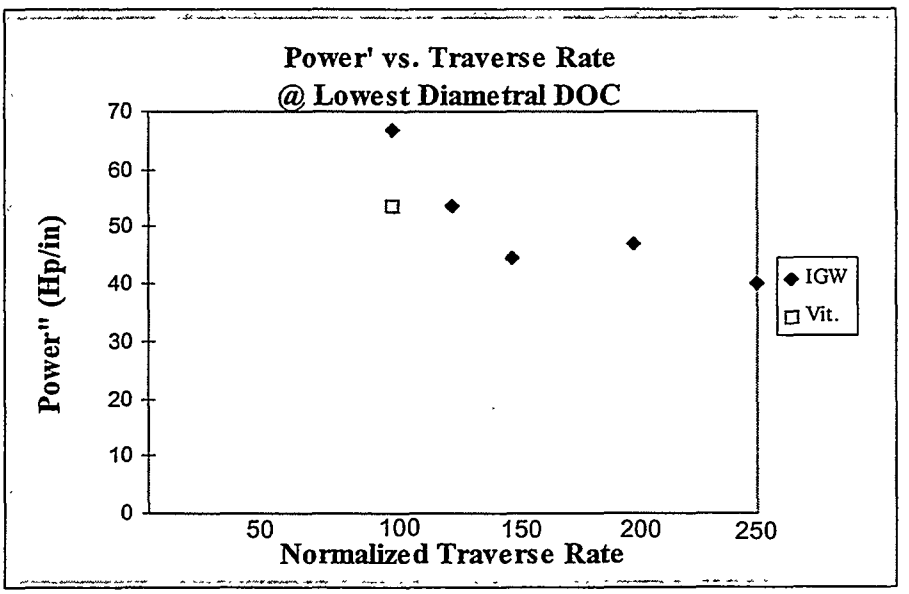


**Figure 32. Grinding power at the various traverse rates and at constant depth of cut.**

7.3.3.5. Supplemental Norton Advanced Ceramics Test at NRDC – Task 3.C.4.2.
After completion of the HGTC test, NAC performed supplementary cylindrical grinding tests at the SGIC Northboro R&D Center comparing the experimental metal-bonded Innovative Grinding Wheel vs a standard resin-bonded wheel. Wheels were evaluated in OD traverse grinding of silicon nitride rolling contact fatigue (RCF) specimens, and cylindrical plunge grinding of alumina disks. The internal test report is included in Appendix 4B.

**Test Wheels** -- The experimental metal-bonded IGW was a 406-mm-diameter AD320-75MXL1994-1/4. For both the traverse and plunge grinding tests the IGW was compared to a standard resin-bonded wheel, 355.6-mm-diameter, SD320R75B69.

**Dressing** -- The first attempt to true the IGW followed a conventional approach utilizing a motorized break dresser with a 4-inch-diameter 5SG80JVS dressing wheel at 0.8 speed ratio and 0.02 mm infeed. Initial attempts to true the IGW proved to be difficult and time consuming. To expedite truing time, the IGW was trued on the motorized break dresser rotating in an asynchronous direction for rapid truing. Once the wheel was trued, an additional 1 mm was trued in a synchronous direction to insure continuity between the resin-bonded wheel and the IGW. Both wheels were dressed manually with a 37C220kv dressing stick. Truing the IGW in a synchronous direction increased truing time by a factor of three when compared to truing a resin-bonded wheel. By reversing the dresser direction and truing in an asynchronous direction, truing time was improved by ~50%. The resin wheel was trued and dressed using the same procedure as the IGW. However, the resin wheel was trued completely in a synchronous direction. By cutting in an asynchronous direction the truing mode changes from a crushing or erosion mode of the bond as in synchronous dressing to a cutting mode and resulted in a less open structure. To insure that both wheels had the same structure, the IGW was trued an additional 1 mm once trued in a synchronous direction.

**Silicon Nitride RCF Rod Grinding Test** -- The first NRDC test evaluated the performance of the wheels on rolling contact fatigue (RCF) rods. The workpiece material was NT551 silicon nitride manufactured by Norton Advanced Ceramics. The test evaluated a semi-finishing OD traverse grinding operation that would simulate the production cycle. Both the IGW and standard resin wheel were 320 grit. Ordinarily, a resin-bonded wheel with a grit size of 6-12 microns (800 grit) is used for producing the finished surface. The final RCF rod has very demanding surface finish and tolerance requirements.

The workpiece rods were glued between two steel cylinders and held between centers on an OD grinding machine and traverse ground at 30 in./min at 250 rpm and 0.0001 in. diametric infeed. The wheel speed was 40 m/s (7874 SFPM). An equivalent of 30 rods were ground for both the IGW and resin wheel. During grinding, wheel spindle power was recorded and wheel diameters were measured before and after grinding.

There was no tangible increase in power above the idle power. There was no detectable wheel wear throughout the test for either wheel. The rod surface finish was the same for both wheels at approximately 0.43 μm Ra (17 μin.). Finer grit and modified grinding conditions would be required in a finishing operation for this part. The lack of increase in spindle power and lack of measurable wheel wear can be attributed to the relatively small infeed on the ceramic rod. The infeed amount was limited to the weak fixturing or holding strength of the glue. Therefore, improved fixturing would be required to test more aggressive grinding conditions to help differentiate between the IGW and standard wheels.

**Alumina OD Disk Grinding** -- The second test was a difficult OD plunge grinding operation of a high purity aluminum oxide disk, approximately 95-mm-diameter x 0.787-mm-thick. Therefore, the workpiece was thinner than the 12.7 mm wheel thickness and only a portion of the wheel face was utilized in grinding the OD.

After dressing (described above), the test consisted of three, 1 mm, plunge grinds. Grinding conditions are shown in Table 15.

**Table 15. OD plunge grinding conditions for alumina disks.**

| Pass Number | Wheel Speed (m/s) | Work Speed (RPM) | Plunge Speed (mm/min) | Radial Plunge Depth (mm) | Workpiece Diam. Start (mm) |
|---|---|---|---|---|---|
| 1 | 40 | 500 | 0.12 | 1.0 | 94.8 |
| 2 | 40 | 500 | 0.5 | 1.0 | 93.8 |
| 3 | 40 | 500 | 0.5 | 1.0 | 92.8 |

NRDC utilized a proprietary test method to measure very small radial wheel wear values. Before the three plunge tests, the wheel face was scanned to establish a reference datum. The wheel face was again scanned after each 1 mm deep grind. This test method can analyze the surface topography of a grinding wheel while it is rotating on the grinding machine. Figure 33 is an typical plot of the total wheel face wear after scanning the resin wheel before grinding and the changes created by each successive grind. The y-axis represents the radial direction displacement on the wheel face. The x-axis shows the wheel face in the direction parallel to the spindle. The wheel wear zone is apparent at approximately 4.5-6 mm on the wheel width. This scanning method allows topographic results to be used to determine changes in the wheel's radial wear to accuracy better then 0.5μm. Additionally, the technique can be utilized for determining truing conditions, spindle run out, and work piece analysis.

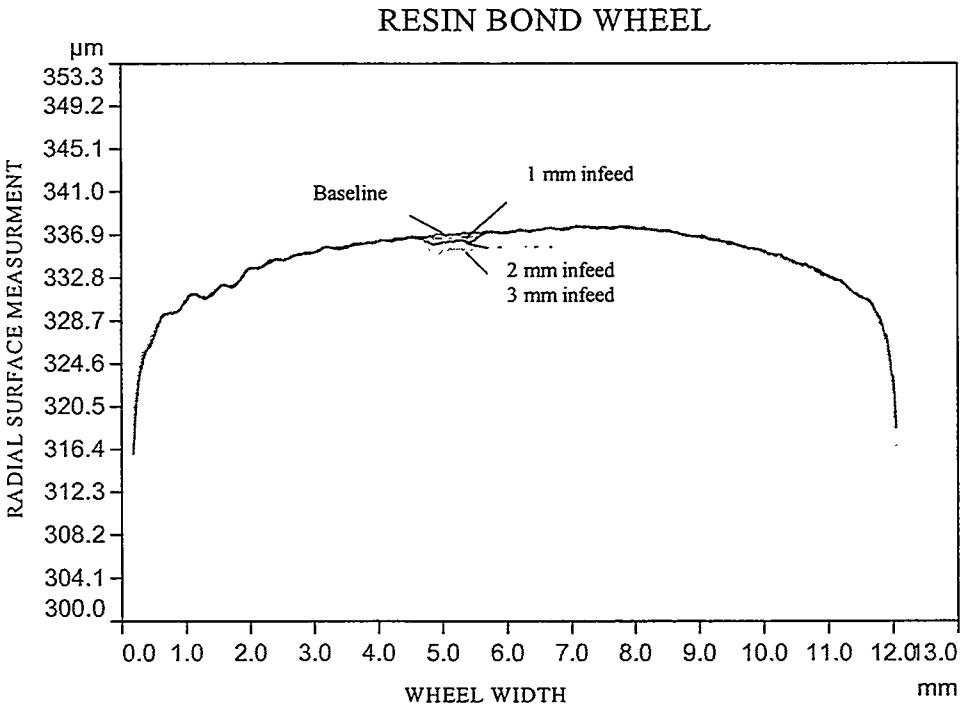


**Figure 33. Example of full wheel wear trace. Standard resin-bonded wheel after each 1 mm grind.**

Figure 34 and Figure 35 show enlarged areas of the wheel face profile throughout the tests for both the resin and innovative grinding wheels, respectively. Wheel profile data during the first 1 mm infeed was lost and not shown in Figure 35. Maximum radial wear was calculated from the differences between the 1, 2, and 3 mm infeed traces and the baseline. The IGW showed less wheel wear from the baseline to the final grind. Total radial wheel wear after 3, 1 mm grinds was 1.81 µm radial wear for the resin-bonded Grinding Wheel and 1.37 µm for the experimental metal-bonded IGW as shown in Figure 34 and Figure 35, respectively. After the disks were ground, the parts were inspected optically at 50x for edge chipping. In this operation, both wheels created continuous chipping along the circumference of the disk. For the IGW typical chip sizes were approximately 1.58 mm x 0.2 mm, whereas the resin-bonded wheel produced chips approximately 0.9 mm x 0.12 mm.

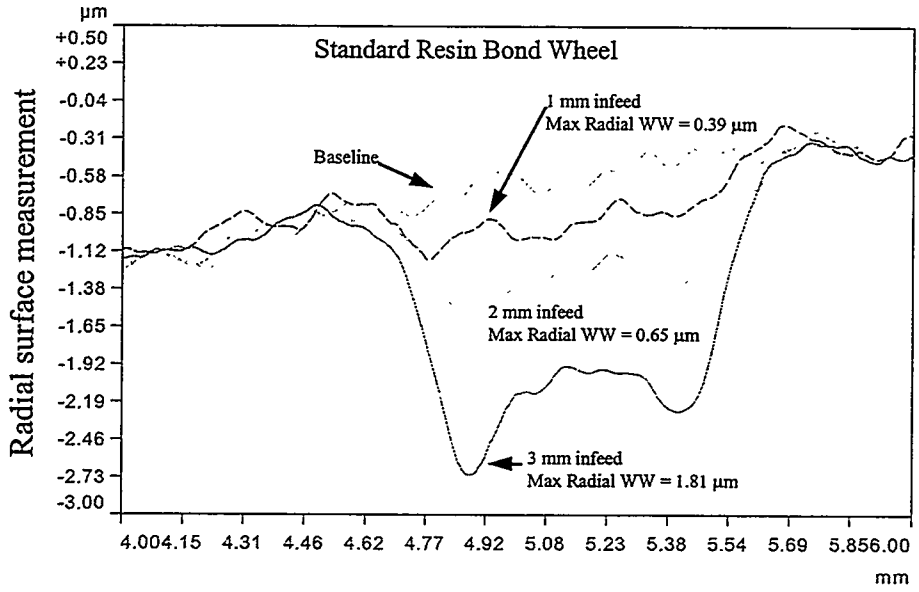


**Figure 34. Wear groove in standard resin-bonded wheel.**

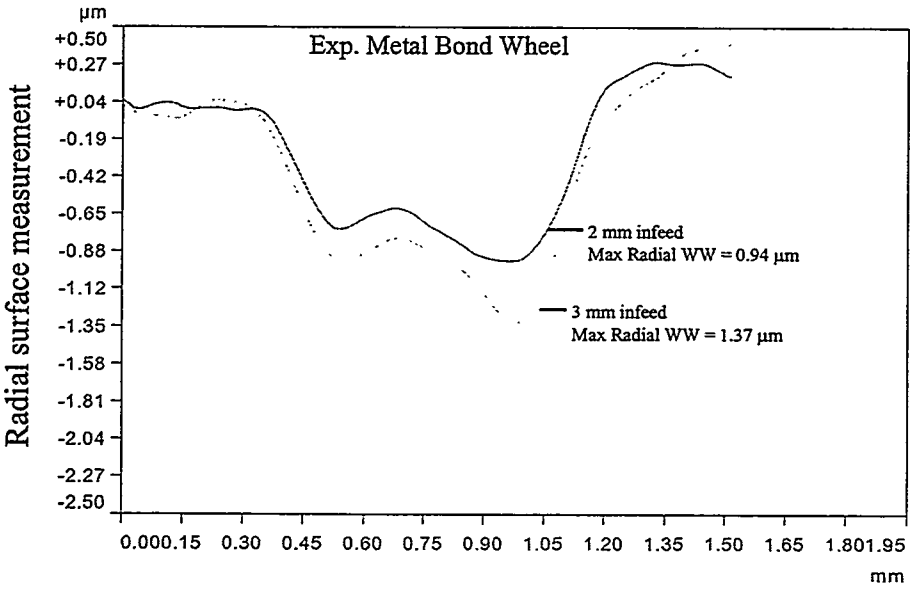


**Figure 35. Wear groove in experimental metal-bonded IGW.**

**Summary of the Supplemental NAC Tests at NRDC** -- Both NAC validation tests performed at the Northboro R&D Center demonstrated that the innovative grinding wheel was comparable to the resin wheel. It tended to have less wheel wear but appeared more difficult to true. In the RCF grinding test there were no differences noted in wheel wear, power, or surface finish. However, the current work fixturing did not allow for high material removal rates that could have better differentiated between the two wheels. In the alumina disk plunge test, the IGW demonstrated less wheel wear but tended to cause a greater degree of chipping than the resin wheel at the severe conditions chosen. Further grinding condition optimization for this OD plunge operation is recommended. Additionally, it should be noted that the IGW was a larger-diameter wheel then the resin wheel, which could contribute to some test variability.

## 7.4. CERAMIC SURFACE INTEGRITY -- TASK 4

The overall objective of this program was to develop a grinding wheel for cost-effective grinding of advanced ceramics. In the advanced ceramics industry, the effect on surface quality must be considered to truly evaluate any new cost-effective machining processes or products. We have used the concept of Surface Integrity as a general surface condition that includes surface finish and part tolerance, machining damage and retained strength, and surface residual stress. The Innovative Grinding Wheel program in both Phase I (small prototype wheels) and II (full size wheels) addressed the effect of the experimental wheels on the ground surface. The goal was to develop a cost-effective grinding wheel product that improved productivity but did not have an adverse effect on surface quality compared to standard commercial grinding wheel products.

In the Phase II program, Task 4.A comprised the surface integrity evaluation of NT551 silicon nitride specimens ground under the Task 2 in-house test. Task 4.B included the selected evaluation of specimens returned after the Task 3 independent grinding tests. Some surface integrity analysis was done by the independent validation test locations and reported under Task 3. In this section, the Task 4 post-grinding surface characterization was done by the Northboro R&D Center.

### 7.4.1. Surface Integrity of the In-House Grinding Test Specimens -- Task 4.A

7.4.1.1. Surface Finish Analysis. All surface finish data from the Task 2 grinding test, were on surfaces created by cylindrical plunge grinding without spark-out. These surfaces are normally rougher than traverse cylindrical grinding. Under Task 2, we reported preliminary surface roughness data measured at Norton's Higgins Grinding Technology Center. These data were shown in Figure 16, 17, 21, and 24 on Pages 30, 31, 34, and 37. Specimens were sent to NRDC for additional surface finish analysis. The NRDC surface finish data presented below were on different specimens or different plunge test surfaces than were reported above. All the HGTC surface finish data were on the twelfth, and last plunge grind of each condition. The NRDC data were taken from surfaces at the sixth plunge.

**Surface Finish Analysis by Contact Profilometry** -- Twenty NT551 silicon nitride samples were evaluated for average surface roughness and total waviness height using the Rank Taylor Hobson S3C 2-D Contact Profilometer. The diamond stylus had a tip radius of 2.5 μm. The results are shown in Table 16. The data cutoff length was 0.8 mm and the total assessment length was 5.6 mm for all parts. The cutoff selected is a typical length for evaluating a standard grinding procedure, and the assessment length was chosen to examine the waviness produced by the wheel within one plunge span.

**Table 16. Surface finish of NT551 samples.**

| Sample Number (Plunge #) | Wheel Bond | MRR ($in^3$/min/in) | Surface Speed (m/s) | Contact Ra 0.8 mm cutoff (μm) | Contact Wt, 0.8 mm cutoff (μm) | Non-Contact Ra (μm) |
|---|---|---|---|---|---|---|
| 13-24 | XL Metal | 0.29 | 32 | 0.65 | 1.1789 | 0.66 |
| 1-12 | XL Metal | 0.29 | 32 | 0.60 | 1.2679 | |
| 145-156 | XL Metal | 0.59 | 32 | 0.70 | 1.2807 | |
| 157-168 | XL Metal | 0.59 | 32 | 0.76 | 1.6447 | |
| 241-252 | XL Metal | 0.59 | 56 | 0.52 | 0.7957 | |
| 253-264 | XL Metal | 0.59 | 56 | 0.52 | 0.7895 | |
| 313-324 | XL Metal | 0.59 | 80 | 0.49 | 1.1532 | |
| 325-336 | XL Metal | 0.59 | 80 | 0.50 | 0.8253 | |
| (improved truing procedure was used for the remaining plunge specimens) | | | | | | |
| 709 | XL Metal | 1.05 | 80 | 0.63 | 0.8904 | |
| 721 | XL Metal | 1.26 | 80 | 0.60 | 1.0031 | 0.57 |
| 781 | XL Metal | 2.31 | 80 | 0.60 | 1.1963 | |
| 793 | XL Metal | 2.52 | 80 | 0.58 | 1.4071 | 0.54 |
| 949 | XL Metal | 4.20 | 80 | 0.51 | 1.0076 | |
| 961 | XL Metal | 4.41 | 80 | 0.49 | 1.4591 | 0.58 |
| 643 | Vitrified | 0.29 | 32 | 0.79 | 2.7131 | 0.80 |
| 655 | Vitrified | 0.84 | 32 | 0.77 | 9.9003 | |
| 973 | Resin | 0.29 | 32 | 0.45 | 0.7211 | 0.37 |
| 992 | Resin | 0.29 | 80 | 0.42 | 1.6577 | |
| 980 | Resin | 0.84 | 32 | 0.64 | 12.9327 | |
| 1004 | Resin | 0.84 | 80 | 0.43 | 1.9387 | |

The experimental metal-bonded samples up to plunge test number 336, used an early truing procedure. During the early part of the Task 2 grinding test, the truing technique was modified and improved and all subsequent surface finish data were on specimens ground after this modified truing technique. The surface finish data reported under Task 2, starting with Figure 16 on Page 30, came entirely from plunge tests using the improved truing technique.

Table 16 shows the average roughness ranged from 0.49 μm to 0.76 μm for the experimental metal-bonded (XL metal) wheel. An important observation was that surface roughness did not increase with an increase in Material Removal Rate (MRR) or surface speed. A similar trend was reported with the HGTC surface finish data. The specimen (#980) ground with the resin-bonded wheel at the higher MRR and lower speed conditions experienced problems during grinding. This is evident by the poor Ra and Wt.

Lower speed, 32 m/s, data analysis -- Figure 36 and Figure 37 show surface and waviness, respectively, versus MRR at a wheel surface speed of 32 m/s for the vitrified, resin, and XL metal-bonded wheels. All surfaces in these two figures were created by plunge grinding with no spark-out. Figure 36 indicates that the resin-bonded wheel gave a finer surface finish at low speed than either the experimental wheel #6 or the vitrified wheel. Results from Figure 37 show that the experimental wheel had a smaller maximum peak to valley height, Wt, in its waviness profile than samples ground with either the vitrified or resin-bonded wheel.

These results do not exactly match the trends reported in Task 2 by HGTC for Ra. At low speed the vitrified bond again had the poorest finish, but the Ra values for the experimental metal bond were poorer than for the resin bond. Under Task 2, we reported that for all tests at low speed, and using the same truing conditions, the experimental metal-bonded wheel was superior to both vitrified and resin-bonded wheels. The use of the improved truing technique should improve the Ra finish of the metal-bonded wheel at these low-speed conditions. Figure 37 shows the experimental metal-bonded wheel results in better waviness, Wt, at low speed conditions vs the vitrified and resin wheels, which is consistent with the data reported previously.

Higher speed, 80 m/s, data analysis -- Roughness and waviness information for the resin-bonded and experimental metal-bonded wheel are shown in Figure 38 and Figure 39 for a wheel surface speed of 80 m/s. The XL metal-bonded wheel maintained a fairly constant surface finish and waviness even at higher material removal rates. The surface finish produced with the resin-bonded wheel at the lower MRR was slightly better while the waviness factor, Wt, was slightly worse than the experimental metal-bonded wheel. These results are similar to those trends reported above under Task 2. Again, the data show remarkable consistency in surface finish of the experimental bond along a very wide range of cut rates.

Figure 40 demonstrates how the surface finish improved with an increase in surface speed at constant MRR for the metal-bonded wheel, as expected. Figure 41 displays the surface roughness data for all the samples for comparison purposes.

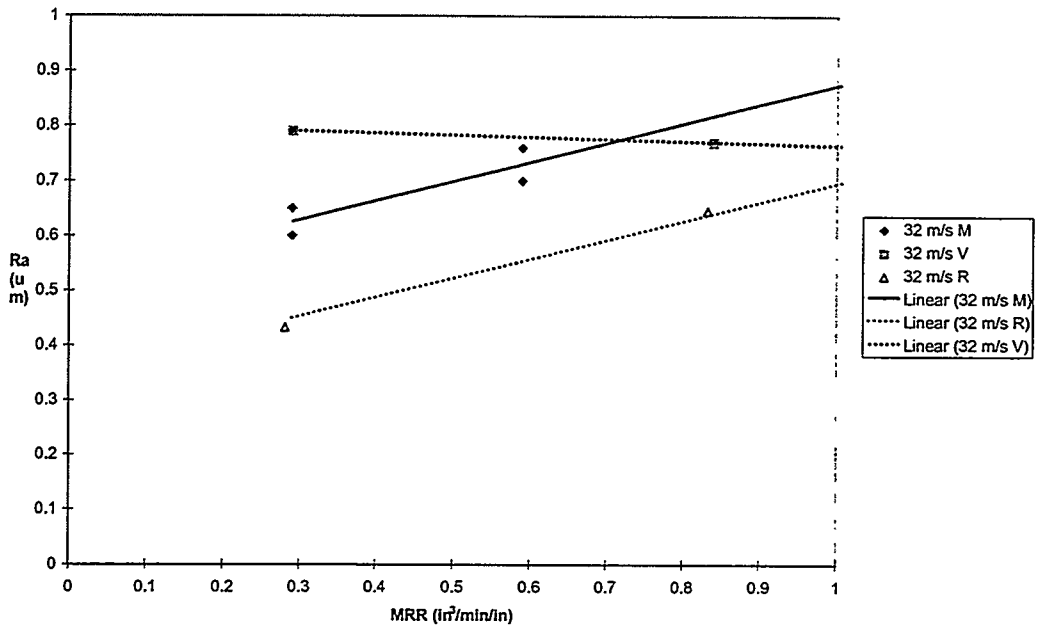


**Figure 36. Surface finish, Ra, vs material removal rate (MRR) at 32 m/s. M = XL metal, V = vitrified, R = resin.**

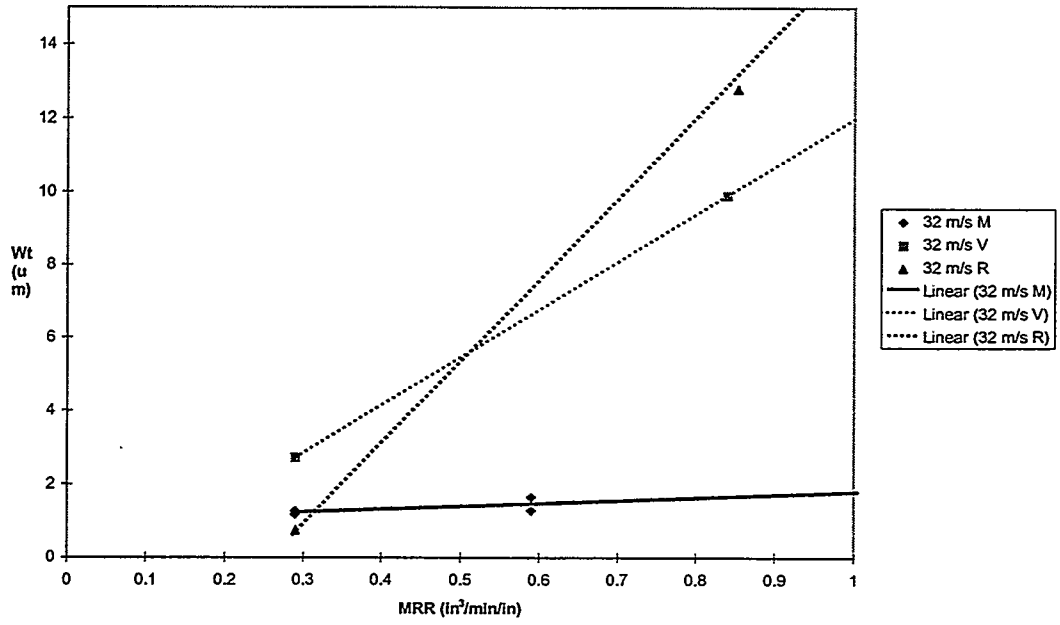


**Figure 37. Waviness, Wt, vs material removal rate at 32 m/s.**

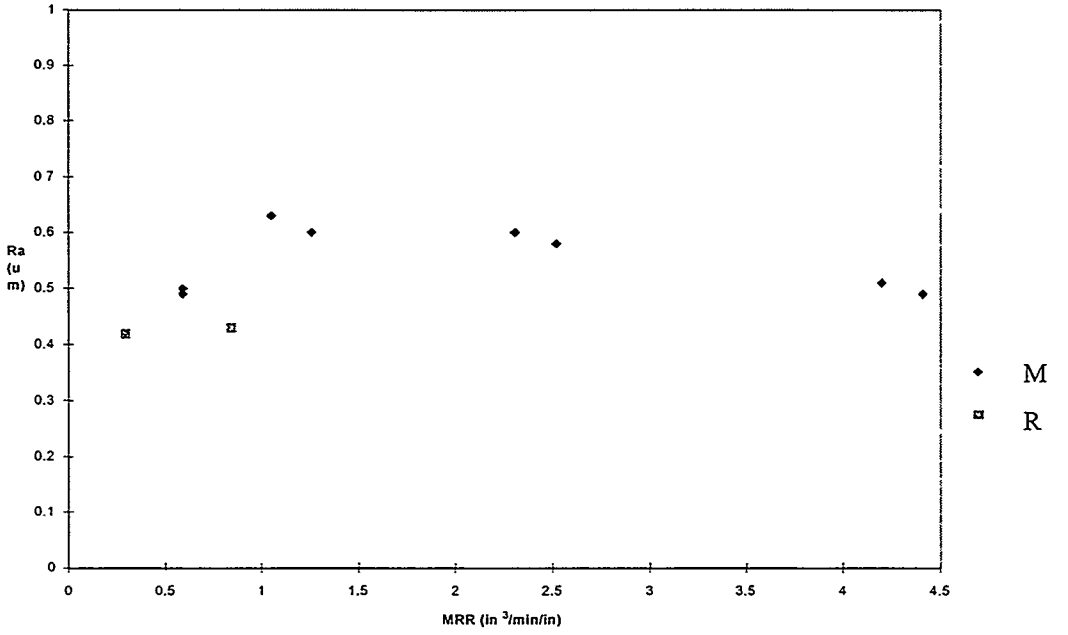


**Figure 38. Surface finish, Ra, vs material removal rate at 80 m/s. M = XL metal, R = resin.**

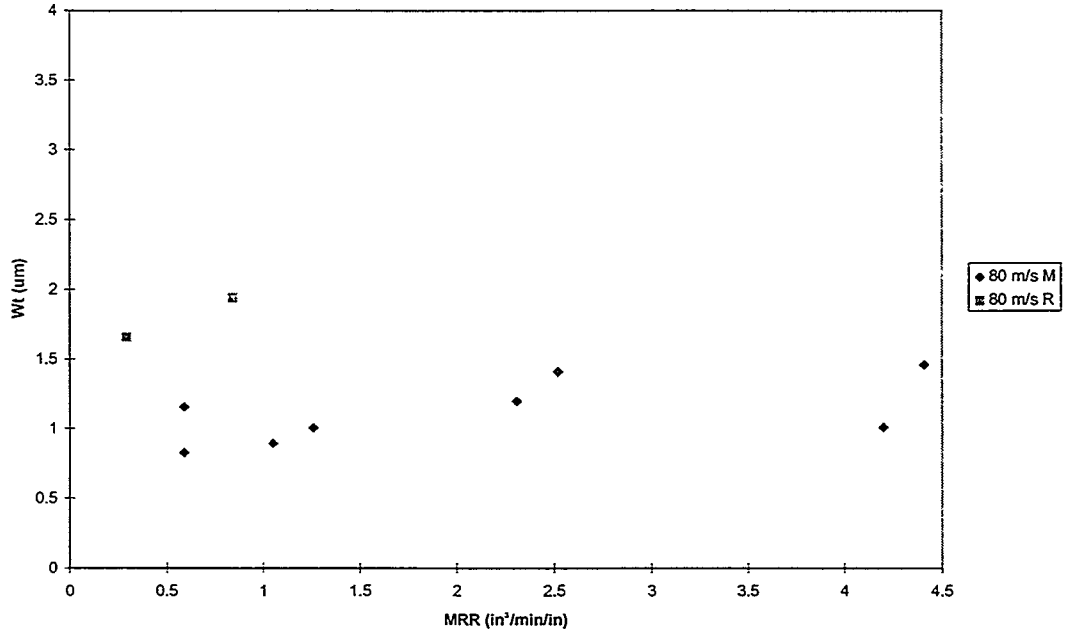


**Figure 39. Waviness vs MRR' at 80 m/s.**

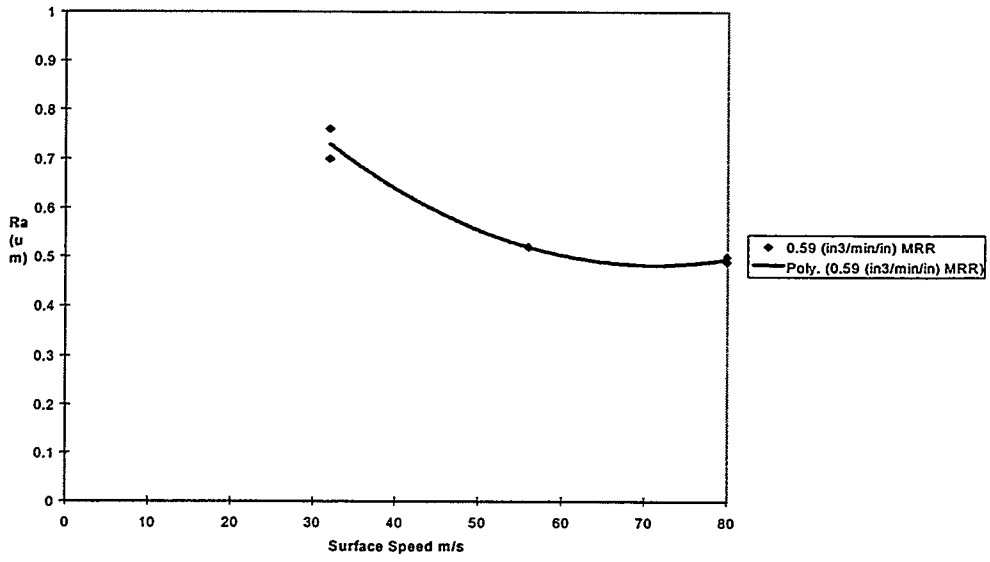


**Figure 40. Surface finish, Ra, vs wheel speed for XL metal-bonded wheel at constant MRR'.**

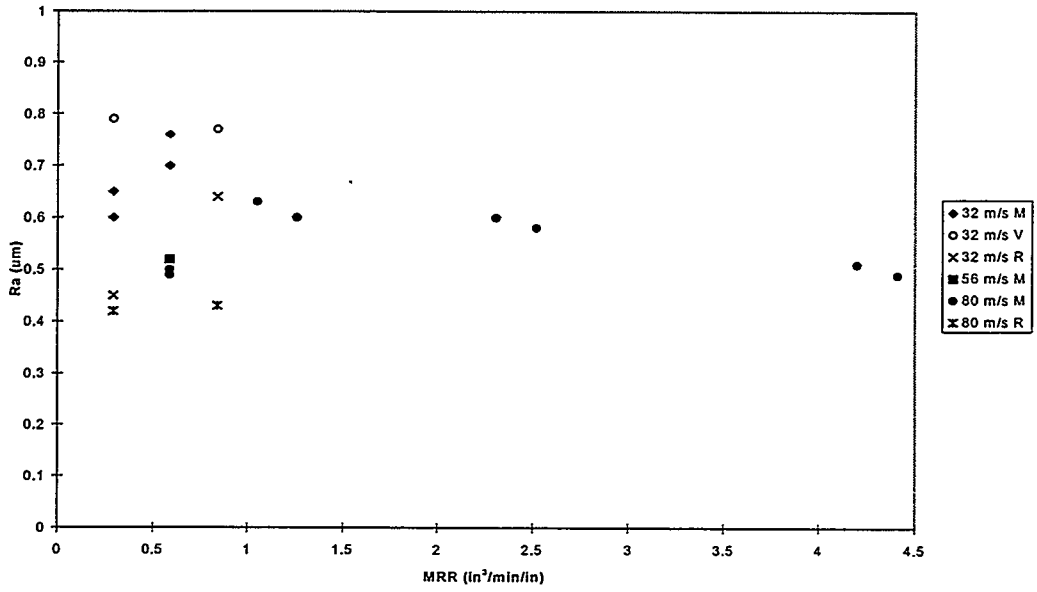


**Figure 41. Surface finish, Ra, vs MRR' for XL metal, vitrified, and resin-bonded wheel at 32, 56, and 80 m/s.**

**Surface Finish Analysis by Non-contact Interferometry** -- Six of the NT551 samples were analyzed using a Zygo NewView 100 Non-contact Scanning White Light Interferometer to confirm measurements made using the Rank Taylor Hobson contact profilometer. A 40x objective with a 1x image zoom was used, which views an area of 0.13 mm x 0.17 mm. A cylinder was removed from the image for evaluation purposes. The non-contact interferometry Ra data are listed above in Table 16 on Page 59. All of the measurements corresponded well with those taken using the contact profilometer.

**Surface Analysis by Atomic Force Microscopy** -- Three silicon nitride samples were selected for evaluation using Atomic Force Microscopy (AFM). Samples 13-24, 643, and 973 (from Table 16) were machined with a surface speed of 32 m/s and an MRR' of 0.29 $in.^3/min/in.$ using an experimental metal, vitrified, and resin-bonded wheel, respectively. An area of size 25 x 25 μm and an area of size 5 x 5 μm were measured on each sample and multiple readings were taken on sample 13-24 and 973. Table 17 summarizes Rq (root mean square value), Ra (average roughness) and Rmax (lowest-valley-to-highest-peak roughness) values for all three samples.

**Table 17. Surface roughness measured by Atomic Force Microscope.**

| Sample | 25 x 25 μm Image | | | 5 x 5 μm Image | | |
|---|---|---|---|---|---|---|
| | Rq(μm) | Ra(μm) | Rmax(μm) | Rq(μm) | Ra(μm) | Rmax(μm) |
| 13-24 | 0.44 | 0.36 | 2.18 | 0.25 | 0.11 | 0.78 |
| 13-24 | 0.26 | 0.20 | 1.75 | 0.17 | 0.18 | 1.13 |
| 973 | 0.23 | 0.19 | 1.46 | 0.14 | 0.08 | 0.59 |
| 973 | 0.69 | 0.57 | 3.30 | 0.20 | 0.12 | 0.82 |
| 643 | 0.51 | 0.43 | 3.61 | 0.16 | 0.14 | 0.81 |

Figure 42 is a typical AFM image, which shows peaks and valleys on its surface. The center valley is approximately 8 μm wide and 2.5 μm lower than its neighboring peaks. The area imaged by the AFM was smaller than the contact length of the wheel and all the valleys observed were less than one third of the abrasive grain size; therefore, it is likely that the peaks and valleys pictured are those produced by a single grit on the wheel. As shown in Table 17, there was a large amount of variability in roughness readings within each sample; therefore no further analysis was done using the atomic force microscope.

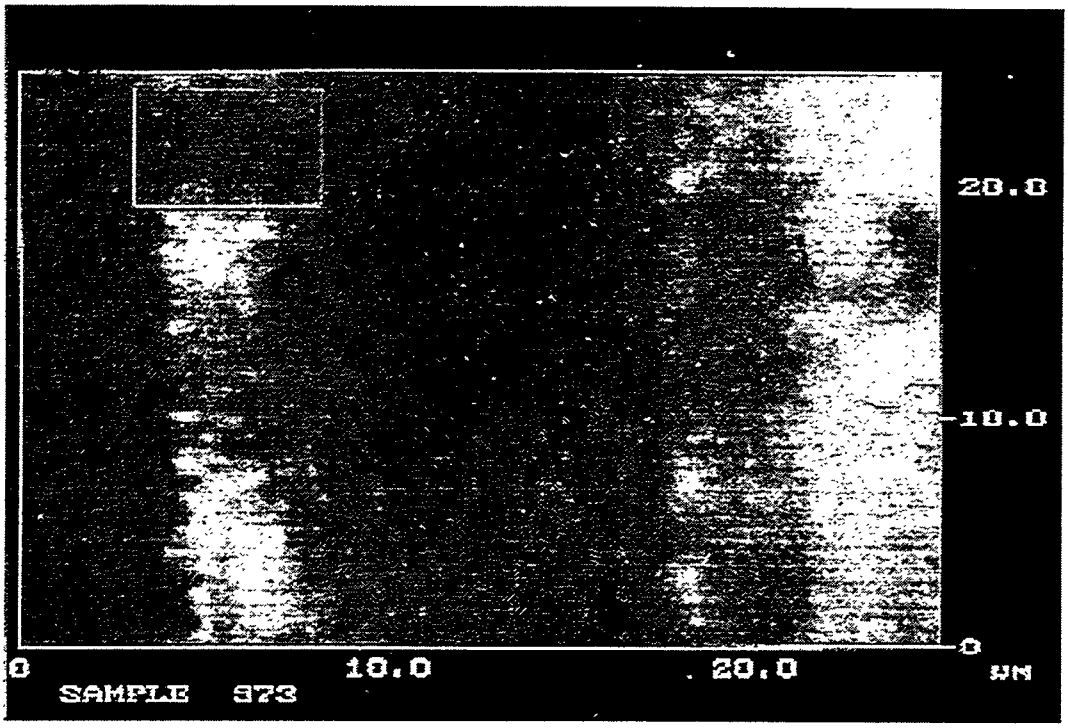


**Figure 42. Atomic Force Microscopy of NT551 silicon nitride, Sample 973, ground with resin-bond wheel at 32 m/s and 0.29 in.$^3$/min/in.**

7.4.1.2. Flexure Testing. NRDC evaluated flexural strength (retained strength) of the Task 2 NT551 rod specimens after conditioning the surface in traverse grinding. While the Task 2 in-house grinding test was in the plunge mode, the specimen surface condition was impractical for bend testing. Additionally, the Task 3 validation test by NAC/WGTC evaluated the experimental metal-bonded wheel in finish traverse grinding of diesel valve stems. For component qualification, it is considered more important to evaluate retained strength characteristics of the experimental wheel vs a conventional ceramic grinding wheel after traverse cylindrical grinding.

After the Task 2 plunge grinding test, some silicon nitride rod specimens were machined in traverse grinding mode using both the experimental metal and standard resin-bonded wheel. The wheel was fed at a depth of 0.127 mm (0.005 in.) to form a shoulder and then traversed to the end of the rod at a rate of 406 mm/min (16 in./min). These conditions are relatively severe compared to standard baseline finishing grinding. This process was repeated until the diameter of the rod was reduced to approximately 5.8 mm (0.23 in.). The total stock removed on each specimen in the traverse mode was approximately 0.25 mm (0.01 in.), which would be more than enough to remove damage from the previous plunge grind. The wheel speed was 80 m/s and the work speed was 750 rpm resulting in a material removal rate of 2.9 in.$^3$/min/in.

Three-point bend, 20-mm-span, flexure testing results for 9 samples machined with the experimental metal-bonded wheel and 10 samples ground with the standard resin-bonded wheel are shown in Table 18 and Table 19. The specimens ground with the resin bond had 5% higher average flexural strength, which is probably not significant. Results for these two data sets did not center around the same mean; however, the range of strengths for samples machined with the resin-bonded wheel overlaps the range of strengths for samples machined using the experimental wheel.

The flexural strengths in Table 18 and 19 appear good, considering they were cylindrically traverse ground, 5.8-mm-diameter specimens. Flexural strengths of ASTM C1161-B longitudinally ground specimens in 4-point bend for this material, including tiles from the same batch, are typically between a mean of 890 to 990 MPa.

Figure 43 is a Weibull-analysis plot for the limited number of data points in Table 18 and Table 19. The figure shows the Weibull modulus, $\beta$, and characteristic strength, $\eta$, for specimens traverse ground with experimental and resin-bonded wheels. There is a 63.2% probability that a sample will fail at or above its characteristic strength. The metal-bonded wheel had a higher Weibull parameter, 28.6, and a 7% lower characteristic strength, 800.89 MPa, than the resin-bonded wheel that had a Weibull modulus and strength of 15.3 and 858.59 MPa, respectively. Originally, it was thought that there might be two separate flaw populations for the experimental metal-bonded wheel data; however, upon SEM examination it was determined that only one mode of failure existed. We do not believe that these Weibull plot differences are significant.

**Table 18. Flexure strength and surface finish of NT551 ground with experimental metal-bonded IGW.**

| Sample Number | Diameter (mm) | Peak Load (kg) | Flexural Strength (MPa) | Avg. Surface Roughness Ra (μm) | Total Waviness Height Wt (μm) |
|---|---|---|---|---|---|
| 55 | 5.849 | 302.10 | 754.02 | 0.337 | 1.9836 |
| 60 | 5.863 | 308.50 | 764.49 | 0.4675 | 0.6118 |
| 61 | 5.811 | 317.10 | 807.09 | 0.3872 | 2.1154 |
| 67 | 5.864 | 330.60 | 818.84 | 0.5351 | 0.7154 |
| 68 | 5.874 | 331.40 | 816.64 | 0.5365 | 1.1956 |
| 69 | 5.861 | 300.50 | 745.43 | 0.4867 | 0.8297 |
| 70 | 5.849 | 331.50 | 827.40 | 0.4614 | 1.5422 |
| 75 | 5.837 | 291.90 | 733.07 | 0.4817 | 0.8155 |
| 76 | 5.848 | 319.90 | 798.86 | 0.5189 | 0.3341 |
| **Mean** | | | **785.09+/-33.78** | **0.468** | **1.127** |

**Table 19. Flexure strength and surface finish of NT551 ground with standard resin-bond wheel.**

| Sample Number | Diameter (mm) | Peak Load (kg) | Flexural Strength (MPa) | Avg. Surface Roughness Ra (μm) | Total Waviness Height Wt (μm) |
|---|---|---|---|---|---|
| 17R | 5.810 | 300.10 | 764.22 | 0.3758 | 0.3857 |
| 18R | 5.827 | 326.70 | 824.69 | 0.3453 | 0.4324 |
| 23R | 5.853 | 354.20 | 882.25 | 0.3993 | 1.1554 |
| 24R | 5.854 | 317.60 | 790.68 | 0.3682 | 1.1019 |
| 31R | 5.841 | 333.70 | 836.32 | 0.3861 | 0.907 |
| 32R | 5.852 | 348.30 | 868.00 | 0.4009 | 0.6923 |
| 39R | 5.900 | 367.40 | 893.43 | 0.3954 | 0.2586 |
| 40R | 5.888 | 261.90 | 640.78 | 0.4057 | 0.7753 |
| 45R | 5.887 | 373.80 | 919.71 | 0.4142 | 0.6401 |
| 46R | 5.886 | 348.60 | 853.78 | 0.3948 | 0.3582 |
| **Mean** | | | **827.39+/-76.48** | **0.3886** | **0.6707** |

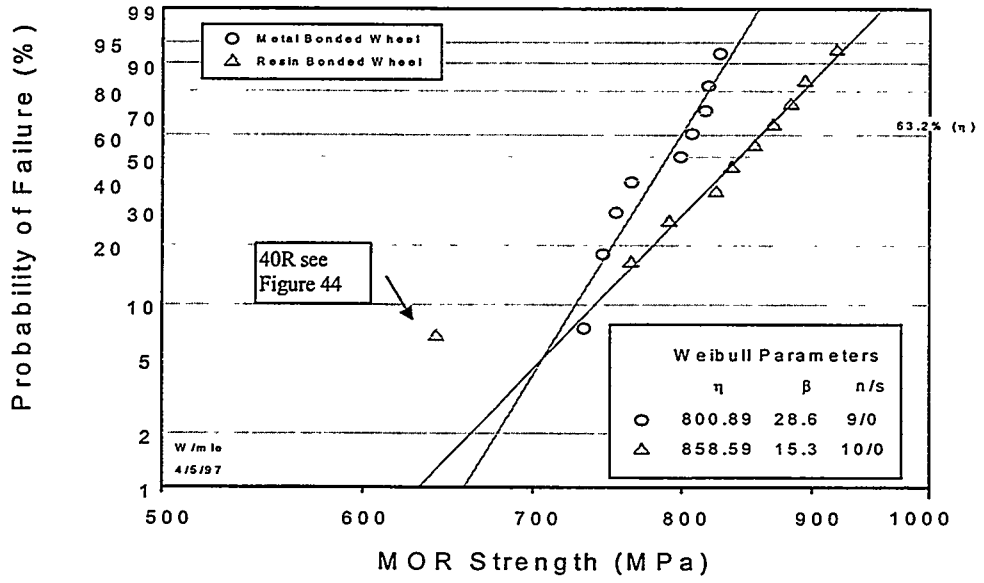


**Figure 43. Weibull analysis for NT551 samples in 3-point bend flexure. η = characteristic strength, β = Weibull Modulus, n = number of samples, s = number of samples suspended.**

**Surface Finish of Flexural Specimens** -- Surface finish of the traverse ground specimens was measured after flexural testing. Samples were evaluated for average surface roughness, Ra, and total waviness height, Wt, using the Rank Taylor Hobson S3C 2-D Contact Profilometer and a 2-μm-tip-radius diamond stylus. The data cutoff length was 0.8 mm and the total assessment length was 5.6 mm. The data are shown in Table 18 and Table 19. For these specimens, surface finish was better for the standard resin-bond wheel. Average Ra, for traverse ground samples with the experimental metal bond were slightly better than roughness measured on plunge-ground samples. The plunge ground specimens at 80 m/s in this MRR' range typically had Ra values of 0.5 to 0.6 μm.

**Fractography** -- Fractography was performed using both optical microscopy and scanning electron microscopy (SEM). As expected, the failure origin was located on or near the tensile surface of the rod. We observed only one failure origin at an area of obviously extreme machining damage. This particular rod, Number 40R, was ground with the resin-bonded wheel and exhibited the lowest flexural strength of any of the specimens, 641 MPa. The data point is shown in Figure 43. The Scanning Electron Micrograph fracture surface of sample 40R is shown in Figure 44. A deep machining groove can be seen at the top of the micrograph and the flaw origin area is pointed out by arrows. This appears to be a classic median-type crack below the grinding groove and parallel to the grinding direction. Note that there is no evidence of unusually rough surface finish on other areas of this specimen, as shown in the Ra and Wt data for 40R in Table 19.

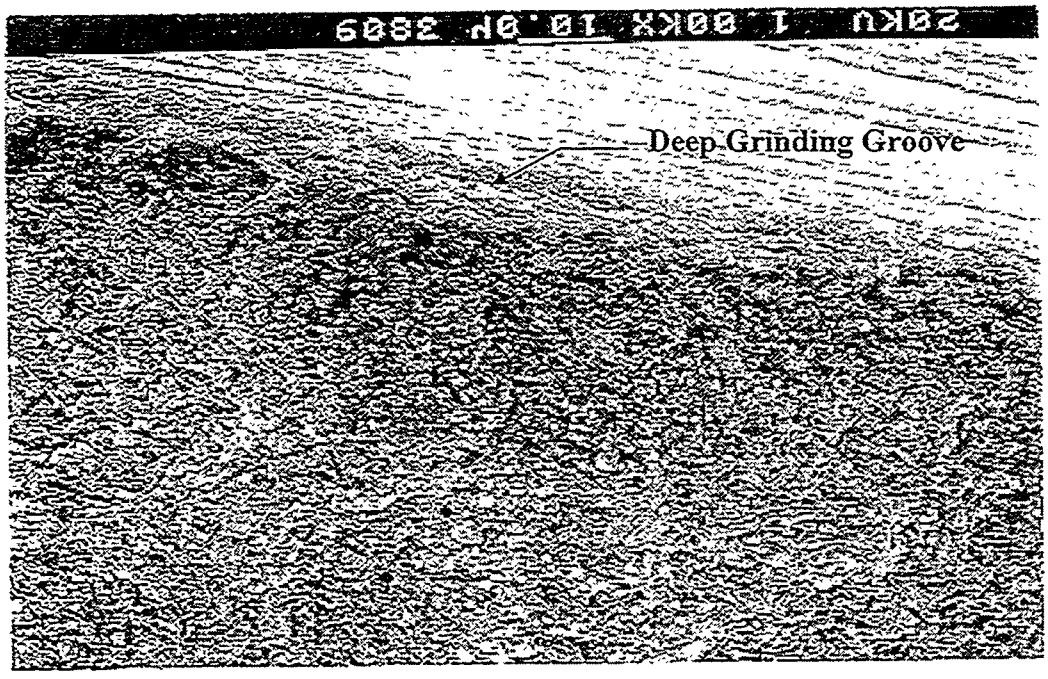


**Figure 44. Fracture surface of Sample 40R showing failure due to machining.**

7.4.1.3. Liquid Dye Penetrant NDE. Selected silicon nitride rod samples were examined for cracks using fluorescent liquid dye penetrant (LDP). Three of the samples (one for each bond-type wheel) were cylindrically plunge ground at a wheel speed of 32 m/s and a material removal rate of 0.29 $in.^3$/min/in. We did not observe any obvious machining-damage cracks in the grinding grooves. LDP highlighted typical edge cracking and chipping. One specimen had a severe catastrophic crack believed to be unrelated to the grinding operation.

We examined two samples after cylindrically traverse grinding at a wheel speed of 80 m/s and an effective MRR' of 2.9 $in.^3$/min/in. One sample was ground with the experimental metal-bonded wheel and one with the standard resin wheel. We observed no machining damage. The sample ground with a standard resin wheel had a longitudinal crack that was not considered machining related.

Fractography and LDP did not give evidence that silicon nitride rods ground with the experimental metal bond resulted in severe or different machining damage than rods ground with either the standard resin or vitrified-bonded wheel.

7.4.1.4. Residual Stress.

**Introduction** -- The Northboro R&D Center and the ORNL High Temperature Materials Laboratory (HTML) Residual Stress User Center collaborated on an experiment to characterize the surface residual stress of the cylindrical $Si_3N_4$ surfaces ground with the experimental metal-bonded versus a standard resin-bonded wheel. As noted in the Introduction Section 5.2.3., Reliability – Ceramic Surface Integrity, residual stress in ground surfaces can affect component strength and wear resistance [6-9]. While grinding conditions and grit size are expected to affect surface residual stress, it was not certain whether different wheel-bond compositions alone would produce significantly different residual stress.

**Experimental** -- Testing was completed at Brookhaven National Lab (BNL) by the experimental team of Dawn Murphy (NRDC), Jian Ming Bai (BNL), and Thomas Watkins (ORNL). The final test report was completed by the research team [25]. Below is a summary of the test report.

Four NT551 samples underwent residual stress testing at Oak Ridge National Lab's X-14A beamline at the National Synchrotron Light Source at Brookhaven National Lab. The experiment evaluated residual-stress characteristics of silicon nitride after grinding with the experimental metal-bonded and the standard resin-bonded wheels, in both the traverse and plunge modes. The samples and their machining conditions are listed in Table 20. In addition to testing these four samples, a spare sample was pulverized, strained through a 325-mesh sieve and used to provide the average strain-free interplanar spacing for calculation purposes.

**Table 20. The β-$Si_3N_4$ samples (NT551) and machining conditions.**

| Sample ID | Wheel type | MRR ($in.^3$/min/in.) | Surface Speed (m/s) | Grind Mode | Diameter (mm) |
|---|---|---|---|---|---|
| 72 | XL Metal | 2.9 | 80 | Traverse | 5.87 |
| 22R | Resin | 2.9 | 80 | Traverse | 5.87 |
| 13-24 | XL Metal | 0.29 | 32 | Plunge | 6.35 |
| 973 | Resin | 0.29 | 32 | Plunge | 6.27 |

Table 21 lists the experimental conditions for the grazing incidence X-ray diffraction (GIXD) measurements conducted at ORNL's X-14A beamline at the National Synchrotron Light Source, BNL [26]. A 6-axis goniometer was employed for the stress measurements using the "Ω-goniometer geometry" [27]. The (323) reflection from the β-$Si_3N_4$ (141.3 °2Θ) was utilized for the strain measurements in the samples. The 2Θ scans were made as a function angle of incidence, α, and azimuthal angle, ϕ. The width of the beam was 6.5 mm for examining the strains in the hoop direction and 0.5 mm for examining the axial direction. The receiving slits were set at 2 x 10 mm (V x H) and 10 x 10 mm for examining the strains in the hoop and axial directions, respectively. Figure 45 is a schematic of the GIXD experimental setup showing the hoop and axial directions. Further details of the experimental setup and procedure are contained in the HTML test report [25].

**Table 21. Experimental conditions of the X-ray measurements.**

| **Parameter** | **Condition** |
|---|---|
| Equipment | 6 Axis Huber goniometer<br>Xe-$CO_2$ proportional counter |
| Radiation | Synchrotron: E=8.054 keV; λ = 1.54058 Å |
| Vertical divergence | <0.03° |
| Horizontal divergence of incident beam | 0.2 & 0.3° |
| Analyzer crystal | (111) oriented Ge crystal (d=3.266 Å):<br>angular acceptance = 0.01° |
| Specimen to back slit distance | 104 cm |
| Tilt axis and angles | Ω=α; 0.4, 0.6, 1.0, 2.0, 3.0, 7.0, 10.0, 30.0° |
| Azimuthal axis and angles | ϕ; 0 & 90° |
| Scans | 0.005 - 0.01 °2Θ/step; 2-4 x$10^6$ cts/step; 140<2θ<142° |

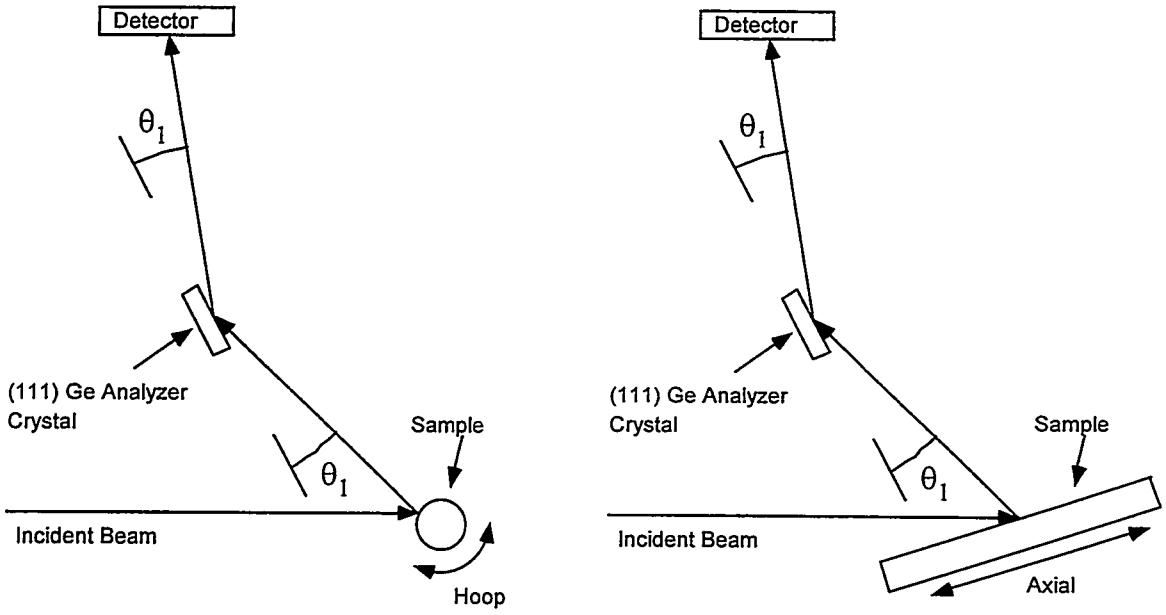


**Figure 45. Schematic of GIXD experimental set-up.**

The 1/e penetration depth, $\tau$, was calculated using Parratt's [28] equation as described by Ballard *et al.* [29]. The data taken at $\alpha \leq 1$ were corrected for the refraction effect [29]. The penetration depth increases steadily as a function of incidence angle after the incidence angle exceeds the critical angle. The residual stresses were calculated using the method of Winholtz and Cohen [30]. Since data could only be obtained in the axial direction, the other directions with respect to the sample surface were assumed to be the same as the axial direction.

**Results** -- No change in peak position (residual stresses) was observed for any of the samples in the hoop direction (direction perpendicular to the grind lines). Since large peak shifts are expected based on previous work with flat specimens [31], it was thought that that the X-rays were penetrating too deeply due to the curved surface. A new procedure was later devised to circumvent this problem, which can be used in the future.

In contrast, large changes in peak position were observed for all samples in the axial direction (perpendicular to the grinding lines in traverse- and plunge-ground rods) indicating large compressive residual stresses relative to the strain-free peak position from the $\beta$-$Si_3N_4$ powder. Figure 46 shows the raw data from the GIXD experiments for rods ground with both wheels in the (A) traverse-ground and (B) plunge-ground modes. This figure plots the two-theta angle vs incidence angle from which the residual stress vs specimen depth were derived. The profiles show the peak position (residual stress) changing rapidly with depth. Here, as the depth of penetration was increased the X-ray penetration volume contained more of the material that was either experiencing tension or no stress at all. Thus, the average signal from this volume results in stresses that approach zero, which makes sense considering force-balance constraints.

Figure 46 (A) for traverse-ground specimens showed effectively the same peak positions for both wheel types, indicating little difference in residual stress. Figure 46 (B) for plunge-ground specimens showed different peak positions indicating different residual stress between the two wheels.

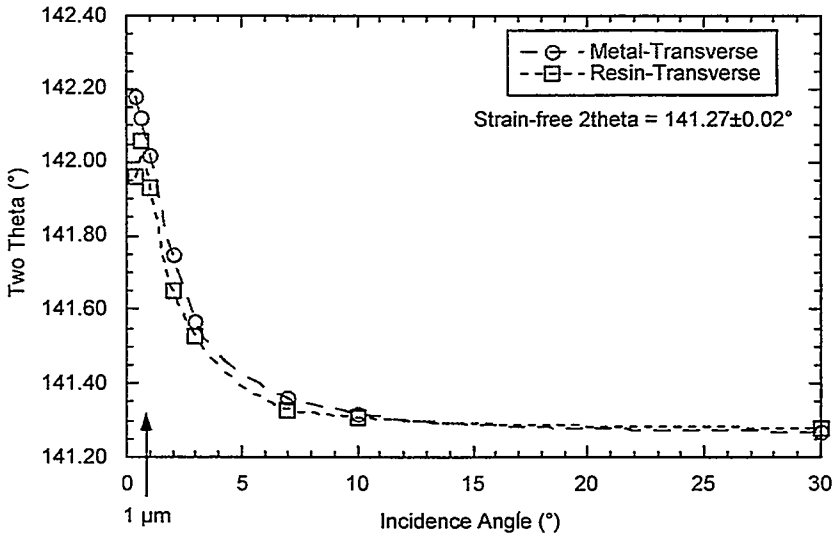


(A) Traverse ground NT551.

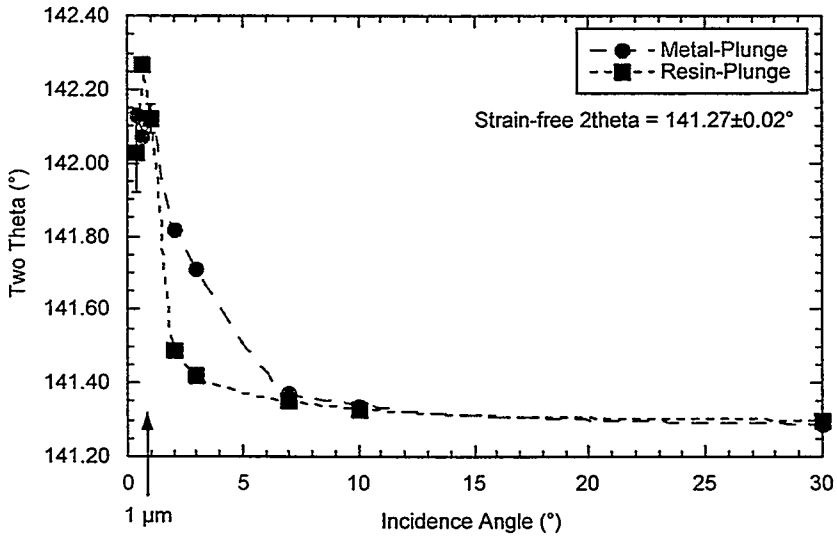


(B) Plunge ground NT551.

**Figure 46 The observed (323) β-$Si_3N_4$ peak positions as a function of the angle of incidence the samples. (A) Traverse ground. (B) Plunge ground.**

Figure 47 and Figure 48 are the summary residual stress plots vs depth below the specimen surface for the traverse-ground rods and plunge-ground rods, respectively. In each figure (A) is the experimental metal-bonded wheel and (B) is the standard resin-bonded wheel. Figure 47 and Figure 48 show the calculated residual stresses (open circles) for each X-ray penetration depth from the tau profile. The Z profile (solid line) represents an estimate of the actual stress as a function of depth from the sample surface and was deconvoluted from the tau profile using the analysis of Zhu *et al.* [32]. Note that the Z-profiles are *estimates* and not unique for the data. The reconstructed tau profile (dotted line) was calculated from the solid line and is a measure of the quality of the solid line. The fits of the reconstructed tau profiles to the original tau profile were reasonable indicating that the Z-profile estimates are good ones. Interestingly, the reconstructed tau profiles from the samples ground with the metal-bonded wheels fit to the original tau profiles better than those from samples ground with the resin-bonded wheels. While the fit could have been improved for the samples ground with the resin-bonded wheels, the resulting Z-profile would have been unrealistic. This suggests that the data from the samples ground with the resin-bonded wheels was not well described by the quadratic function used in the Z-profile calculation.

In general, the tau profiles show the residual stresses decaying rapidly with depth. Interestingly, a maximum is observed at low angles of incidence for both traverse- and plunge-ground samples with resin-bonded wheels. In Figure 47 and Figure 48, the residual stresses transition from compressive to tensile between 2 and 6 μm. Table 22 summarizes the residual stress gradient from Figures 48 and 49 showing the maximum compressive and tensile stresses and zero stress depth for each wheel and grinding mode. Data from this procedure on curved surfaces tend to give higher stresses and shallower zero stress depth than previous data on silicon nitride on flat surfaces using a curvature residual stress technique by Samuel *et al.* [7].

As noted, Figure 46 (A) indicated that the samples that were traverse-ground with the metal-bonded and resin-bonded wheels have effectively the same peak positions, indicating little difference in residual stress state between them. A comparison of the data in Figure 47 (A) and (B) and Table 22 confirms that the residual stresses were similar.

In contrast as noted above in Figure 46 (B), the samples that were plunge-ground with the metal-bonded and resin-bonded wheels have different peak positions, indicating different residual stress states between the two wheel types. Specifically, as shown in Figure 48 (A) and (B) and Table 22, the residual stress gradient was steepest in the sample that was plunge ground with the resin-bonded wheel than for any wheel/grinding mode combination. The data in Figure 48 also indicate that a significant reduction of residual stress occurs in between the 2 and 8 μm range for the sample that was plunge ground with the resin-bonded wheel relative to the metal-bonded wheel.

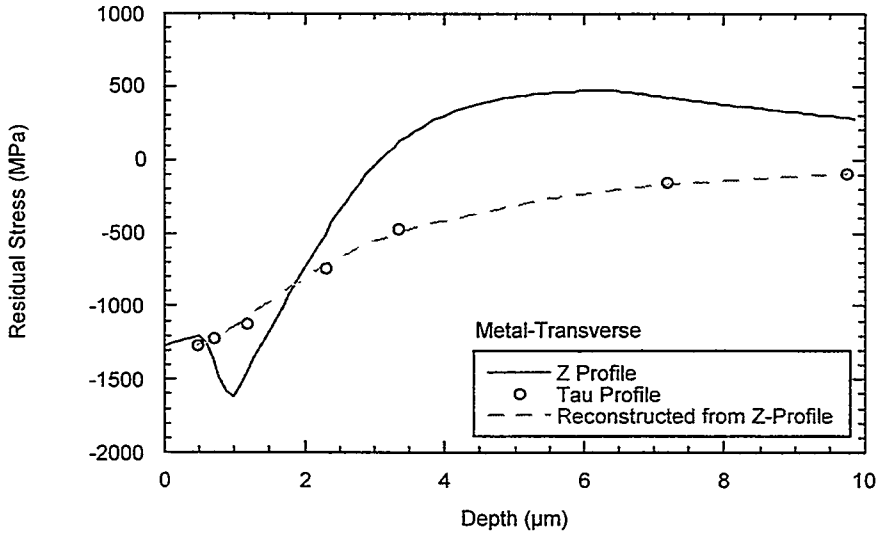


(A) Experimental metal-bonded wheel, traverse grinding.

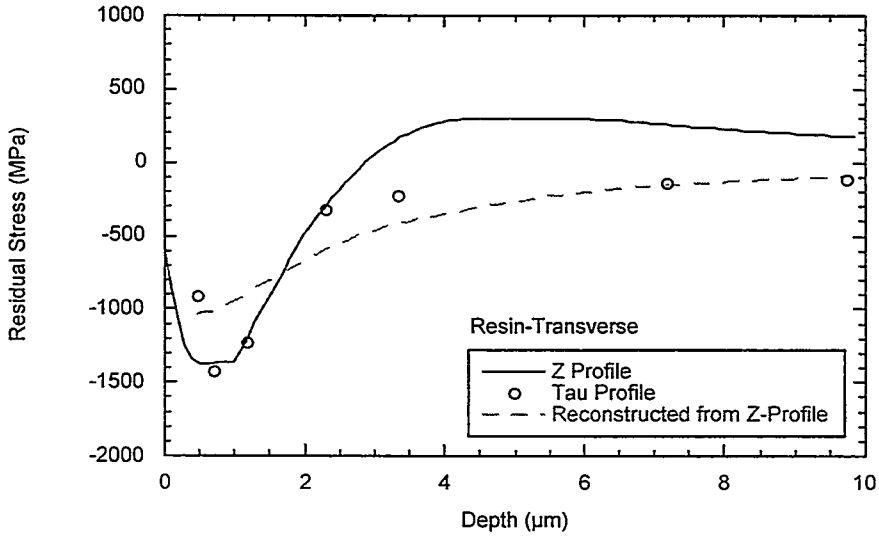


(B) Resin-bonded wheel, traverse grinding.

**Figure 47. Residual stress tau and Z-profiles vs depth for traverse-ground NT551 silicon nitride. (A) Experimental metal-bond. (B) Standard resin-bond.**

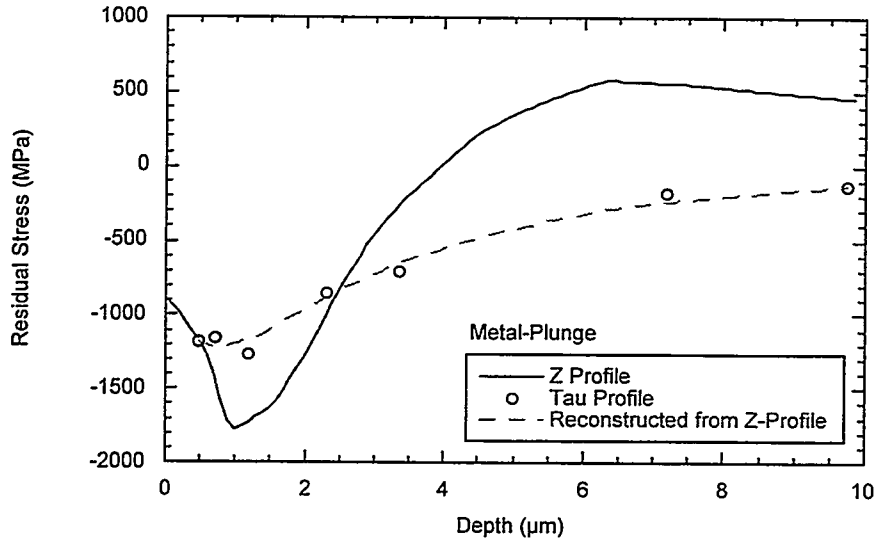


(A) Experimental metal-bond, plunge grinding.

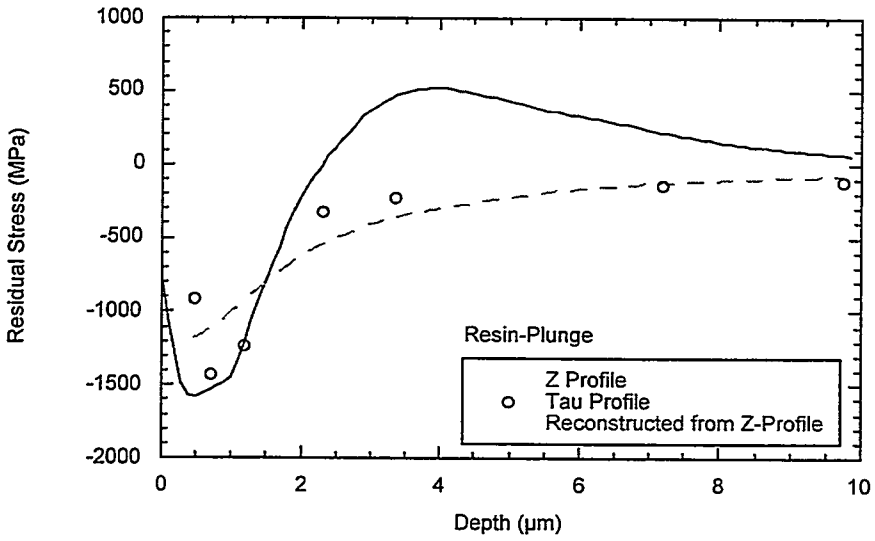


(B) Resin-bonded wheel, plunge grinding.

**Figure 48. Residual stress tau and Z-profiles vs depth for plunge-ground NT551 silicon nitride. (A) Experimental metal-bond. (B) Standard resin-bond.**

**Table 22. A comparison of the residual stress gradient features of the tau- and Z-profiles for the β-$Si_3N_4$ samples examined.**

| Sample ID | Wheel type | Grinding Mode | Maximum Compressive/ Tensile Residual Stresses (MPa) | Zero Stress Depth (μm) |
|---|---|---|---|---|
| 72 | XL Metal | Traverse | -1300/ 400 | 3 |
| 22R | Resin | Traverse | -1400/ 300 | 3 |
| 13-24 | XL Metal | Plunge | -1250/ 500 | 4 |
| 973 | Resin | Plunge | -1450/ 500 | 2.5 |

**Residual Stress Characterization Summary and Conclusions** -- Cylindrical β-$Si_3N_4$ samples (NT551) were examined using grazing incidence X-ray diffraction. Synchrotron radiation was used to provide the necessary intensity with the parallel beam optics required for these highly curved samples (6-mm-diameter). A large residual stress gradient as a function of depth was observed in the axial direction of the samples. The resulting τ- and Z-profiles indicated that the residual stresses in the samples that were traverse-ground were effectively the same, independent of wheel type. In contrast, substantial differences in residual stresses were found in the samples that were plunge ground. The residual stresses at the surface were the severest in the sample that was plunge ground with a resin-bonded wheel. The residual stresses at the surface were the mildest in sample that was plunge ground with a metal-bonded wheel. The residual stresses at the surface for the samples that were traverse ground were intermediate between those of the aforementioned plunge-ground sample.

While high compressive surface stresses are considered beneficial in advanced ceramics, the specimen plunge-ground with the experimental metal-bonded wheel would be considered superior to the resin-bond wheel because of the relatively deeper tensile zone and lower stress gradient. Additional work is suggested to confirm that these differences are significant and repeatable. The overall conclusion is that the experimental metal-bonded wheel does not appear to adversely affect the grinding residual stress profile.

Hoop direction residual stress characterization was not successful. Subsequent independent work at HTML has refined the hoop direction residual stress techniques. Additional work is warranted to evaluate hoop stress.

7.4.2. Surface Integrity of the Independent Grinding Test Specimens -- Task 4.B

Specimens returned from the independent tests were not able to be tested for residual stress as part of the HTML user center experiment because of test priorities and time constraints.

Surface integrity at the independent validation test sites was reported in Section 7.3.3., Independent Validation Tests at Subcontractors -- Task 3.C, starting on Page 39.

The following summarizes the surface integrity data from these validation tests showing that the experimental-metal bond produced equal or slightly superior surfaces as the standard production wheels.

Caterpillar evaluated surface finish on zirconia and silicon nitride as reported in Table 9 and Table 10, respectively, starting on Page 40. There was no apparent difference in surface finish for the experimental metal-bond wheel vs a standard vitrified-bonded wheel grinding zirconia. The vitrified-bond wheel produced poorer finish than the experimental wheel on silicon nitride at higher thrufeed rates due to wheel breakdown. As shown in Table 10, Caterpillar also evaluated residual stress for both wheels in the radial and axial directions. The differences among wheels were inconclusive although higher residual stress in the specimens ground by the vitrified-bond wheel at the high thrufeed rate was noted.

Chand Kare, in Section 7.3.3.2 on Page 41, reported that depth of cut followed by wheel speed had the most significant influence on surface finish. The experimental metal-bond wheel resulted in slightly better and more consistent surface roughness, but this was not considered significant.

Eaton in Section 7.3.3.3 on Page 45, evaluated surface finish, Ra, and Rt for all tests as reported in Table 12. The experimental metal-bond wheel was reported superior to the standard resin-bond; however, this result was not conclusive because the grit size of the experimental wheel was finer.

The Norton Advanced Ceramics valve grinding test at the HGTC, as shown in Figure 30 on Page 52 reported that the experimental metal-bond wheel produced very stable and acceptable stem surface finish over a wide range of material removal rates. These material removal rates exceeded the capability of the standard vitrified-bond wheel.

## 7.5. PROGRAM MANAGEMENT -- TASK 5

### 7.5.1. Reporting

Norton Company submitted the required bimonthly and semiannual reports to the LMER Project Manager.

### 7.5.2. Communications/Visits/Travel (after Phase I and during Phase II)

R. H. Licht attended the Annual Review of Projects in Cost-Effective Ceramic Machining, Pollard Auditorium, Oak Ridge, TN, September 20, 1995.

R. H. Licht attended the Annual Automotive Technology Development Contractors' Coordination Meeting, Dearborn, MI, October 24-26, 1995.

R.H. Licht and P. Kuo to Oak Ridge, Cost-Effective Ceramic Machining (CECM) Annual Project Review and High Temperature Materials Lab (HTML) User Center, September 11-12, 1996.

James Blackmore, AlliedSignal Ceramic Components, during a visit to Norton Company Superabrasives, Worcester MA, reviewed ASCC planned independent validation test with Norton project personnel, October 4, 1996.

Michael A. Laurich, Eaton Corp. Manufacturing Technologies Center, during a visit to Norton Company Superabrasives, Worcester MA, reviewed Eaton's planned independent validation test with Norton project personnel, October 23, 1996.

R.H. Licht, P. Kuo, and L.A. Broderick to Chand Kare Technical Ceramics, November 8, 1996.

A meeting with NAC and HGTC was held on March 28, 1997, at the HGTC to finalize plans for conducting the NAC valve grinding experiment for the experimental metal bond.

R.H. Licht to ORNL, Program Review of Propulsion System Materials, April 22-24, 1997. Discussion of residual stress testing at the HTML with C. Hubbard and T. Watkins.

HTML User Proposal, No., 97-061, "Evaluation of Residual Stress in Silicon Nitride Ground With A New Innovative Grinding Wheel," submitted to HTML Program Office, July 8, 1997.

R.H. Licht to ORNL, HTML Tenth Anniversary Celebration/User Forum, July 14-16, 1997. Discussion of residual stress testing at the HTML with C. Hubbard and T. Watkins.

Final Test Report, "Metal Bond Diamond Wheels, IGW Project - Phase II, Task 3, NAC Independent Validation Test, O.D. Grinding on $Si_3N_4$," WGTC Test Results, S. Liu, D.A. Wakefield, and R.H. Licht, Submitted April 16, 1997.

Final Test Report, "Testing of the New Experimental Metal Bond Wheel", Changsheng Gho, Chand Kare Technical Ceramics, Submitted to R.H. Licht, Norton Company, July 15, 1997.

Final Test Report, "Innovative Grinding Wheel Design for Cost Effective Machining of Ceramics," Michael Haselkorn, Caterpillar Inc., Submitted to Norton Company, August 28, 1997.

Final Test Report, "An Evaluation of The Norton Innovative Grinding Wheel Design for Cost Effective Machining of Ceramics," Michael A. Laurich and Joseph A. Kovach, Eaton Manufacturing Technologies Center, Submitted to Norton Company, September 1997.

R.H. Licht to the Annual DOE Automotive Technology Development Customers' Coordination Meeting, Dearborn, MI, October 27-29, 1997.

D. Murphy to Brookhaven National Laboratory to perform the Residual Stress User Center experiment with Tom Watkins, November 11-15, 1997.

D. Murphy, J. M. Bai, and T. Watkins, "Evaluation of Residual Stresses in Silicon Nitride Ground with a New 'Innovative Grinding Wheel," HTML Experimental Report, Proposal Number 97-061, April 13, 1998.

Petitions for Identified Waiver of Patent Rights to Inventions S-87,062 (BD-3560 "Method of Grinding Ceramic Components" and S-87,063 (BD-3561 "Abrasive Tool for Grinding Ceramics" Made Under Contract No. DE-AC05-84OR21400; LMES Subcontract No. 86X-SU697V [W(I)97-028; ORO-667 and W(I)97-029; ORO-668], L.A. Broderick, Norton Company, to E.G. Schneider, U.S. Department of Energy.

Approval of Norton Company's request for waiver (above), E.G. Schneider, DOE, March 25, 1998.

7.5.3. Contract-Related Publications/Presentations

R.H. Licht (presenter), S. Ramanath, M. Simpson, E. Lilley, "Development of a Next-Generation Grinding Wheel," Annual Review of Projects in Cost-Effective Ceramic Machining, Ceramic Technology Project, Propulsion System Materials Program, Pollard Auditorium, Oak Ridge, TN, September 20, 1995.

R.H. Licht (presenter), S. Ramanath, M. Simpson, E. Lilley, "Innovative Grinding Wheel Design for Cost-Effective Machining of Dense Ceramics," Annual Automotive Technology Development Contractors' Coordination Meeting, Propulsion System Materials, No. 2, Dearborn, MI, October 25, 1995.

R.H. Licht and P. Kuo (presenters), and S. Ramanath, "Development of a Next-Generation Grinding Wheel," presented at the Cost-Effective Ceramic Machining (CECM) Annual Project Review, Oak Ridge, September 11, 1996.

P.J. Blau, "Cost-Effective Ceramic Machining Effort Celebrates Five Years of Accomplishments," *Abrasives Magazine*, February/March 1997.

Presentation, "The Evaluation of Surface Integrity in Ground Silicon Nitride Components," R.H. Licht, D. Murphy, M.R. Foley, and V.K. Pujari, American Ceramic Society Annual Meeting & Exposition, Cincinnati, May 6, 1997.

Presentation, "Innovative Grinding Wheel Design for Cost-Effective Machining of Advanced Ceramics", J.W. Picone (Presenter), R.H. Licht, S. Liu, P. Kuo, and D. Murphy, at "Discover Ceramics, '97," Columbus Convention Center, September 24, 1997.

Presentation, R.H. Licht (presenter), P. Kuo, S. Liu, J.W. Picone, and D. Murphy, "Innovative Grinding Wheel Design for Cost-Effective Machining of Advanced Ceramics," Annual Automotive Technology Development Customers' Coordination Meeting, Dearborn, MI, October 29, 1997.

L.M. Sheppard, Editor, "Toward Economical Machining of Advanced Ceramics," *Ceramic Industry*, October 1997.

J. Picone, R.H. Licht, S. Liu, P. Kuo, S. Ramanath, and D. Murphy, "New Wheels for Cost-Effective Manufacturing," *Ceramic Industry*, December 1998.

7.5.4. Schedule and Status of Milestones

| Task Number | Milestone | Due Date (Mod. 6) | Status |
|---|---|---|---|
| 1 | **Process Scale-Up** | | |
| 1.A | Experimental Design and Definition | 3/31/96 | Completed |
| 1.B | Strength Characterization and High Speed Core Development | 6/30/96 | Completed |
| 1.C | Manufacture and Characterization of Large Wheels and Task 1 Decision Point | 8/31/96 | Completed |
| 2 | **In-House Wheel Testing** | | |
| 2.A | Ceramic Specimen Preparation | 6/30/96 | Completed |
| 2.B | Preliminary Grinding Tests at HGTC | 10/30/96 | Completed 1/15/97* |
| 3 | **Independent Validation Testing** | | |
| 3.A | Selection of sites and wheel specs | 8/15/96 | Completed |
| 3.B | Wheel Fabrication and Delivery | 12/31/96 | Completed |
| 3.C | Tests at Subcontractors and Test Reports | 3/31/97 | Completed 9/18/97* |
| 4 | **Ceramic Surface Integrity** | | |
| 4.A | Ceramic Surface Integrity of In-House Specimens | 12/31/96 | Completed |
| 4.B | Independent Validation Test Specimens | 10/31/97 | Completed 12/2/97* |
| 5 | **Program Management** | | |
| 5.A | Bimonthly and Semiannual Reports | | Completed |
| 5.B | Delivery of Draft Final Report | (10/31/98) | Completed |
| 5.C | Delivery of Final Final Report | (12/31/98) | Completed |

*Comments on completion dates: The decision to do supplemental testing and some unforeseen delays in Tasks 2, 3, and 4 delayed completion as shown. All other milestones completed on or ahead of schedule.

## 7.6. PHASE 3 -- COMMERCIALIZATION BY NORTON CO., SUPERABRASIVES

With the successful completion of Phase II, Norton Company did not propose further Phase III development under the DOE program. Norton Company concluded that an additional DOE-supported program was not required to make a new, innovative grinding wheel product available to the U.S. advanced ceramics industry.

### 7.6.1. Patents Filed under the Phase II Program

Norton Company made the following U.S. Patent Application filings on March 27, 1998. Inventors of both: S. Ramanath, S.Y. Kuo, W.H. Williston, and S.T. Buljan.

1. Serial No. 09/049,628, "Method for Grinding Precision Components"
2. Serial No. 09/049,623, "Abrasive Tool"

Norton Company submitted a Petition for Identified Waiver of Rights to Invention for two inventions made under the Innovative Grinding Wheel Phase II program. The U.S. Department of Energy granted the petition. Norton Company agreed to accept DOE's standard waiver terms and conditions and to abide by the conditions relating to Government license, march-in rights, and preference for U.S. Industry.

### 7.6.2. Product Launch in the U.S.

In addition to the program independent test sites review in Task 3, Section 7.3 beginning on Page 38, Norton supplied the experimental innovative grinding wheel to the ORNL High Temperature Material Laboratory Machining and Inspection User Center, and to other customer sites.

Norton Company, Superabrasives Division, Worcester, Massachusetts, initiated the new product launch of this innovative grinding wheel at the April 1998 American Ceramic Society Annual Meeting and Exposition. The metal-bonded grinding wheel product designation is Scepter™, as shown in the latest product flyer in Appendix 5.

In addition to abiding by the conditions specified by DOE in the Identified Waiver of Rights, Norton Company pledged to make the new Scepter product available exclusively to U.S. industry for at least one year after the product launch. This U.S. availability "head-start" was first offered in Norton's 1993 Phase I proposal to DOE.

The new Scepter product is being manufactured in the Norton Company Superabrasive Industrial Wheel facility in Worcester, Massachusetts. This Superabrasive facility became ISO 9001 certified in 1998.

# 8. CONCLUSIONS

Norton Company completed the Phase II technical effort and successfully met the program objectives to develop a novel grinding wheel for cost-effective cylindrical grinding of advanced ceramics. Ceramic machining, predominantly diamond grinding, is a major cost factor in advanced ceramics manufacturing. The abrasive wheel performance significantly influences the grinding costs. Additionally, the quality of the grinding operation greatly affects ceramic surface integrity, tolerance, and manufacturing yield. Commercialization of the new metal-bonded Innovative Grinding Wheel (IGW) should contribute to improved cost-effective manufacturing of advanced ceramics vital for energy conservation and pollution reduction in new transportation systems.

The segmented-wheel approach facilitated prototype fabrication of larger-diameter wheels. Norton requested a modification of the original statement of work to change the test wheel diameter requirement from 356 mm, to include a range of between 356 mm and 406 mm. This larger-diameter capability is preferable for some of the newer OD grinding machines and current grinding trends in the ceramic industry. The successful manufacture of the larger-diameter wheels should expedite new wheel commercialization at the conclusion of this Phase II contract.

A core material was chosen that would more than exceed the required spin test speeds for test wheels by a factor of 3. Abrasive segment manufacturing trials were successfully completed that demonstrated improved segment property consistency. Wheel assembly trials were completed that demonstrated net-shape segment manufacture and successful segment-core adhesion. Three partial wheel specimens with only four segments were made for a burst speed study to evaluate cements. Failure occurred at over 200 m/s with the failure at the cemented interface. Fractography confirmed successful interface preparation and expected failure patterns. The manufacturing trials demonstrated segment curvature and side-angle control for the rim and segment-to-segment interfaces. Speed tests of the wheels to be used in grinding tests rated them at up to 120 m/s. Burst tests of 4 of the prototype wheels conservatively rated this design for a maximum operating speed (MOS) of at least 90 m/s. Further enhancements of the cement and core are expected to increase the MOS beyond this conservative limit.

Confirmatory grinding tests were performed in Task 2, in-house grinding tests, and Task 3, independent validation tests at customer sites. Norton's Higgins Grinding Technology Center completed preliminary in-house tests under Task 2 on the large-diameter wheel at three grinding speeds and several grinding conditions, in both plunge- and traverse-grinding modes.

- The experimental metal-bonded wheel significantly outperformed both the standard vitrified and resin-bonded wheels. The experimental metal-bonded wheel demonstrated superior wheel life with less need for truing and dressing during the extended grinding tests.

- Experimental wheel improvements were more pronounced at higher-material-removal-rate conditions.
- The IGW achieved cut rates of over 5 times of that practical by a standard resin-bond diamond grinding wheel, and demonstrated G-ratios over an order of magnitude greater. This advantage was more pronounced when considering that the standard resin-bond wheel had a higher diamond concentration.

In Task 3, independent customer validation tests of the experimental metal-bonded innovative grinding wheel (IGW) were performed by Caterpillar Corporation, Chand Kare Technical Ceramics, Eaton Manufacturing Technologies Center, and Norton Advanced Ceramics. All these validation tests reported excellent results and operator preference with the IGW over standard diamond wheel products when grinding NT551 silicon nitride and other ceramics. The general results of these tests showed that the IGW gave lower and more stable wheel wear, grinding force, and power over a wide range of material removal rates.

- Caterpillar demonstrated significantly lower wheel wear with the IGW compared to their standard vitrified-bonded wheel in centerless grinding on both NT551 silicon nitride and Mg-PSZ. At higher thrufeed rates, the IGW had superior surface finish because it did not breakdown compared to the standard wheel.
- Weibull analysis of post-ground zirconia bend bars suggested less machining damage for the IGW.
- At Caterpillar, the IGW did not appear more difficult to true and dress but required less dressing, especially in the higher thrufeed tests.
- Chand Kare, testing at lower grinding speed than the other tests, reported significantly lower specific energy with the IGW with similar surface roughness, form holding, and truing time as the standard resin-bonded wheel. The operator preferred the IGW.
- As expected, the Chand test showed that higher depth of cut, higher work speed, and lower wheel speed had the greatest effect on increasing wheel wear of both test wheels. Surprisingly, the IGW had slightly higher wheel wear in the Chand test (the opposite result from all other tests).
- Eaton tested the wheel at three speeds up to 18,000 SFPM. The Eaton test showed the 320-grit IGW had higher G-ratio, lower wheel wear, lower grinding force, and better surface finish compared to an even coarser 240-grit resin-bonded wheel.
- At Eaton, the IGW performance was less sensitive to grinding speed than the resin-boded wheel. The superiority of the IGW was more pronounced at lower grinding speeds and higher-material-removal-rate conditions.
- The metal-bonded IGW is capable of dressing by electrolytic techniques. Eaton's Electrocontact Discharge Dressing (EDD) technique was tested against conventional dressing but EDD appeared to be too aggressive.
- NAC in collaboration with the HGTC successfully demonstrated high productivity ceramic valve stem finishing with the IGW. The IGW was tested at cut rates over 6 times higher and traverse rates 2½ times greater than could be achieved with the

vitrified-bonded wheel, while the IGW met the surface-finish specification at all grinding test conditions.

- A supplemental NAC test at NRDC evaluated the IGW machining NT551 silicon nitride rolling contact fatigue specimens and cylindrical-plunge grinding of aluminum oxide disks. In these preliminary trials at NRDC, no significant differences were noted compared to a standard resin-bonded wheel. For the aluminum oxide disks, the IGW had less wheel wear but did tend to cause greater amounts of edge chipping.

During the development of cost-effective machining processes or the development of new grinding wheels, it is critically important to maintain and characterize the surface integrity of the ground ceramic. In this program, we characterized the surface integrity of the ground surfaces of the new wheels vs standard wheels including surface finish, component flexural strength, failure origin analysis, and surface residual stress. There was no evidence of unusual surface integrity problems with the new IGW.

- Most notably, the IGW showed excellent surface-finish stability at very high material removal rates in several tests.
- Conventional contact profilometry was effective in characterizing surfaces generated by different wheels and machining conditions. Non-contact interferometry proved consistent to contact profilometry data. Atomic force microscopy was discontinued as a surface characterization tool because of large variability in the data.
- Flexural testing of traverse-ground specimens did not result in significantly different strength differences or any observed severe machining damage with the IGW. Actually, severe damage was observed in isolated examples with the standard resin-bonded wheel, not the IGW, after the in-house HGTC test and the Caterpillar test. The lower normal force and specific grinding energy observed in several IGW tests would tend to indicate a tendency for lower grinding damage with this new wheel.
- Liquid Dye Penetrant NDE did not identify machining damage in selected samples.
- Residual stress studies were performed at Brookhaven National Lab under an ORNL HTML User Center project. Traverse- and plunge-ground cylindrical surfaces ground with the IGW and standard resin-bond wheel were compared. No significant differences in residual stress profiles were observed, except that a more severe stress gradient was shown in the plunge-ground surface produced by the resin-bond wheel.

The Innovative Grinding Wheel Phase II program successfully demonstrated manufacturing scale-up of 16-inch-diameter wheels for cylindrical grinding. The new experimental metal-bonded grinding wheel demonstrated significant improvements over conventional resin- and vitrified-bonded wheels when grinding silicon nitride and other advanced ceramics. The new wheel product should result in significant cost-effective improvements in the cylindrical grinding of advanced ceramics, while maintaining the required component quality achieved by conventional grinding wheels.

# 9. ACKNOWLEDGEMENTS

The Innovative Grinding Wheel Phase II program was a collaborative effort among several groups in Norton Company. The roles (and organizations) of each of the authors are as follows: **Robert Licht,** Program Manager (SGIC Government Programs Group); **Peter Kuo** and **S. (Ram) Ramanath**, Principal Investigators for bond development (Norton Company, Superabrasives R&D); **Steve Liu**, in-house and NAC wheel testing (Norton Company HGTC); **Dawn Murphy**, Principal Investigator for surface integrity (Northboro R&D Center, NRDC); and **Joseph Picone**, independent validation test coordination (Norton Company, Superabrasives Division).

Norton Company is greatly appreciative of the sponsorship given by the U.S. Department of Energy, Assistant Secretary for Energy Efficiency and Renewable Energy, Office of Transportation Technologies, as part of the Heavy Vehicle Propulsion System Materials Program, under contract DE-AC05-96OR22464 with Lockheed Martin Energy Research Corporation.

The authors gratefully acknowledge the advice and guidance of **Peter Blau** and **Susan Winslow**, ORNL Program Monitors. We acknowledge the efforts of **D. Ray Johnson**, ORNL Program Manager of the Heavy Vehicle Propulsion Materials, **Robert B. Schulz** and **Sidney Diamond**, U.S. Department of Energy OTT, for their efforts over the years in support of reliable and cost-effective ceramics.

The independent validation tests in Task 3 were the heart of this program. The authors gratefully acknowledge the professional wheel testing support given by the following Principal Investigators and organizations: **Michael Haselkorn** (Caterpillar, Inc.), **Changsheng Gho** (Chand Kare Technical Ceramics), and **Joseph A. Kovach** and **Michael A. Laurich** (Eaton Manufacturing Tech. Center). **Vimal Pujari**, (Program Manager of ACMT, NAC R&D) provided technical support to Steve Liu and Bob Licht regarding the NAC valve grinding tests and NT551 properties. **William Folsom** (NRDC Machining Lab) performed the NAC supplemental grinding test.

**Tom Watkins** (HTML Residual Stress User Center) and **Jian Ming Bai** (Brookhaven National Lab) worked with Dawn Murphy on arduous curved-surface residual stress experiments that resulted in very useful surface characterization data.

The success of this program was a team effort by many contributors in Norton Company Abrasives and Saint-Gobain Industrial Ceramics, for which we are grateful. **Bob Block**, Business Manager, Glass, Ceramics, and Composites, provided invaluable market information and encouragement, and is now spearheading the Scepter™ new-wheel product launch. Bond development support came from **Tom Buljan**, Manager, Superabrasives R&D, and **Harold Williston**. The authors wish to thank the following from Norton's Higgins Grinding Technology Center for grinding technology expertise: **K. (Subbu) Subramanian**, Director, HGTC; **Douglas Wakefield**, who ran the grinding tests, and **John Hagan**, who led the ACMT-valve grinding trials.

The authors acknowledge the ceramic science technical support given at the SGIC NRDC. **Mike Foley, Peter Pope, Paul R. Paldino,** and **Tom Thibaudeau** processed the silicon nitride specimens. **Paul Pelletier, Bill Hackett, Josh Kilgore, Dave Goodmacher,** and **Dave Jacobs** provided NDE and material-characterization support.

The SGIC Government Program Group in Northboro provided contract support. We are grateful to **Linda Broderick**, Senior Contract Administrator, for her professionalism and perseverance. We thank **Fred Van Slett**, Manager of Contract Compliance, and **Colleen Carhart**, SGIC Sr. Government Accountant, for their support to the program regarding financial and contract compliance issues.

# 10. REFERENCES

1. R.H. Licht, S. Ramanath, M. Simpson, E. Lilley, *Innovative Grinding Wheel Design for Cost-Effective Machining of Advanced Ceramics, Phase I Final Report,* Subcontract No. 87X-SM037V, published by Oak Ridge National Laboratory Ceramic Technology Project, Report Number ORNL/Sub/93-SM037/1, February 1996.

2. G.E. Superabrasives, Worthington, OH., Personal Communication, "GE's Guidelines to Markets and Applications," 1996 and 1997.

3. P. J. Blau, *Report on the Planning Workshop on Cost-Effective Ceramic Machining,* ORNL/M – 1745, November 1991.

4. *DOE/ORNL Workshop, Superabrasives and Grinding Wheel Technology for Machining Ceramics,* May 28-29, 1992, Oak Ridge, TN.

5. R. H. Licht, Norton Company presentation at ORNL, White Paper WP-912, (1990), from Internal White Paper, "Machining in [Norton Company] Advanced Ceramics."

6. D. Johnson-Walls, A. G. Evans, D. B. Marshall, and M. R. James, "Residual Stresses in Machined Ceramic Surfaces," *J. Am. Ceram. Soc.,* **69** [1] 44-49 (1986).

7. R. Samuel, S. Chandrasekar, T. N. Farris, and R. H. Licht, "Effect of Residual Stresses on the Fracture of Ground Ceramics," *J. Am. Ceram. Soc.*, Vol. **72**, No. 10, 1960-1966 (October 1989).

8. D. J. Snoha and M. R. Foley, "An Investigation of Residual Stresses in Machined Silicon Nitride", *U.S. Army MTL Report MTL TR 92-46*, Watertown, MA (July 1992).

9. E.S. Zanoria, et. al., "Assessment of Techniques for Characterizing the Surface Quality of Ground Silicon Nitride," *Journal of Materials Engineering and Performance,* Volume 7(4), 533-547 (August 1998).

10. K. Subramanian, "Superabrasives," *ASM Handbook, Machining,* 1985.

11. K. Subramanian, "Precision Finishing of Ceramic Components with Diamond Abrasives," *American Ceram. Soc. Bull.*, Vol. 67 (No. 6), 1026-1029 (June 1988).

12. K. Subramanian and S. Ramanath, Mechanism of Material Removal in the Precision Grinding of Ceramics," *Proceedings of the Symposium on Precision Machining,* PED –Vol. 58, American Society of Mechanical Engineers, 1-20 (1992).

13. J. A. Kovach and S. Malkin, 'High-Speed, Low-Damage Grinding of Advanced Ceramics," ORNL/TM-12778, *Ceramic Technology Project Semiannual Progress Report for October 1993 Through March 1994*, U.S. DOE Office of Transportation Technologies.

14. B. P. Bandyopadhyay and P. J. Blau, *Survey of Ceramic Machining in Japan,* ORNL/M-2881, U.S. DOE Office of Transportation Technologies (July 1993).

15. V. K. Pujari et al., *Development of Improved Processing and Evaluation Methods for High Reliability Structural Ceramics for Advanced Heat Engine Applications, Phase I. Final Report,* ORNL/Sub/98-SB182/1 ORNL Ceramic Technology Project, U.S. DOE Office of Transportation Technologies, August 1993.

16. E. Lilley, G. A. Rossi and P. J. Pelletier, *Tribology of Improved Transformation Toughened Ceramics – Heat Engine Test. Final Report,* ORNL /Sub/90-SG372/1, ORNL Ceramic Technology Project, U.S. DOE Office of Transportation Materials, April 1992

17. J. F. Braza, R. H. Licht, and E. Lilley, "Ceramic Cam Roller Follower Simulation Tests and Evaluation," *STLE Preprint No. 92-AM-2F-1*, 47th Annual Meeting of STLE, Philadelphia, PA, May 4-7, 1992.

18. V.K. Pujari, et. al., "Development of Advanced Ceramic Manufacturing Technology," *Heavy Vehicle Propulsion System Materials Program Semiannual Progress Report for April Through September 1997* and *October 1997 Through March 1998*, published by Oak Ridge National Laboratory, Report Number ORNL/TM-13562 and ORNL/TM-13648, Publication date, January 1998 and June 1998.

19. M. R. Foley, R. H. Licht, L. C. Sales, and D. M. Tracey, "Surface Integrity in Advanced Structural Ceramics," Presented at the *Workshop on Superabrasives and Grinding Wheel Technology for Machining Ceramics*, ORNL, May 1992.

20. M. R. Foley and V. K. Pujari, "Tensile Testing in the Development of Processing Methods for High Strength/High Reliability Silicon Nitride," *Ceramic Engineering and Science Proceedings,* Sept. -- Oct. 1992, 16th Annual Conference on Composites and Advanced Ceramic Materials.

21. O. M. Jadaan, D. L. Shelleman, J. C. Conway, J. J. Mecholsky, and R. E. Tressler, "Prediction of the Strength of Ceramic Tubular Components: Part I—Analysis," *ASTM J. of Testing and Evaluation,* 19[3], 181-191 (May 1991).

22. G. R. Anstis, P. Chantikul, B. R. Lawn, and D. B. Marshall, "A Critical Evaluation of Indentation Techniques for Measuring Fracture Toughness: I, Direct Crack Measurements," *J. Am. Cer. Soc.*, **64**, 533-538 (1981).

23. ASTM Standard C 1161 - 94 "Standard Test Method for Flexural Strength of Advanced Ceramics at Ambient Temperature." *Annual Book of ASTM Standards*, Vol. 15.01 (February 1995).

24. H. Ohmori, I. Takahashi, and B.P. Bandyopadhyay, "Highly Efficient Grinding of Ceramic Parts by Electrolytic In-Process Dressing (ELID) Grinding," *Materials and Manufacturing Processes*, Vol. 11, No. 1, 31-44 (1996).

25. D. Murphy, J. M. Bai, and T. Watkins, "Evaluation of Residual Stresses in Silicon Nitride Ground with a New 'Innovative Grinding Wheel,'" *HTML Experimental Report*, Proposal Number: 97-061, April 13, 1998.

26. A. Habenschuss, G. E. Ice, C. J. Sparks, and R. A. Neiser, "The ORNL Beamline at the National Synchrotron Light Source," *Nuc. Instr. and Meth.*, A266 215-9 (1988).

27. I. C. Noyan and J. B. Cohen, "Residual Stress, Measurement by Diffraction and Interpretation," *Springer-Verlag*, New York, p. 101 (1987).

28. L. G. Parratt, *Phys. Rev.*, **95**, 359-69 (1954).

29. B. Ballard, X. Zhu, P. Predecki, and D. Braski, "Depth-Profiling of Residual Stresses by Asymmetric Grazing Incidence X-Ray Diffraction (GIXD)," pp. 1133-43 in *Proc. Fourth Int. Con. on Residual Stresses,* Soc. for Exp. Mech., Bethel, CT (1994).

30. R. A. Winholtz and J. B. Cohen, "Generalized Least-squares Determination of Triaxial Stress States by X-ray Diffraction and the Associated Errors," *Aust. J. Appl. Physics,* 41, 189-99 (1988).

31. R. D. Ott, K. Breder, T. R. Watkins, M. K. Ferber, and J. M. Rigsbee, "Characterization of Machining-Induced Sub-Surface Damage of a High Strength Silicon Nitride," *Ceramic Engineering and Science Proceedings,* V. 18, [4] pp. 93-103 (1997).

32. X. Zhu, B. Ballard, and P. Predecki, "Determination of Z-Profiles of Diffraction Data from t-Profiles Using a Numerical Linear Inversion Method," *Adv. X-Ray Anal.,* V. 38, Plenum Press, New York, pp. 255-62 (1995).

# 11. APPENDIX

**Task 3 Independent Validation Grinding Test Final Reports**

1. "Innovative Grinding Wheel Design for Cost-Effective Machining of Advanced Ceramics – Phase II", M. Haselkorn, Caterpillar, Inc., August 28, 1997.

2. "Diamond Wheel Test Report", Changsheng Guo, Chand Kare Technical Ceramics, July 15, 1997.

3. "An Evaluation of the Norton Innovative Grinding Wheel Design for Cost-Effective Machining of Ceramics", Michael A. Laurich and Joseph A. Kovach, Eaton Manufacturing Technologies Center, September 8, 1997.

4. A) "Metal Bond Diamond Wheels, IGW Project – Phase II Task 3. NAC Independent Validation Test, OD Grinding on $Si_3N_4$", HGTC and Norton Advanced Ceramics, S. Liu and R.H. Licht, April 16, 1997.

   B) "Innovative Grinding Wheel Performance Evaluation", William W. Folsom, Northboro Research and Development Center (NRDC) and NAC, TM-97-218, January 14, 1998.

5. New Product Flyer, "Superior Metal Bond Diamond Wheels for Advanced Ceramic Grinding", Norton Company, © 1998.

Note: Individual reports available from Heavy Vehicle Propulsion System Materials Program, Oak Ridge National Laboratory, Building 4515, Oak Ridge, Tennessee 37831-6066, Phone (865) 574-4827.

ORNL/Sub/93-SM037/2

INTERNAL DISTRIBUTION

L. F. Allard, Jr.
P. F. Becher
T. M. Besmann
P. J. Blau
R. A. Bradley
K. Breder
C. R. Brinkman
T. D. Burchell
A. Choudhury
D. D. Conger
S. A. David
M. K. Ferber
R. L. Graves
C. R. Hubbard
M. A. Janney
D. R. Johnson (5)
R. R. Judkins
M. A. Karnitz
R. J. Lauf
K. C. Liu
W. D. Manly
S. B. McSpadden
T. A. Nolan
A. E. Pasto
M. H. Rawlins
A. C. Schaffhauser
D. P. Stinton
T. N. Tiegs
S. G. Winslow
R. E. Ziegler
Laboratory Records - RC

EXTERNAL DISTRIBUTION

Jeffrey Abboud
U.S. Advanced Ceramics Assoc.
1600 Wilson Blvd., Suite 1008
Arlington VA 22209

B. P. Bandyopadhyay
University of North Dakota
Box 8359 University Station
Grand Forks ND 58202-8359

Donald F. Baxter, Jr.
Advanced Materials & Processes
ASM International
9639 Kinsman Road
Materials Park OH 44073-0002

M. Brad Beardsley
Caterpillar Inc.
Technical Center Bldg. E
P.O. Box 1875
Peoria IL 61656-1875

Ramakrishna T. Bhatt
NASA Lewis Research Center
MS-106-1
21000 Brookpark Road
Cleveland, OH 44135

Bruce Boardman
Deere & Company, Technical Ctr.
3300 River Drive
Moline IL 61265-1792

Michael C. Brands
Cummins Engine Company, Inc.
P.O. Box 3005, Mail Code 50179
Columbus IN 47201

Donald J. Bray
Advanced Refractory Technologies
699 Hertel Avenue
Buffalo NY 14207

Jeff Bougher
Caterpillar Inc.
Technical Center, Bldg. E
P.O. Box 1875
Peoria IL 61656-1875

Mike Bowling
Cummins Engine Company, Inc.
1900 McKinley Avenue
P.O. Box 3005
Columbus IN 47202-3005

Walter Bryzik
U.S. Army Tank Automotive
Command
R&D Center, Propulsion Systems
Warren MI 48397-5000

David Carruthers
Kyocera Industrial Ceramics
5713 East Fourth Plain
Vancouver WA 98661

Ronald H. Chand
Morton Advanced Materials
185 New Boston Street
Woburn MA 01801

William J. Chmura
Torrington Company
59 Field Street, P.O. Box 1008
Torrington CT 06790-1008

William S. Coblenz
Defense Adv. Research Projects Agency
3701 N. Fairfax Drive
Arlington VA 22203-1714

Gloria M. Collins
ASTM
100 Barr Harbor Drive
West Conshohocken PA 19428-2959

Shawn Cooper
FEV Engine Technology
4554 Glenmeade Lane
Auburn Hills MI 48326-1766

Douglas Corey
AlliedSignal, Inc.
2525 West 190th Street, MS:T52
Torrance CA 90504-6099

Keith P. Costello
Chand/Kare Technical Ceramics
2 Coppage Drive
Worcester MA 01603-1252

Gary M. Crosbie
Ford Motor Company
P.O. Box 2053, 20000 Rotunda Drive
MD-3182, SRL Building
Dearborn MI 48121-2053

Pamela Cunningham
WETO Technical Library
MSE, Inc.
Industrial Park, P. O. Box 4078
Butte MT 59702

S. Keoni Denison
Norton Company
1 New Bond Street
Worcester MA 01615-0008

Sidney Diamond
U.S. Department of Energy
Office of Transportation Technologies
EE-33, Forrestal Building
Washington DC 28505

Ernest J. Duwell
3M Abrasive Systems Division
3M Center, Bldg. 251-01-34
St. Paul MN 55144

Michael Easley
AlliedSignal Engines
P. O. Box 52181
MS 551-11
Phoenix AZ 85072-2181

James J. Eberhardt
U.S. Department of Energy
Office of Transportation Technologies
EE-33, Forrestal Building
Washington DC 20585

Jim Edler
Eaton Corporation
26201 Northwestern Highway
P.O. Box 766
Southfield MI 48037

William A. Ellingson
Argonne National Laboratory
Energy Technology Division, Bldg. 212
9700 S. Cass Avenue
Argonne IL 60439-3848

John W. Fairbanks
U.S. Department of Energy
Office of Transportation Technologies
EE-33, Forrestal Building
Washington DC 20585

Ho Fang
Applied Materials
2695 Augustine Drive, MS-0962
Santa Clara CA 95054

Dan Foley
AlliedSignal Ceramic Components
MS:1/5-1, 26000
2525 West 190th Street
Torrance CA 90504

Douglas Freitag
DuPont Lanxide Composites
21150 New Hampshire Avenue
Brookeville MD 20833

Richard Gates
NIST
Bldg. 223, Rm. A-256
Rt. 270 & Quince Orchard Road
Gaithersburg MD 20899

Ludwig J. Gauckler
ETH Zurich
Nonmetallic Materials
Sonneggstr. 5
CH-8092 Zurich, SWITZERLAND

Allan E. Goldman
U.S. Graphite, Inc.
907 W. Outer Drive
Oak Ridge TN 37830

Robert J. Gottschall
U.S. Department of Energy
Metal & Ceramic Sciences, ER-131
19901 Germantown Road
Germantown MD 20874-1290

Thomas J. Gross
U.S. Department of Energy
Office of Transportation Technologies
EE-30, Forrestal Building
Washington DC 20585

Changsheng Guo
United Technologies Research Center
Machining Systems, MS 129-46
East Hartford CT 06108

Darryl Gust
Cummins Engine Company, Inc.
1900 McKinley Avenue
P.O. Box 3005
Columbus IN 47202-3005

Nabil S. Hakim
Detroit Diesel Corporation
13400 Outer Drive West, A08
Detroit MI 48239-4001

Alan M. Hart
Dow Chemical Company
1776 Building
Midland MI 48674

Michael H. Haselkorn
Caterpillar Inc.
Technical Center, Building E
P.O. Box 1875
Peoria IL 61656-1875

Deborah A. Haught
U.S. Department of Energy
Ofc. of Industrial Crosscut Technologies
EE-23, Forrestal Bldg.
Washington DC 20585

Daniel Hauser
Edison Welding Institute
Microjoinint & Plastics Tech. Team
1250 Arthur E. Adams Drive
Columbus OH 43221-3585

John Haygarth
Wah Chang
P.O. Box 460
Albany OR 97321-0460

Gene Huber
Precision Ferrites & Ceramics
5432 Production Drive
Huntington Beach CA 92649-1525

Thomas A. Johnson
Lanxide Corporation
1300 Marrows Road
P.O. Box 6077
Newark DE 19714-6077

Adam Jostsons
ANSTO
PMB1
Menai, NSW, Australia 2234

Yury Kalish
Detroit Diesel Corporation
Mechanical Systems
13400 Outer Drive West
Detroit MI 48239-4001

Roy Kamo
Adiabatics, Inc.
3385 Commerce Park Drive
Columbus IN 47201

Ralph Kelly
Cincinnati Milacron
P.O. Box 9013
Cincinnati OH 45209

W. C. King
Mack Truck, Z-41
1999 Pennsylvania Avenue
Hagerstown MD 21740

Tony Kirn
Caterpillar Inc.
Defense Products Dept., JB7
Peoria IL 61629

Joseph A. Kovach
Parker Hannifin Corporation
6035 Parkland Boulevard
Cleveland OH 44124-4141

Edwin H. Kraft
Kyocera Industrial Ceramics
5713 E. Fourth Plain Boulevard
Vancouver WA 98661

Oh-Hun Kwon
Norton Company
Saint Gobain Industrial Ceramics
1 Goddard Road
Northboro MA 01532-1545

S. K. Lau
B. F. Goodrich Aerospace R&D
9921 Brecksville Road
Brecksville OH 44141

Elaine Lentini
Saint-Gobain Industrial Ceramics
Goddard Road
Northboro MA 01532

Stan Levine
NASA Lewis Research Center
21000 Brookpark Road, MS:106/5
Cleveland OH 44135

Robert H. Licht
Norton Company
Saint Gobain Industrial Ceramics
1 Goddard Road
Northboro MA 01532-1545

E. Lilley
Norton Company
Saint Gobain Industrial Ceramics
1 Goddard Road
Northboro MA 01532-1545

B. J. McEntire
Applied Materials Corporation
3050 Bowers Avenue
Santa Clara, CA 95054

James McLaughlin
Sundstrand Power Systems
4400 Ruffin Road
P.O. Box 85757
San Diego CA 92186-5757

Biljana Mikijelj
Ceradyne, Inc.
3169 Red Hill Avenue
Costa Mesa CA 92626

Carl E. Miller
Delphi Energy & Engine Mgmt. Systems
4800 S. Saginaw Street, MC 485-301-150
P. O. Box 1360
Flint MI 48501-1360

Curtis V. Nakaishi
U.S. Department of Energy
Federal Energy Tech. Center
3610 Collins Ferry Rd.
P.O. Box 880
Morgantown WV 26507-0880

Malcolm Naylor
Cummins Engine Company, Inc.
P.O. Box 3005, Mail Code 50183
Columbus IN 47202-3005

Dale E. Niesz
Ceramic & Materials Engineering
607 Taylor Road, Rm. 204
Piscataway, NJ 08854-8065

Thomas J. Paglia
Coors/ACI
3315 Boone Road
Benton AR 72015

Richard Palicka
CERCOM, Inc.
1960 Watson Way
Vista CA 92083

Vijay M. Parthasarathy
Solar Turbines
2200 Pacific Highway, M.Z. R-1
San Diego CA 92186

Magan Patel
Cummins Engine Company, Inc.
Mail Code 50183
Box 3005
Columbus IN 47202-3005

James W. Patten
Cummins Engine Company, Inc.
P.O. Box 3005, Mail Code 50183
Columbus IN 47202-3005

Joe Picone
Norton Company
1 New Bond Street
Box 15008
Worcester MA 01615-0008

Stephen C. Pred
Pred Materials International, Inc.
60 East 42nd Street, Suite 1456
New York NY 10165

Vimal K. Pujari
Norton Company
Saint Gobain Industrial Ceramics
1 Goddard Road
Northboro MA 01532-1545

Fred Quan
Corning Inc.
Sullivan Park, FR-2-8
Corning NY 14831

George Quinn
NIST
I-270 & Clopper Road
Ceramics Division, Bldg. 223
Gaithersburg MD 20899

Mike Readey
Caterpillar, Inc.
Technical Center, Bldg. E
P.O. Box 1875
Peoria IL 61656-1875

Harold Rechter
Chicago Fire Brick Company
7531 S. Ashland Avenue
Chicago IL 60620-4246

Jack A. Rubin
CERCOM, Inc.
1960 Watson Way
Vista CA 92083

Robert J. Russell
Riverdale Consulting, Inc.
24 Micah Hamlin Road
Centerville MA 02632-2107

J. Sankar
North Carolina A&T State Univ.
Dept. of Mechanical Engineering
Greensboro NC 27406

Maxine L. Savitz
AlliedSignal, Inc.
Ceramic Components
2525 West 190th Street
P.O. Box 2960, MS:1/5-1, 26000
Torrance CA 90509-2960

Jim Schienle
AlliedSignal Aerospace
1130 West Warner Road
M/S 1231-K
Tempe AZ 85284

Gary Schnittgrund
Transfer Technology
16401 Knollwood Drive
Granada Hills CA 91344

Robert S. Shane
Shane Associates
1904 NW 22nd Street
Stuart FL 34994-9270

Subu Shanmugham
MicroCoating Technologies
3901 Green Industrial Way
Chamblee GA 30341-1913

Albert J. Shih
North Carolina State University
Mechanical & Aerospace Engineering
2217 Broughton Hall, Box 7910
Raleigh NC 27695

Charles Spuckler
NASA Lewis Research Center
21000 Brookpark Road, MS: 5-11
Cleveland OH 44135-3127

Gordon L. Starr
Cummins Engine Company, Inc.
P.O. Box 3005, Mail Code:50182
Columbus IN 47202-3005

Marian Swirsky
Cambridge Scientific Abstract
Commerce Park, Bldg. 4, Suite 804
23200 Chagrin Blvd.
Beachwood OH 44122

Victor J. Tennery
113 Newell Lane
Oak Ridge TN 37830

Malcolm Thomas
Allison Engine Company
P. O. Box 420 (W06)
Indianapolis IN 46206

Marc Tricard
Norton Company
Superabrasives Division
1 New Bond Street, MS-412-301
P. O. Box 15008
Worcester MA 01615-0008

Marcel H. Van De Voorde
Commission of the European Union
Eeuwigelaan 33
1861 CL Bergen
THE NETHERLANDS

V. Venkateswaran
Materials Solutions International, Inc.
P.O. Box 663
Grand Island, NY 14072-0663

Robert M. Washburn
ASMT
11203 Colima Road
Whittier CA 90604

R. W. Weeks
Argonne National Laboratory
Bldg. 362, E313
9700 S. Cass Avenue
Argonne IL 60439

Sheldon M. Wiederhorn
NIST
Building 223, Room B309
Gaithersburg MD 20899

Matthew F. Winkler
Seaworthy Systems, Inc.
P.O. Box 965
Essex CT 06426

Thomas J. Wissing
Eaton Corporation
26201 Northwestern Highway
P.O. Box 766
Southfield MI 48037

James C. Withers
MER Corporation
7960 S. Kolb Road
Tucson AZ 85706

Dale E. Wittmer
Southern Illinois University
Mechanical Engineering Dept.
Carbondale IL 62901

Egon E. Wolff
Caterpillar Inc.
Technical Center
P.O. Box 1875
Peoria IL 61656-1875

Roy Yamamoto
Ethyl Petroleum Additives, Inc.
500 Spring Street
P. O. Box 2158
Richmond VA 23218-2158

R. L. Yeckley
Kennametal, Inc.
P.O. Box 231
Latrode, PA 15650

Thomas M. Yonushonis
Cummins Engine Company, Inc.
1900 McKinley Avenue
P.O. Box 3005, Mail Code 50183
Columbus IN 47202-3005

S. Charles Yoon
Cincinnati Milacron, Inc.
P.O. Box 9013
3000 Disney Street
Cincinnati OH 45209-9013

Jong Yung
Sundstrand Aerospace
Dept. 789-6
4747 Harrison Avenue
Rockford IL 61125

A. L. Zadoks
Caterpillar Inc.
Technical Center, Building L
P.O. Box 1875
Peoria IL 61656-1875

Zhenqi Zhu
Stevens Institute of Technology
Department of Mechanical Engineering
Castle Point on Hudson
Hoboken NJ 07030

Department of Energy
Oak Ridge Operations Office
Assistant Manager for Energy
Research and Development
P. O. Box 2001
Oak Ridge TN 37831-8600

For distribution by microfiche
as shown in DOE/OSTI-4500,
Distribution Category UC-332
(Ceramics/Advanced Materials).